

Models of Learning in the Visual System: Dependence on Retinal Eccentricity

Dissertation

Presented in Partial Fulfillment
of the Requirements for the Degree of

Doctor of Natural Sciences

(Dr. rer. nat.)



Submitted to the Faculty of Physics,
Philipps-University Marburg

by

Basim Samir Al-Shaikhli

Marburg/Lahn

June 2006

Vom Fachbereich Physik der Philipps-Universität

angenommen am: 12.07.2006

Erstgutachter: Prof. Dr. R. Eckhorn

Zweitgutachter: Prof. Dr. H. Neumann

Tag der mündlichen Prüfung: 13.07.2006

Learning is not compulsory... neither is survival.

W. Edwards Deming (1900 - 1993)

Zusammenfassung

Im primären Sehkortex von Primaten nimmt die Repräsentation des zentralen Sehfeldes einen verhältnismäßig größeren Raum ein als die des peripheren Sehfeldes. Experimentell überprüfbare Theorien bezüglich der Faktoren und Mechanismen, die zu dieser inhomogenen Repräsentation geführt haben, können wertvolle Hinweise auf allgemeine Verarbeitungsprinzipien im Sehsystem liefern. Ich habe daher untersucht, an welche Sehsituationen diese inhomogene Repräsentation des Sehfeldes angepasst ist und welche Mechanismen zu ihrer Verfeinerung und Stabilisierung während der individuellen Entwicklung beitragen könnten. Weiterhin habe ich die funktionelle Bedeutung dieser inhomogenen Repräsentation für die visuelle Verarbeitung an zentralen und peripheren Orten des Sehfeldes untersucht.

Die Verarbeitung von Sehinformationen spielt während Eigenbewegung eine wichtige Rolle und sollte daher gut an diese spezielle Situation angepasst sein. Ich habe daher angenommen, dass retinale Geschwindigkeitsverteilungen, die durch statische Objekte während Eigenbewegung entlang der Blickrichtung auftreten, durch die inhomogene kortikale Repräsentation des Sehfeldes im Mittel in räumlich homogene kortikale Geschwindigkeitsverteilungen transformiert werden. Dies hätte den Vorteil, dass die kortikalen Mechanismen zur Verarbeitung von Eigenbewegung über das gesamte Sehfeld identisch aufgebaut sein könnten. Das ist der Fall, wenn die Anordnung der Sehobjekte relativ zum Beobachter in etwa einem Ellipsoid mit dem Beobachter im Mittelpunkt entspricht. Das daraus resultierende Flussfeld habe ich benutzt, um ein neuronales Netzwerkmodell mittels einer Hebb'schen Lernregel zu trainieren. Die räumliche Verteilung der gelernten rezeptiven Felder entspricht der inhomogenen kortikalen Repräsentation des Sehfeldes. Diese Ergebnisse zeigen, dass Eigenbewegung eine wichtige Rolle bei der Evolution des Sehsystems gespielt haben könnte, und dass die inhomogene kortikale Repräsentation des Sehfeldes während der individuellen Entwicklung durch Hebb'sche Lernmechanismen in natürlichen Sehsituationen verfeinert und stabilisiert werden kann.

Neben der Verarbeitung von Eigenbewegung spielt die Gruppierung und Trennung lokaler räumlicher Sehmerkmale in Sehobjekte eine wichtige Rolle bei der visuellen Verarbeitung. Daher habe ich mir die Frage gestellt, wie die entsprechenden Mechanismen von der repräsentierten Position des Sehfeldes abhängen. Es wird vermutet, dass neuronale Verbindungen innerhalb des primären Sehkortex diesen Gruppierungsprozess unterstützen. Diese Verbindungen werden erst nach der Geburt in Abhängigkeit von der Seherfahrung spezifiziert. Wie hängt die laterale Verschaltungsstruktur von der repräsentierten Position des Sehfeldes ab? Mit zunehmendem Sehwinkel werden die rezeptiven Felder der Neuronen im

primären Sehkortex größer, und die kortikale Vergrößerung des Sehfeldes nimmt ab. Daher habe ich die räumliche Statistik von realen Sehszenen in Abhängigkeit von den räumlichen Filtereigenschaften kortikaler Neuronen an unterschiedlichen Positionen des Sehfeldes untersucht. Ich zeige, dass die Korrelationen zwischen kollinear angeordneten Filtern gleicher Orientierung und Größe mit zunehmender Filtergröße längerreichweitig werden. Normiert man die Abstände der Filter aber auf die Filtergröße, fallen die kollinearen Korrelationen zwischen großen Filtern schneller mit zunehmendem Abstand ab als die zwischen kleinen Filtern. Das spricht gegen eine homogene kortikale laterale Verschaltungsstruktur über den gesamten Sehraum bezüglich der Codierung von Objektkonturen.

Zwei wichtige retino-kortikale Signalverarbeitungspfade sind der magnozelluläre (M) und der parvozelluläre (P) Pfad. Während Neuronen des M-Pfades eine zeitliche Bandpass-Charakteristik aufweisen, zeigen Neuronen des P-Pfades zeitliches Tiefpassverhalten. Das Verhältnis von P- zu M-Neuronen ist nicht über das gesamte Sehfeld konstant, sondern nimmt mit zunehmendem Sehwinkel ab. Ich habe daher untersucht, wie sich die unterschiedlichen zeitlichen Antworteigenschaften von Neuronen des M- und des P-Pfades auf die Selbstorganisation im Sehkortex auswirken und was dies für die Codierung von Sehobjekten an unterschiedlichen Orten des Sehfeldes bedeutet. Exemplarisch habe ich den Einfluss der Bewegung von Sehreizen auf die Selbstorganisation horizontaler Verbindungen an einem Netzwerkmodell mit impulscodierenden Neuronen und Hebb'schem Lernen untersucht. Niedrige Reizgeschwindigkeiten führen zu lateralen Verbindungen, die der räumlichen Struktur der Sehreize angepasst sind, wohingegen höhere Reizgeschwindigkeiten zu einer Verschaltungsstruktur führen, die die Codierung der Bewegungsrichtung der Sehreize unterstützt. Dies lässt vermuten, dass die zeitlichen Tiefpasseigenschaften von P-Neuronen die Codierung von räumlichen Reizmerkmalen (Form) unterstützen, wohingegen die zeitlichen Bandpasseigenschaften der M-Neuronen die Codierung von raum-zeitlichen Reizmerkmalen (Bewegungsrichtung) unterstützen. Das deutet darauf hin, dass besonders das zentrale Sehfeld, mit seinem hohen Anteil an P-Neuronen, für die Codierung von räumlichen Objektmerkmalen geeignet ist, wohingegen das periphere Sehfeld besser an die Codierung der Bewegung von Sehobjekten angepasst ist.

Abstract

In the primary visual cortex of primates relatively more space is devoted to the representation of the central visual field in comparison to the representation of the peripheral visual field. Experimentally testable theories about the factors and mechanisms which may have determined this inhomogeneous mapping may provide valuable insights into general processing principles in the visual system. Therefore, I investigated to which visual situations this inhomogeneous representation of the visual field is well adapted, and which mechanisms could support its refinement and stabilization during individual development. Furthermore, I studied possible functional consequences of the inhomogeneous representation for visual processing at central and peripheral locations of the visual field.

Vision plays an important role during navigation. Thus, visual processing should be well adapted to self-motion. Therefore, I assumed that spatially inhomogeneous retinal velocity distributions, caused by static objects during self-motion along the direction of gaze, are transformed on average into spatially homogeneous cortical velocity distributions. This would have the advantage that the cortical mechanisms, concerned with the processing of self-motion, can be identical in their spatial and temporal properties across the representation of the whole visual field. This is the case if the arrangement of objects relative to the observer corresponds to an ellipsoid with the observer in its center. I used the resulting flow field to train a network model of pulse coding neurons with a Hebbian learning rule. The distribution of the learned receptive fields is in agreement with the inhomogeneous cortical representation of the visual field. These results suggest that self motion may have played an important role in the evolution of the visual system and that the inhomogeneous cortical representation of the visual field can be refined and stabilized by Hebbian learning mechanisms during ontogenesis under natural viewing conditions.

In addition to the processing of self-motion, an important task of the visual system is the grouping and segregation of local features within a visual scene into coherent objects. Therefore, I asked how the corresponding mechanisms depend on the represented position of the visual field. It is assumed that neuronal connections within the primary visual cortex subserve this grouping process. These connections develop after eye-opening in dependence on the visual input. How does the lateral connectivity depend on the represented position of the visual field? With increasing eccentricity, primary cortical receptive fields become larger and the cortical magnification of the visual field declines. Therefore, I investigated the spatial statistics of real-world scenes with respect to the spatial filter-properties of cortical neurons at different locations of the visual field. I show that correlations between collinearly

arranged filters of the same size and orientation increase with increasing filter size. However, in distances relative to the size of the filters, collinear correlations decline more steeply with increasing distance for larger filters. This provides evidence against a homogeneous cortical connectivity across the whole visual field with respect to the coding of spatial object properties.

Two major retino-cortical pathways are the magnocellular (M) and the parvocellular (P) pathways. While neurons along the M-pathway display temporal bandpass characteristics, neurons along the P-pathway show temporal lowpass characteristics. The ratio of P- to M-cells is not constant across the whole visual field, but declines with increasing retinal eccentricity. Therefore, I investigated how the different temporal response-properties of neurons of the M- and the P-pathways influence self-organization in the visual cortex, and discussed possible consequences for the coding of visual objects at different locations of the visual field. Specifically, I studied the influence of stimulus-motion on the self-organization of lateral connections in a network-model of spiking neurons with Hebbian learning. Low stimulus velocities lead to horizontal connections well adapted to the coding of the spatial structure within the visual input, while higher stimulus velocities lead to connections which subserve the coding of the stimulus movement direction. This suggests that the temporal lowpass properties of P-neurons subserve the coding of spatial stimulus attributes (form) in the visual cortex, while the temporal bandpass properties of M-neurons support the coding of spatio-temporal stimulus attributes (movement direction). Hence, the central representation of the visual field may be well adapted to the encoding of spatial object properties due to the strong contribution of P-neurons. The peripheral representation may be better adapted to the processing of motion.

Statement of Originality

Large parts of Chapter 2 were written in co-authorship with Thomas Wachtler and Reinhard Eckhorn and are accepted for publication in a special issue of BioSystems (in press, 2006). All other parts of this thesis are originally composed by the author unless explicitly indicated otherwise. Models and data analyses were developed and implemented self-dependently, including the development of new software for the N.A.S.E. simulation environment. Simulations and visualizations base in part on elementary routines, which were developed in cooperation with other members of the Neurophysics group led by Reinhard Eckhorn.

This thesis has not been submitted, either in whole or part, for a degree at this or any other university or institution.

Contents

| | | |
|----------|--|-----------|
| 1 | Introduction | 1 |
| 1.1 | About this Thesis | 2 |
| 1.1.1 | Aim | 2 |
| 1.1.2 | Methods | 4 |
| 1.2 | Parallel Processing in the Visual System | 5 |
| 1.2.1 | Retino-Cortical Processing Pathways | 5 |
| 1.2.2 | Cortical Processing Pathways | 7 |
| 1.3 | Spatially Inhomogeneous Retino-Cortical Mapping | 9 |
| 1.3.1 | Physiology and Anatomy | 9 |
| 1.3.2 | Scale Invariance and Log Polar Transformation | 11 |
| 1.3.3 | Eccentricity-Dependent Projections Between Cortical Areas | 13 |
| 1.4 | Self Organization | 13 |
| 1.4.1 | Role of Input-Driven Self-Organization on Cortical Development | 13 |
| 1.4.2 | Synaptic Plasticity | 14 |
| 1.5 | Thesis Outline | 16 |
| 2 | Inhomogeneous Retino-Cortical Mapping and Self-Motion | 17 |
| 2.1 | Abstract | 17 |
| 2.2 | Introduction | 18 |
| 2.3 | Relating Cortical Magnification to Self-Motion | 18 |
| 2.4 | Model Simulations | 22 |
| 2.4.1 | Network Model and Input Stimuli | 23 |
| 2.4.2 | Results | 28 |
| 2.5 | Discussion | 31 |
| 2.5.1 | Summary of Results | 31 |
| 2.5.2 | Relating Optical Flow to Cortical Magnification | 32 |

| | | |
|----------|--|-----------|
| 2.5.3 | Minimal Network Model | 34 |
| 2.5.4 | Extensions to the Model | 37 |
| 2.5.5 | Related Studies | 39 |
| 3 | Spatial Statistics of Local Contour Elements in Real-World Scenes | 41 |
| 3.1 | Abstract | 41 |
| 3.2 | Introduction | 42 |
| 3.2.1 | Contour Grouping in Human Perception | 42 |
| 3.2.2 | Spatial Statistics of Contours in Real-World Scenes | 43 |
| 3.2.3 | Neurophysiology and Anatomy | 44 |
| 3.2.4 | Ontogenetic Development of Grouping Mechanisms | 45 |
| 3.2.5 | Models of Contour Grouping | 45 |
| 3.2.6 | Dependence of Contour Grouping Mechanisms on Retinal Eccentricity | 46 |
| 3.2.7 | Aim of the Current Study | 47 |
| 3.3 | Methods | 47 |
| 3.3.1 | Real-World Scenes | 47 |
| 3.3.2 | Extraction of Local Contour Elements | 49 |
| 3.3.3 | Data Analysis | 51 |
| 3.4 | Results | 53 |
| 3.4.1 | Average Normalized Wavelet Responses | 53 |
| 3.4.2 | Two-Dimensional Autocorrelation Matrices | 55 |
| 3.4.3 | Collinear Correlations | 56 |
| 3.4.4 | Shuffled Images | 60 |
| 3.4.5 | Non-Normalized Wavelet Responses | 63 |
| 3.5 | Discussion | 65 |
| 3.5.1 | Summary of Results | 65 |
| 3.5.2 | Anisotropy of Normalized Wavelet Responses | 65 |
| 3.5.3 | Scale Invariance of Contour Integration | 67 |
| 3.5.4 | Dependence of Spatial Scene Statistics on Eccentricity | 67 |
| 4 | Self-Organization of Lateral Connections | 71 |
| 4.1 | Abstract | 71 |
| 4.2 | Introduction | 72 |
| 4.2.1 | Conduction Velocities of Lateral Connections | 72 |
| 4.2.2 | Parallel Retinal and Cortical Processing Streams | 73 |

| | | |
|----------|--|------------|
| 4.2.3 | Goal of the Model | 74 |
| 4.3 | Methods | 75 |
| 4.3.1 | Network Architecture | 75 |
| 4.3.2 | Input Stimuli | 77 |
| 4.3.3 | Self Organization | 78 |
| 4.3.4 | Data Analysis | 78 |
| 4.4 | Results | 79 |
| 4.4.1 | No Lateral Conduction Delays | 79 |
| 4.4.2 | Finite Lateral Conduction Velocity | 82 |
| 4.4.3 | Random Stimulus Velocities during Learning | 85 |
| 4.5 | Discussion | 86 |
| 4.5.1 | Summary of Results | 86 |
| 4.5.2 | Network Scaling | 88 |
| 4.5.3 | Grouping Mechanisms for Static and Motion-Defined Contours | 89 |
| 4.5.4 | Grouping Mechanisms at Different Eccentricities | 90 |
| 4.5.5 | Conclusion | 91 |
| 5 | Conclusion and Outlook | 93 |
| 5.1 | Specific Results | 94 |
| 5.2 | Proposals for Future Research | 95 |
| 5.2.1 | Retinal Velocity Distribution During Self-Motion | 95 |
| 5.2.2 | Spatial Statistics of Contour Elements Across the Whole Visual Field | 96 |
| 5.2.3 | Lateral Connections in the Primary Visual Cortex | 96 |
| | Bibliography | 97 |
| | Acknowledgements | 115 |
| | Scientific CV | 117 |

Chapter 1

Introduction

The human visual system is a highly complex system, able to rapidly process huge amounts of sensory information. We are able to recognize known objects in different views and distances, under different lighting conditions, and we perceive locations in space as stable. This is a remarkable achievement, especially if one considers the continuously changing projections of the external visual world on our retinas due to self-motion, eye-movements, and the movement of objects like other people or animals. These accomplishments enable us to successfully navigate in and interact with our environment, which is a crucial precondition for our survival.

From the moment when light is absorbed by the photoreceptors of our retinas, visual information is processed in highly parallel networks of nerve cells (neurons), in order to form an internal representation of the outer visual world. To allow an organism to successfully interact with its environment, the structure of this internal representation must correspond well to the structure of the external world. Although the raw structure of the visual system is determined genetically, many properties depend on visual experience during individual development, as can be demonstrated by altering specific aspects of the visual input an organism receives during early stages of development (e.g., Wiesel and Hubel, 1963; Hubel et al., 1977).

Many scientific disciplines, including neurophysiology, neurobiology, neurophysics, and psychophysics, have spent much time and effort to better understand the characteristics of this internal representation and how it adapts on evolutionary and ontogenetic timescales according to the characteristics of the environment. A better understanding can lead to the development of flexible technical systems which are able to dynamically and effectively adapt to spatio-temporal regularities in their environment.

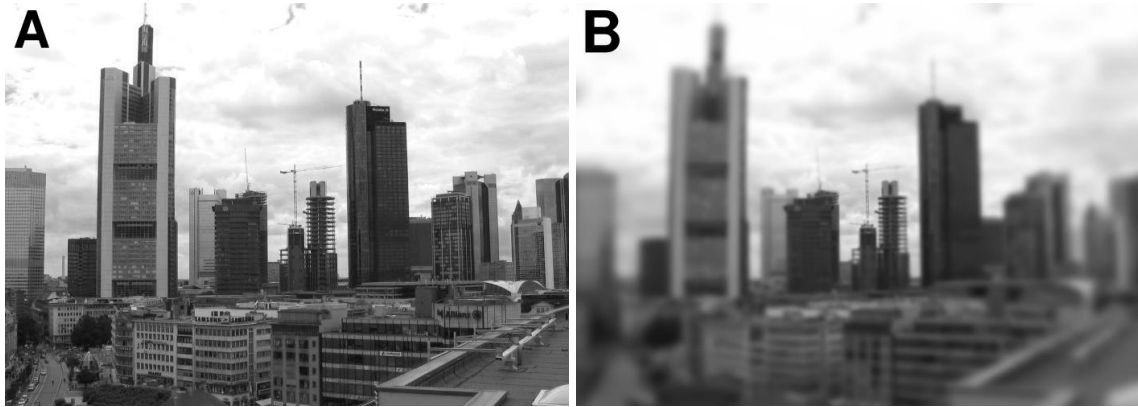


Figure 1.1: LINEAR DECREASE IN SPATIAL RESOLUTION. (A) Original image with constant resolution across the whole image. (B) The image is computed from the original image by replacing each pixel by a Gaussian weighted average of its original intensity value and its surrounding intensity values, with the standard deviation of the Gaussian kernel increasing linearly with distance from the center. Note that the crane in the center of the image appears crisp and sharp, while spatial details are lacking in the surrounding scene.

1.1 About this Thesis

1.1.1 Aim

The human visual system samples the external world in a spatially inhomogeneous fashion (e.g., Daniel and Whitteridge, 1961). Spatial resolution is highest along the direction of gaze and drops sharply with increasing retinal eccentricity¹. Thus, an object whose image falls on the central region of the retina (fovea) is perceived with higher spatial resolution than an object whose image falls outside the central region. This decrease in spatial resolution is illustrated in Figure 1.1, where a photograph was spatially blurred, with the amount of blur increasing linearly with distance from the center.

Several factors may have played a role during the evolution of this spatially inhomogeneous mapping. High spatial resolution enables us to perform actions which require fine visual and visuo-motor control, like building intricate tools, the visual distinction of friends from enemies (possibly even at larger distances), or reading this thesis. Limiting factors are, however, the volume of the eyes, the diameter of the optic nerve, and the size of the brain. The inhomogeneous retino-cortical mapping may be seen as an evolutionary solution to these antagonistic constraints. The visual system provides high spatial resolution only in

¹*Retinal Eccentricity* or *Eccentricity* is the angular deviation of a visual target from the direction of gaze.

the fovea, and requires eye movements over large areas of the visual field for the perception at high spatial resolution. This explanation, however, cannot quantitatively account for the shape of the inhomogeneous retinal cortical mapping. Experimentally testable theories about the factors and mechanisms which may have determined this inhomogeneous mapping may provide valuable insights into general processing mechanisms of the visual system.

Therefore, we² investigated to which properties of the visual input the spatially inhomogeneous retino-cortical mapping of visual space is well adapted and which biologically plausible principles could lead to its emergence and stabilization under natural viewing conditions. Furthermore, we studied possible functional consequences for visual processing at central and peripheral locations of the visual field.

We demonstrate that the global retino-cortical mapping may be well adapted to self-motion of an observer in its environment. Vision plays an important role in the control of goal-directed movements during self-motion, thus it seems plausible that the structure of visual systems is well adapted to this special situation. The importance of motion for the processing of visual information can be anticipated by the ubiquity of visual motion processing mechanisms in different species. From insects (Hassenstein and Reichardt, 1956; Egelhaaf and Borst, 1993), frogs (Barlow, 1953), cats (Hubel and Wiesel, 1962) to primates (Hubel and Wiesel, 1968), every organism with a visual system has developed mechanisms for the processing of visual motion, despite their vastly different natural environments and lifestyles.

However, in addition to the processing of self-motion, an important task of the visual system is to group and segregate local spatial features within a visual scene into coherent objects. Real-world³ visual scenes have characteristic statistical spatial properties that distinguish them from random noise distributions (e.g., Field, 1987; Ruderman and Bialek, 1994; Zetsche and Röhrbein, 2001). Several studies have demonstrated a correspondence between the statistical structure of real world scenes on the one hand and the neurophysiological and perceptual properties of visual processing on the other hand (e.g., Olshausen and Field, 1996; Bell and Sejnowski, 1997; Geisler et al., 2001).

How well is the spatially inhomogeneous retino-cortical mapping adapted to the spatial structure of the external environment? To investigate this question, we studied the statistics

²Although major parts of this thesis, and all of the computations, are the work of a single author, *I* use the form *we* throughout this thesis to account for the fact that many ideas arose from discussions with colleagues and the study of scientific publications written by others.

³Throughout the thesis we make a distinction between *natural scenes*, containing only natural objects, and *real-world scenes*, which can also contain man-made objects, like cars or houses.

of real-world scenes with respect to the spatial filter-properties of cortical neurons at different eccentricities.

Visual information is processed along parallel neuronal pathways with different spatial and temporal filter properties. Two major retino-cortical pathways are the magnocellular (M) and the parvocellular (P) pathways, originating in the retina (Perry et al., 1984). While neurons along the M-pathway exhibit temporal bandpass characteristics and provide an achromatic, spatially coarse representation of the visual world, neurons along the P-pathway display temporal lowpass characteristics and provide spatially fine chromatic details (Merigan et al., 1991a,b). The ratio of P- to M-neurons is not constant across the whole visual field. The central visual field is sampled more densely by the P-pathway than by the M-pathway. With increasing eccentricity, the ratio of P- to M-inputs to the visual cortex declines from approximately 35:1 in the fovea to 5:1 at 15° eccentricity in monkeys (e.g., Azzopardi et al., 1999).

What is the influence of the retino-cortical M- and P-pathways on the self-organization in the visual cortex according to spatial and temporal properties in the visual input? What are the functional consequences of the inhomogeneous representation of the visual field by neurons of the M- and the P-pathways for visual processing at different eccentricities? We investigated how the different temporal response properties of neurons along the P- and M-pathways may subserve the learning of either object-properties corresponding to the spatial structure of the visual input (object forms), or properties corresponding to the spatio-temporal structure of the visual input (object motion).

1.1.2 Methods

This thesis is theoretical in nature. We performed numerical simulations and calculations which aimed to mimic basic known aspects of early stages of visual processing. The human brain consists of approximately 10^{11} neurons, which are believed to be the substrate of the cognitive processing. Each neuron interacts directly with about 10,000 other neurons (Braitenberg and Schüz, 1991). This enormous complexity alone prevents us to envision a model of the entire human brain. Another limitation is the fact that current experiments, intricate as they are, fail to provide data about how these neurons interact. This is where biologically motivated theoretical models come into play. The interaction between experiments and theoretical models can iteratively lead to new insights into the principles of neural processing. While experiments can provide models with biologically realistic constraints, models can make predictions which can be verified experimentally and in turn provide new

input for more sophisticated models.

Although we are primarily interested in how the human visual system works, we treat the human and the mammalian cortex in parallel throughout this thesis and highlight distinctions only where necessary. At first sight, the brains of cats, monkeys and humans do not have much in common, besides the fact that we do not understand any of them. However, there are considerable similarities in the structure of their visual systems, due to the similarities in their natural environments and their common evolutionary heritage.

In the following we will provide the biological background for this thesis.

1.2 Parallel Processing in the Visual System

1.2.1 Retino-Cortical Processing Pathways

In the eyes, light is focused by cornea and eye lens to form a two-dimensional image on each retina. The retinal photoreceptors, which can be divided into rods and cones, transduce the absorbed light into electrical activity. Rods dominate achromatic vision at low levels of illumination, while cones provide color vision at higher levels of illumination. From the photoreceptors information is passed to the retinal bipolar cells. Bipolar cells have spatial classical receptive fields (cRFs) with a so-called center-surround organization: The direct input from a group of photoreceptors is balanced by a group of antagonistic inputs from a larger spatial region, presumably mediated by neighboring horizontal cells (e.g., Dacey et al., 2000). Half of the bipolar cells are hyperpolarized by light onset in their cRF center (OFF-center bipolar cells), the other half is depolarized by light onset (ON-center bipolar cells). The bipolar cells project to approximately 1.5 million retinal ganglion cells (Rodieck, 1988). Two important morphologically distinct classes of retinal ganglion cells are the *midget or parvocellular (P) cells* and the *parasol or magnocellular (M) cells*. Approximately 80% of the retinal ganglion cells are of the P-type and have small cell bodies, thin axons, and small dendritic trees. In contrast, M-type ganglion cells have large cell bodies, thick axons and large dendritic trees⁴ (Watanabe and Rodieck, 1989). Via the optic nerve, most of the retinal ganglion cells project to the lateral geniculate nucleus (LGN). The LGN has a layered structure, consisting of six main layers. The upper four layers (parvocellular or P-layers) receive inputs from retinal P-cells, while the lower two layers (magnocellular or M-layers) receive inputs from retinal M-cells. The functionally distinct M- and P-fibers from the LGN project to segregated sublamina of the primary visual cortex.

⁴The dendritic tree of M-cells resembles a parasol, hence the name.

Neurons along the M- and P-pathways differ in their sensitivity with respect to different stimulus attributes:

Spatial sensitivity. While P-cells have relatively small cRFs, the diameters of the cRF centers of neighboring M-cells are approximately 2 times larger (e.g., De Monasterio and Gouras, 1975; Derrington and Lennie, 1984; Croner and Kaplan, 1995). Additionally, some M-cells exhibit nonlinear spatial summation, while the remaining M- and P-cells show nearly linear spatial summation (Marrocco et al., 1982; Kaplan and Shapley, 1982).

Temporal sensitivity. P-cells respond in a more sustained fashion (resembling a temporal lowpass filter) to light onset or offset in comparison to M-cells (resembling a temporal bandpass filter) (Marrocco et al., 1982; Hicks et al., 1983; Purpura et al., 1990; Kaplan and Bernadete, 2001). P-cells respond best to stimuli temporally modulated at about 10 Hz and they generally cannot follow temporal modulations at frequencies higher than 20-30 Hz. M-cells, on the other hand, respond best to temporal modulations at 20 Hz and greater and can follow temporal modulations up to 60-80 Hz (review: Van Essen and Anderson, 1995).

Spectral sensitivity. P-cells encode most of the chromatic information within a visual scene due to the spectral opponency of their cRF center and surround, while M-cells are virtually insensitive to color (e.g., De Monasterio, 1978; Reid and Shapley, 1992; De Valois and De Valois, 1993).

Contrast sensitivity. While M-cells respond to changes in luminance contrast as low as 1%, P-cells rarely respond to contrasts below 10% (Purpura et al., 1988; Sclar et al., 1990; Shapley et al., 1981; Derrington and Lennie, 1984).

Perceptually, lesions of the parvocellular layers of the LGN cause a 3- to 4-fold reduction in spatial acuity in monkeys while magnocellular lesions do not affect acuity (Merigan et al., 1991a,b). Luminance and chromatic contrast sensitivities for static gratings of high spatial frequencies are reduced for parvocellular lesions, but not for magnocellular lesions. However, luminance contrast sensitivity for low spatial frequency gratings, modulated at 10 Hz is reduced by both parvocellular and magnocellular lesions.

In conclusion, the retino-cortical parvocellular pathway provides a chromatic representation of the visual world at high spatial but low temporal frequencies, while the magnocellular pathway provides an achromatic representation at low spatial but high temporal frequencies.

Nevertheless, the sensitivities of neurons along both pathways overlap considerably in both the temporal and the spatial domain.

1.2.2 Cortical Processing Pathways

The visual cortex is commonly divided into functionally different regions called cortical areas, which can be distinguished by the response properties of their neurons. There are at least 32 distinct areas involved in visual processing (e.g., Felleman and Van Essen, 1991). Neurons within each area form numerous connections with neurons in the same area, and provide feedback and feed-forward connections to neurons of other cortical areas, often in a reciprocal fashion (e.g., Felleman and Van Essen, 1991; Van Essen and Gallant, 1994). Early visual areas such as V1, V2, and MT have a retinotopic organization, which means that the spatial arrangement of neurons preserves the local topography of the visual field with respect to their cRFs.

The Primary Visual Cortex

The primary visual cortex (area V1, striate cortex) constitutes the first stage of cortical visual processing and receives an organized array of projections from the LGN. Neurons in V1 process information in a localized fashion, generating various representations which are distributed to other, more specialized areas. The response properties of neurons in V1 are substantially different from the center-surround organization of the cRFs of neurons in retina and LGN. Many neurons in V1 show selectivity for the orientation of stimuli (like bars), spatial frequency, ocular dominance and color (e.g., Hubel and Wiesel, 1959). Depending on their response properties, neurons in V1 are commonly classified as simple or complex cells (Hubel and Wiesel, 1962). The cRFs of simple cells can be subdivided into separate antagonistic subregions whose spatial profiles can be approximated by a sine wave, weighted with a Gaussian envelope (Marčelja, 1980; Pollen and Ronner, 1981; De Valois et al., 1982; De Valois and De Valois, 1988). Complex cells, on the other hand, are also orientation selective, but insensitive to the exact position of the stimulus within their cRF (Hubel and Wiesel, 1962). Some simple and complex cells are selective for the direction of stimulus motion (Hubel and Wiesel, 1968). They respond strongly to oriented bars or gratings moving in a specific direction, but only weakly to stimuli moving in the opposite direction.

V1 can be divided into six different layers. M- and P-fibers from the LGN terminate in separate sublamina within layer 4C, 4C α and 4C β , respectively. From there, fibers project to layers 2, 3, and 4B before projecting to higher cortical areas. Layers 2 and 3 can be divided

into a mosaic of small regions called blobs, with dividing areas called inter-blobs. Blob regions, which receive both M- and P-input, are sensitive to color and stimulus contrast, but less to stimulus orientation or motion. Neurons in inter-blob regions which receive mainly P-input are selective for stimulus orientation, but insensitive to color and motion. Neurons in layer 4B, which mainly receive M-input, are selective for the orientation and direction of motion, but not for color (Livingstone and Hubel, 1984, 1988).

Higher Visual Areas - Dorsal and Ventral Pathways

The many visually driven cortical areas are commonly divided into a ventral and a dorsal pathway. The ventral pathway leads from area V1 to the inferior temporal cortical areas, while the dorsal pathway leads from V1 to the posterior parietal cortex (Ungerleider and Mishkin, 1982). Experimental findings in monkeys and humans support the possibility that these two pathways serve different visual functions. The ventral pathway is thought to be involved in the identification of objects (*What-path*), while the dorsal pathway is crucial for the spatio-temporal localization of objects (*Where-path*). Ungerleider and Mishkin (1982) found that monkeys with lesions of the inferotemporal cortex had deficits in the discrimination and recognition of visual patterns, but not in solving distance discrimination tasks. Lesions of the posterior parietal cortex produced impaired performance for the distance discrimination task while retaining the performance during object discrimination learning. Human patients with lesions in the parietal cortex, but with intact temporal cortex, are able to discriminate objects according to their shape, but have difficulties grasping them. Conversely, patients with lesions in the temporal cortex can respond to a stimulus with a grasping action but are not able to discriminate the stimulus according to its shape (Goodale et al., 1991, 1994).

Neurons in the higher temporal cortical visual areas of monkeys have large, translation-invariant RFs and encode shapes and objects in a distributed fashion (Perrett et al., 1982; Desimone et al., 1984; Logothetis et al., 1995; Rolls, 2000; Quiroga et al., 2005). In the parietal lobe neurons are sensitive to the location of stimuli with respect to the animal's head- or eye-position (e.g., Duhamel et al., 1997), often in a multimodal fashion (Andersen et al., 1997; Schlack et al., 2002; Bremmer, 2005). In addition, the dorsal pathway seems to play an important role in the encoding of self-motion (reviews: Duffy, 2000; Bremmer et al., 2000).

Taken together, these findings suggest that the ventral pathway plays a major role in the perceptual identification of objects, while the dorsal pathway mediates the spatio-temporal localization of objects and performs sensorimotor transformations for visually guided ac-

tions (Goodale and Milner, 1992).

1.3 Spatially Inhomogeneous Retino-Cortical Mapping

1.3.1 Physiology and Anatomy

While spatial resolution in the fovea is extremely high, reaching the optical resolution limits of the eye (Snyder and Miller, 1977), spatial resolution declines in an approximately linear fashion with increasing eccentricity (Westheimer, 1979). The neural basis for the decline in spatial resolution with increasing eccentricity lies mainly in the retina. In primates, the density of retinal ganglion cells is highest in the fovea, with about 60,000 cells/mm², and decreases by a factor of more than 1,000 towards the periphery (Wässle et al., 1990). For both M and P ganglion cells, dendritic field sizes increase linearly with eccentricity (Perry et al., 1984; Watanabe and Rodieck, 1989). However, this increase has a steeper slope for M-cells than for P-cells, shown in Figure 1.2. Over a wide range of eccentricities, the RF sizes of M ganglion cells are 2–3 times larger than the RF-sizes of P ganglion cells at the same eccentricity (e.g., De Monasterio and Gouras, 1975; Derrington and Lennie, 1984). In the far periphery this ratio increases to approximately 5 in macaques (Watanabe and Rodieck, 1989) and up to 10 in humans (Dacey and Petersen, 1992). In the fovea, approximately 5-6% of the retinal ganglion cells are of the M-type (Grünert et al., 1993). However, the portion of M-cells reaches values of 20% in the far periphery (Silveira and Perry, 1991). The sampling density, i.e. the number of overlapping RFs of retinal ganglion cells at any given position in the visual field, seems to be relatively constant at about 3-4 for both M- and P-cells (review: Van Essen and Anderson, 1995).

From the retinal ganglion cells to the primary visual cortex there is an additional increase in machinery devoted to the processing of foveal in comparison to peripheral stimuli in monkeys (e.g., Perry and Cowey, 1985; Azzopardi and Cowey, 1996; Adams and Horton, 2003) and humans (Popovic and Sjöstrand, 2001). There is a great emphasis on the representation of central vision, causing nearly a quarter of the striate cortex to be devoted to the processing of the central 2.5 degrees of the visual field (De Valois and De Valois, 1988). The dependence of the spatial RF density of neurons in the primary visual cortex on retinal eccentricity can be quantitatively described by the linear cortical magnification factor M (Daniel and Whitridge, 1961; Van Essen et al., 1984), which is defined as the cortical distance corresponding to one degree of visual angle. M depends strongly on the retinal eccentricity E and can be approximated by

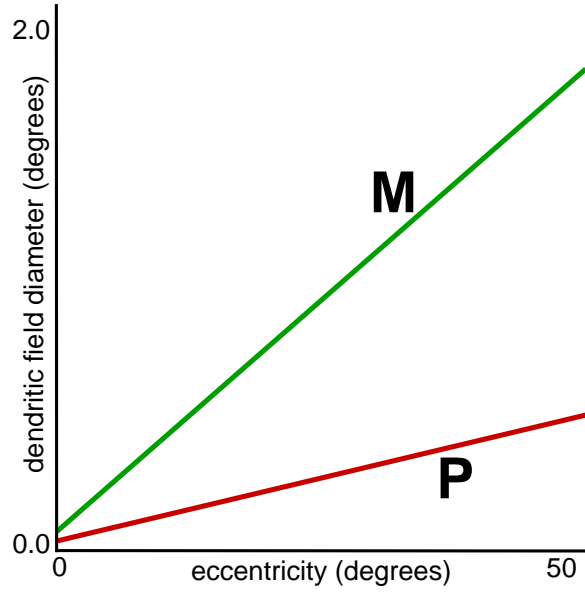


Figure 1.2: CHANGE OF DENDRITIC FIELD SIZES WITH ECCENTRICITY FOR P AND M GANGLION CELLS. Dendritic field sizes of P and M retinal ganglion cells increase linearly with eccentricity, with a steeper slope for M ganglion cells. Modified from Van Essen and Anderson (1995).

$$M(E) = \frac{A}{B + E}, \quad (1.1)$$

where A is a scaling factor and the quotient A/B is the cortical magnification in the fovea ($E = 0$).

The *inverse* cortical magnification factor $M^{-1}(E)$ increases linearly with eccentricity:

$$M^{-1}(E) = \frac{B}{A} + \frac{1}{A}E. \quad (1.2)$$

By integrating $M(E)$ from the fovea to a given retinal eccentricity E , one obtains the corresponding *cortical* eccentricity, or cortical distance from the position of the cortical foveal representation, E_c :

$$E_c(E) = \int_0^E M(e)de = A \ln \left(1 + \frac{E}{B} \right). \quad (1.3)$$

Thus, retinal coordinates are logarithmically mapped to cortical coordinates.

1.3.2 Scale Invariance and Log Polar Transformation

The linear increase in inverse cortical magnification, accompanied by a linear increase in RF-sizes, provides a spatially scale-invariant cortical representation of fixated objects at different distances from the observer (e.g., Schwartz, 1980; Reitboeck and Altmann, 1984; Van Essen et al., 1992). If a fixated object is brought closer to the observer, its retinal image becomes larger, and its outline moves towards the periphery. Cortical magnification is such that the decrease in cortical magnification with increasing eccentricity compensates for this increase in size. Thus, the resolution of extrafoveal object parts is not altered by changes of viewing distance. There is experimental evidence that if a stimulus is scaled according to the inverse cortical magnification factor (a procedure called M-scaling) it becomes equally resolvable across the visual field. Examples include spatial contrast sensitivity and spatial acuity for static and moving sine gratings (Rovamo et al., 1978; Virsu and Rovamo, 1978; Rovamo and Virsu, 1979; Virsu et al., 1982), vernier acuity (Levi et al., 1985), or the detection of coherent motion in stroboscopically moving random-dot patterns (van de Grind et al., 1983). However, M-scaling cannot account for the decreased performance of contour-grouping with increasing eccentricity (e.g., Hess and Dakin, 1997, 1999) or the identification of faces (Makela et al., 2001).

The two-dimensional mapping of retinal coordinates onto the primary visual cortex of monkeys can be approximated by a log-polar transformation. An ideal log-polar transformation, which has originally been suggested by Fischer (1973), has the form

$$w = \log(z), \quad (1.4)$$

where z and w are complex numbers⁵ representing points in retinal and cortical space, respectively. Later, Schwartz (1977, 1980) proposed an extension which provides a better description of the central region of the visual field:

$$w = \log(z + a), \quad (1.5)$$

where the parameter a accounts for deviations of the retino-cortical mapping from an ideal log-polar mapping for small eccentricities.

⁵The logarithm $\log z$ of a complex number z is the set of complex numbers w , for which the equation $e^w = z$ holds. With $r = |z|$ and $\phi = \arg z$, the logarithm of a complex number can be reduced to the real-valued logarithm: $\log z = \log r + i\phi$. Thus, the complex logarithm separates magnitude and phase of a complex number.

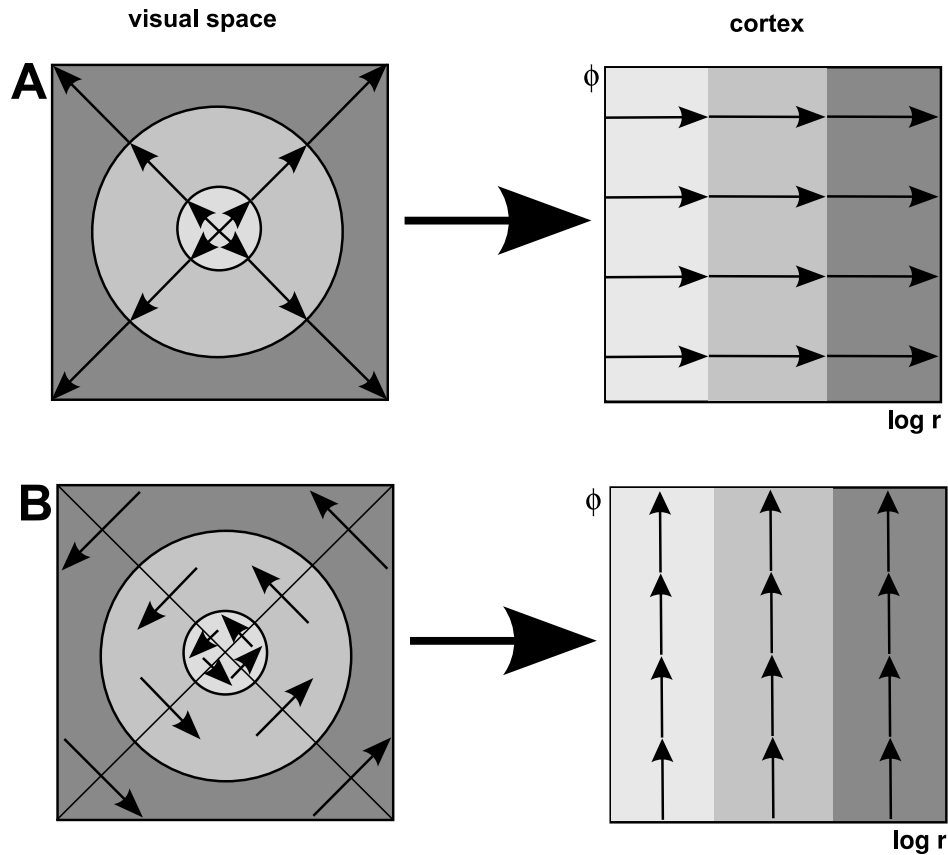


Figure 1.3: LOG-POLAR MAPPING. (A) Retinal scaling of a stimulus corresponds to translations in cortical space, (B) rotation around the direction of gaze corresponds to cortical translations in the perpendicular direction. Modified from Grossberg et al. (1999).

An ideal log-polar transform (Equation 1.4) converts centered scaling and rotation of objects in visual space into translations along perpendicular directions in cortical space (e.g., Schwartz, 1977; Reitboeck and Altmann, 1984) (Figure 1.3). Thus, the spatial cortical activation profile of a fixated object which is scaled or rotated undergoes a translation on the cortical surface while retaining its shape. This means that the amount of information about the extrafoveal parts of an object in the visual field remains roughly constant as it is moved closer or further away from the observer, or is centrally rotated with respect to the direction of gaze.

Several studies have highlighted the possible role of the log-polar mapping of visual space for the processing of form and motion information. It has been proposed that the log-polar mapping may play a role in the scale- and rotation-invariant recognition of visual objects (Schwartz, 1981; Reitboeck and Altmann, 1984). In the model of Reitboeck and Altmann

(1984), the retinal images of scaled and rotated objects are transformed into cortical translations according to the log-polar mapping. These cortical activations are extracted with a translation-invariant mechanism, leading to scale- and rotation-invariant object representations. A recent model employs the log-polar representation of visual space to account for the response properties of neurons in area MSTd with respect to optic flow stimuli generated during self-motion (Grossberg et al., 1999).

1.3.3 Eccentricity-Dependent Projections Between Cortical Areas

There is evidence that inter-areal projections depend on the eccentricity of the corresponding cortical representations (review: Gattass et al., 2005). On the one hand, the foveal, but not the peripheral, portion of V1 projects to area V4 (Zeki, 1969; Nakamura et al., 1993). On the other hand, peripheral V1, but not central V1, projects to area V3A (Zeki, 1980). Additionally V3A receives projections from the peripheral, but not the foveal portion of area MT (Ungerleider and Desimone, 1986). Gattass et al. (1997) found that the peripheral, but not the central field of V2 projects to areas MST, VIP and VTF in the dorsal pathway.

These findings suggest that cortical areas along the ventral pathway, associated with the encoding of object form, receive mainly input from the foveal portion of the visual field. Areas along the dorsal pathway, concerned with the encoding of motion and spatial coordination, predominantly receive input from the peripheral portion of the visual field (Gattass et al., 1990, 1999).

1.4 Self Organization

1.4.1 Role of Input-Driven Self-Organization on Cortical Development

It is generally believed that visual input plays an essential role for many aspects of self-organization in the visual system. Kittens raised in either horizontally or vertically striped environments developed less neurons sensitive to vertically or horizontally oriented stimuli, respectively (Blakemore and Cooper, 1970). Experiments on monocular deprivation (Wiesel and Hubel, 1963) and strabism (Hubel and Wiesel, 1965) demonstrate that missing or conflicting visual information can disturb the development of ocular dominance columns. In a series of experiments on ferrets, projections from the retina were directed to the immature auditory pathway (review: Sur and Leamey, 2001). After some weeks, the auditory cortex exhibited visually driven orientation maps and characteristic horizontal connections between

neurons. This demonstrates the flexibility of input-driven self-organization of cortical connectivity.

Although plasticity is typically greatest within a few weeks or months after birth (e.g., Wiesel and Hubel, 1963; Daw et al., 1992), it is important to note that some input-driven synaptic modifications are not restricted to certain critical periods during early development, allowing cortical sensory maps to be modified continuously by experience: In adult cats, asynchronous visual stimulation of two adjacent retinal regions induced rapid modifications of intracortical connectivity and shifts in the positions of cortical RFs, depending on the temporal interval between the visual stimuli (Fu et al., 2002). A similar stimulation paradigm caused shifts in human spatial perception. Comparable effects were found for the pairing of visual stimuli of two orientations, which caused a shift in the orientation tuning of cortical neurons in cats and a shift in orientation-perception in human subjects (Yao and Dan, 2001). Synchronous visual stimulation of the RF center and a location in the RF's surround can induce a spatial expansion of the RF towards the stimulated surround region in cats (Eysel et al., 1998). In patients with macular degeneration, a loss of central vision, cortical regions normally devoted to the processing of foveal stimuli have been shown to become responsive to peripheral stimuli (Baker et al., 2005).

Taken together, these findings demonstrate convincingly that the initial development of cortical circuits and their later refinement depends critically on the spatio-temporal structure of the visual input, and that certain statistical regularities in the visual environment are reflected in the cortical connectivity.

1.4.2 Synaptic Plasticity

Information transmission between neurons is thought to occur mainly via chemical synapses, whose efficiency can undergo long-term changes under certain conditions. The idea that learning and adaptation in neural systems is due to changes in synaptic connectivity is very old (Cajal, 1894). However, Hebb (1949) was the first to propose a rule based on theoretical considerations, suggesting under which circumstances these changes in synaptic efficiency should occur:

When an axon of a cell A is near enough to excite cell B or repeatedly or consistently takes part in firing it, some growth or metabolic change takes place in one or both cells such that A's efficiency, as one of the cells firing B, is increased.

An important feature in Hebb's formulation is the principle of causality. In order to cause a change in synaptic efficiency, the firing of neuron A must be causally related to the firing

of neuron B. Furthermore, the formulation implicitly underlines the importance of the timing of single spikes in the learning process.

Nevertheless, the principle of causality and the influence of single spikes on synaptic changes were underrepresented for a long time in both experimental and theoretical works. Experimentally it has been shown that synaptic efficiency can be increased by a brief, high-frequency stimulation of the presynaptic axon (Lomo, 1971; Bliss and Lomo, 1973), an effect called long term potentiation (LTP). This effect has been demonstrated in many cortical areas and species and can last for hours or days (review: Bi and Poo, 2001). This stimulation paradigm suggests an underlying correlational rule, relying on the firing rates of pre- and postsynaptic neurons. This can be summarized by the phrase "cells that fire together, wire together" (Zigmond, 1999). Theoretical models employing correlation based Hebbian learning rules can account for many adaptive processes. This includes the formation of topographic maps (e.g., Kohonen, 1989; Sirosh and Miikkulainen, 1997), the extraction of independent component filters from natural images (e.g., Falconbridge et al., 2006), which resemble the spatial filter properties of cortical simple cells, and the self-organization of long-range intra-cortical lateral connections (e.g., Grossberg and Williamson, 2001; Prodhöhl et al., 2003).

The temporal specificity of synaptic modifications has become of greater interest only in the last decade, stimulated by the development of better recording-techniques. An important discovery was the fact that action potentials do not only travel along the axon, but also back-propagate into the neuron's dendrite (Stuart and Sakmann, 1994). A backpropagating action potential which was evoked 10 ms after the onset of the postsynaptic potential induced LTP, while a reversal of the order caused a weakening of the synapse, an effect called long term depression (LTD) (Markram et al., 1997; Magee and Johnston, 1997). Neither action potential nor postsynaptic potential alone was sufficient to evoke synaptic changes. The critical temporal difference of pre- and postsynaptic activation for which LTP or LTD is evoked (time window or learning window) is about 50 ms (e.g., Bi and Poo, 1998; Zhang et al., 1998; Feldman, 2000; Froemke and Dan, 2002). Recent studies suggest that learning does not only depend on the temporal interval between pre- and post-synaptic activity, but also on the history of the pre- and postsynaptic activation (e.g., Sjöström et al., 2001; Froemke and Dan, 2002), and the location of the synapse on the dendritic tree (Saudargiene et al., 2004; Froemke et al., 2005).

1.5 Thesis Outline

The thesis consists of three self-contained chapters, each endowed with separate introduction and discussion intended for readers with an elementary background in neuroscience. In order to preserve the self-containedness of the chapters, parts of the description of the used model-neurons in Chapter 2 and Chapter 4 are identical.

- In *Chapter 2* we identify visual situations to which the spatially inhomogeneous retino-cortical mapping is well-adapted. We demonstrate that cortical magnification is well adapted to self-motion of an observer walking in the direction of gaze, under the assumption that the retino-cortical mapping transforms an inhomogeneous retinal velocity distribution into a homogeneous cortical velocity distribution. Applying flow fields similar to those during self-motion along the direction of gaze to train a simple network of pulse coding neurons with Hebbian learning, we demonstrate that the distribution of learned RFs is consistent with primate cortical magnification.
- With increasing eccentricity, the RFs of neurons in V1 become larger and their preferred spatial frequency shifts to lower values. In *Chapter 3* we investigate how the spatial statistics of real-world scenes change with respect to the spatial filter properties of cortical neurons at different eccentricities. We show that the collinear correlations between filters of the same orientation and wavelength are not scale-invariant, which provides evidence against a homogeneous lateral cortical connectivity across the visual field with respect to the spatial statistics of natural scenes.
- In *Chapter 4* we study the influence of stimulus velocity and the conduction velocity of lateral connections on the self-organization of lateral connectivity due to Hebbian learning mechanisms. We show that stimulus velocities much lower than the conduction velocity of the lateral connections favor the development of lateral connections which are well adapted to the spatial structure of the visual input. High stimulus velocities lead to lateral connections which support the coding of the spatio-temporal structure of the visual input. We discuss possible implications for the self-organization within cortical M- and P-dominated visual pathways and for the self-organization of lateral connections at different positions in the visual field.

Chapter 2

Inhomogeneous Retino-Cortical Mapping and Self-Motion

Inhomogeneous Retino-Cortical Mapping is Supported and Stabilized with Correlation-Learning During Self-Motion

2.1 Abstract

In primates, the area of primary visual cortex representing a fixed area of visual space decreases with increasing eccentricity. We identify visual situations to which this inhomogeneous retino-cortical mapping is well adapted and study their relevance during natural vision and development. We assume that cortical activations, caused by stationary objects during self-motion along the direction of gaze, travel on average with constant speed across the cortical surface, independent of retinal eccentricity. This is the case if the distribution of objects corresponds to an ellipsoid with the observer in its center. We apply the resulting flow field to train a simple network of pulse coding neurons with Hebbian learning and demonstrate that the density of learned receptive field centers is in close agreement with primate cortical magnification. In addition, the model reproduces the increase of receptive field size and the decrease of receptive field peak sensitivity with increasing eccentricity. Our results suggest that self-motion may have played an important role in the evolution of the visual system and that cortical magnification can be refined and stabilized by Hebbian learning mechanisms in ontogenesis under natural viewing conditions.

Major parts of this Chapter have been accepted for publication in a special issue of BioSystems (Proceedings on Neural Coding 2005, in press).

2.2 Introduction

The spatial resolution of the representation of the visual field in primate primary visual cortex decreases strongly with increasing eccentricity (e.g., Daniel and Whitteridge, 1961) in parallel with the increase of receptive field (RF) sizes of retinal, thalamic and cortical neurons (Hubel and Wiesel, 1974; Dow et al., 1981; Croner and Kaplan, 1995; Xu et al., 2002). A large number of cortical neurons process stimuli near the fovea, while relatively few represent the periphery. This inhomogeneous mapping keeps the number of retino-cortical connections relatively low, but requires eye movements over larger areas of the visual field for perception at high spatial resolution. The inhomogeneous retino-cortical mapping is to a large part determined genetically, but development of theories on its underlying principles and its shaping during ontogeny may help to understand fundamental coding mechanisms in the visual system. We investigate whether visual situations exist to which the inhomogeneous retino-cortical mapping is well adapted and ask how relevant these situations are during natural vision and development. Because vision plays an important role during navigation, visual processing should be well adapted to self-motion. Thus, it is reasonable to hypothesize that self-motion plays a role in determining retino-cortical mapping and magnification. Virsu and Hari (1996) showed that cortical magnification can be estimated by linear self-motion in a world, idealized as a sphere, under the assumption that cortical activations, caused by stationary objects, travel at constant cortical speed, independent of eccentricity. We take the complementary approach and investigate which average geometrical arrangement of static objects in the environment is best suited to predict cortical magnification from flow fields arising during self-motion along the direction of gaze. Furthermore, we demonstrate that an RF distribution, whose density is consistent with cortical magnification, can be learned in a basic network model of spiking neurons by training with flow fields similar to those experienced during self-motion.

2.3 Relating Cortical Magnification to Self-Motion

The dependence of RF density of neurons in primary visual cortex on retinal eccentricity can be quantitatively described by the linear cortical magnification factor M (e.g., Daniel and Whitteridge, 1961; Van Essen et al., 1984), which is defined as the cortical distance corresponding to one degree of visual angle. M depends on the retinal eccentricity E and can be approximated as

$$M(E) = \frac{C_2}{C_1 + E}, \quad (2.1)$$

where C_2 is a scaling factor and the quotient C_2/C_1 is the cortical magnification in the fovea ($E = 0$).

In the following we make the assumption that cortical magnification has the effect that during self motion along the direction of gaze, representations of static objects shift on average the same cortical distance, independent of eccentricity. This would have the important advantage that the neuronal modules, concerned with the processing of self-motion, can be identical in their spatial and temporal properties across the representation of the whole visual field.

For convenience, we introduce the inverse cortical magnification factor M^{-1} , which has the form

$$M^{-1}(E) = \frac{C_1}{C_2} + \frac{1}{C_2}E. \quad (2.2)$$

M^{-1} specifies the change in visual angle that corresponds to a fixed cortical distance. Thus, cortical activations travel at constant speed, if the angular velocity $\omega(E)$ of the corresponding retinal activations is proportional to the inverse cortical magnification factor $M^{-1}(E)$ for all eccentricities:

$$\omega(E) \propto M^{-1}(E). \quad (2.3)$$

In the following, we neglect the term C_1 of the cortical magnification factor ($C_1 \ll E$), which cannot be explained by self-motion along the direction of gaze (Virsu and Hari, 1996), because a finite C_1 corresponds to non-zero retinal velocities in the fovea. One possibility to explain a non-vanishing value of C_1 would be to assume velocity jitter across the visual field, due to eye and body-motion. However, we will show (Section 2.4) that even a vanishing retinal velocity in the fovea can lead to a magnification factor with $C_1 \neq 0$, due to the finite size of the retinal RFs.

According to the experimentally estimated linear inverse cortical magnification factor (Equation 2.2, for $C_1 \ll E$), angular velocity increases linearly with eccentricity for the condition of constant velocity across the visual cortical representation:

$$\omega(E) \propto E. \quad (2.4)$$

In the next step, we determine the geometrical arrangement of objects surrounding an observer which leads to angular velocities increasing linearly with eccentricity. The retinal speed of objects depends on their distance, their eccentricity, and the velocity of self-motion.

Therefore, we have to derive a mathematical expression for the angular velocity of an object at a given position in visual space during self motion of an observer with velocity v . We assume rotational symmetry around the axis of fixation, which allows us to solve the problem in the horizontal plane. We choose a coordinate system that originates in the observer's eye, with positive y -direction in the direction of gaze. The distance r of an object in the horizontal plane at position $P = (x, y)$ from the observer is

$$r = \sqrt{x^2 + y^2}, \quad (2.5)$$

and its retinal eccentricity is

$$E = \arctan \frac{x}{y}. \quad (2.6)$$

To obtain the angular velocity $\omega(E)$ of the object we differentiate E with respect to t , using the derivative of the arcus tangens

$$\frac{d}{dx} \arctan x = \frac{1}{1 + x^2}, \quad (2.7)$$

which yields

$$\omega(E) = \frac{1}{1 + \left(\frac{x}{y}\right)^2} \cdot \frac{\dot{x}y - \dot{y}x}{y^2} \quad (2.8)$$

$$= \frac{\dot{x}y - \dot{y}x}{r^2}. \quad (2.9)$$

We examine the case of the observer moving with velocity v in the positive y -direction. The coordinates of an object which is initially ($t = 0$) at position $P = (x_0, y_0)$ relative to the observer's eye, change according to

$$y(t) = y_0 - vt, \quad (2.10)$$

$$x(t) = x_0 = \text{const.} \quad (2.11)$$

With Equation 2.9, and $x_0 = r \sin E$ we obtain

$$\omega(E) = \frac{v \sin(E)}{r}. \quad (2.12)$$

This is the general expression for the angular velocity of an object at eccentricity E with distance r from the observer's eye.

According to our initial assumption (Equation 2.4), for a fixed velocity v of the observer, angular velocity increases linearly with increasing eccentricity:

$$E \propto \frac{\sin(E)}{r}. \quad (2.13)$$

Thus, we obtain

$$r \propto \frac{\sin(E)}{E}. \quad (2.14)$$

The solid curve in Figure 2.1 shows the arrangement of objects according to this theoretical relationship.

In the following we examine two simple geometrical arrangements of objects, straight line and ellipse, to test how well they match the required linear increase of angular velocity with eccentricity.

Objects on a Straight Line. For objects lying on a straight line perpendicular to the movement direction of the observer, with distance y_{\perp} , we obtain the following dependence of an object's $P = (x, y_{\perp})$ distance on its eccentricity:

$$r = \frac{y_{\perp}}{\cos(E)}. \quad (2.15)$$

Thus, angular velocity increases according to

$$\omega(E) = \frac{v \sin(E)}{r} = \frac{v}{y_{\perp}} \sin(E) \cos(E). \quad (2.16)$$

Objects on an Ellipse. The representation of an ellipse in polar coordinates is

$$r = \frac{b}{\sqrt{1 - \epsilon^2 \cos^2(E)}}, \quad (2.17)$$

with ϵ as the numerical eccentricity of the ellipse, defined as

$$\epsilon = \frac{\sqrt{a^2 - b^2}}{a}. \quad (2.18)$$

a and b being semimajor and semiminor axis, respectively. For the angular velocity we obtain

$$\omega(E) = \frac{v}{b} \sin(E) \sqrt{1 - \epsilon^2 \cos^2(E)}. \quad (2.19)$$

The special case of objects on a circle ($\epsilon = 0$) yields

$$\omega(E) \propto \sin(E), \quad (2.20)$$

which is identical to the result of Virsu and Hari (1996).

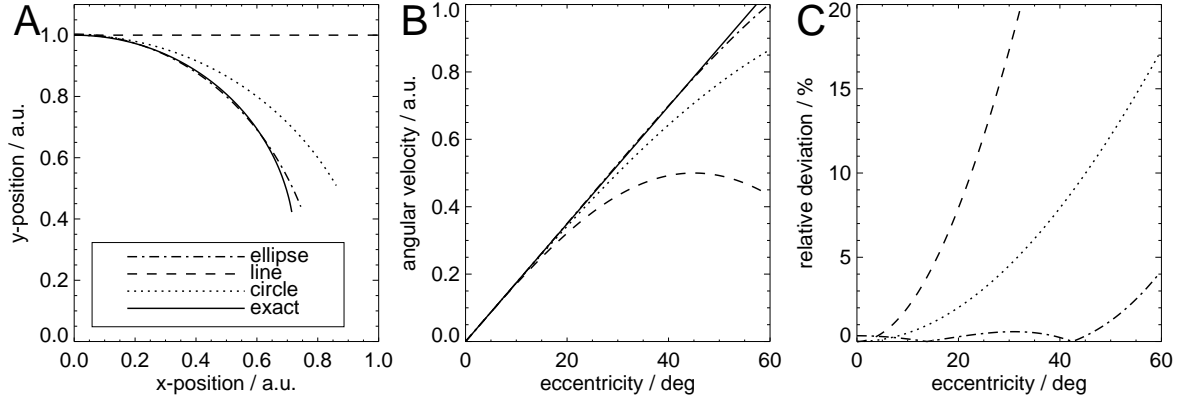


Figure 2.1: DIFFERENT GEOMETRIES OF OBJECT LOCATIONS AND THEIR RESULTING INSTANTANEOUS, ANGULAR VELOCITY DISTRIBUTIONS. (A) The four examined geometries (exact, circle, line, and ellipse). The observer is located at (0,0), facing in positive y -direction. The ellipse corresponds to a numerical eccentricity of $\epsilon \approx 0.56$, obtained by least squares fitting. (B) The corresponding velocity distributions. The increase in angular velocity is similar for the four examined object-geometries at small eccentricities, but diverges for larger eccentricities. (C) The relative deviations of the predicted velocities of the examined geometries (circle, line, and ellipse) from a linear increase in velocity.

Figure 2.1 illustrates the different object geometries and their corresponding velocity-distributions. Figure 2.1C shows that the resulting velocity distributions for the different geometries are similar for small eccentricities, but diverge for larger eccentricities. The velocity distribution of objects on a straight line increases nearly linearly for small eccentricities, but diverges for larger eccentricities. Points on a circle are a closer match, but for larger eccentricities these velocities also diverge from the predicted linear increase. The elliptic geometry with slightly elongated axis along the viewing direction yields the closest match to the linearly increasing magnification factor for eccentricities larger than $\approx 7^\circ$.

2.4 Model Simulations

Here we demonstrate that a minimal network model with spiking neurons and other biologically plausible properties can learn an RF distribution whose density is consistent with the experimental cortical magnification factor, if trained with flow fields similar to those present during self motion along the direction of gaze.

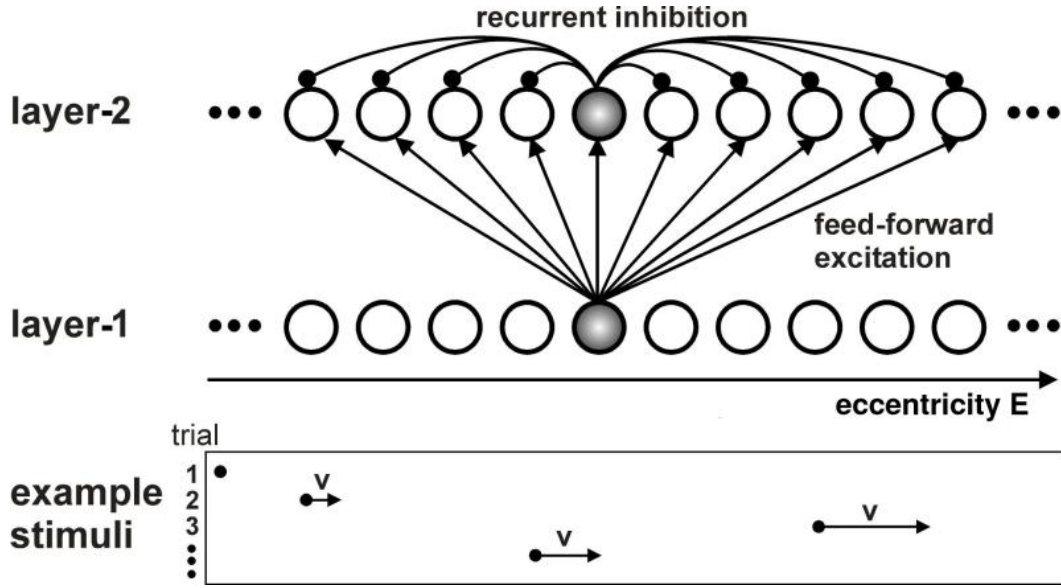


Figure 2.2: MODEL ARCHITECTURE AND SAMPLE INPUT STIMULI. The network consists of two layers of spiking neurons. The connections between layer-1 and layer-2 are subject to Hebbian learning. Neurons in layer-2 interact via global inhibitory connections. For clarity, only projections from a single neuron in each layer are plotted. Input stimuli for the layer-1 neurons are small moving dots with a lifetime of 100 ms and velocities that increase linearly with eccentricity.

2.4.1 Network Model and Input Stimuli

Network Architecture

The model (Figure 2.2) consists of two one-dimensional layers of pulse coding neurons (Eckhorn et al., 1990). Neurons in the first layer are directly driven by the visual input. They have retinotopically arranged, equally spaced RFs, i.e., each neuron is sensitive to stimuli at a given retinal eccentricity. This choice is not crucial for the results. However, equally spaced RFs of layer 1 neurons allow us to conveniently assess the learned RFs of layer-2 neurons in terms of the matrix of synaptic connection strengths from layer-1 to layer-2.

Layer-1 consists of 80 neurons, while layer-2 consists of 30 neurons. The connections between the first and the second layer represent the transformation between retinal surface and primary visual cortex. They are adapted during learning according to a temporal Hebbian learning rule. Every neuron in the first layer can form connections with every neuron in the second layer. Neurons within the second layer inhibit each other mutually (connection strength w^I , Table 2.1). This inhibitory competition prevents learned RFs of the layer-2

neurons from overlapping substantially. The direct inhibitory interaction between layer-2 neurons was chosen for computational convenience, ignoring the fact that cortical neurons inhibit each other via inhibitory interneurons. However, the exact form of competitive interactions between layer-2 neurons is not crucial for the functioning of the model.

Model Neurons

We used pulse coding neurons with realistic synaptic potentials and an adaptive spike encoder with dynamic threshold (Eckhorn et al., 1990). The input stage of a neuron i consists of synapses $S_{ij}(t)$ to presynaptic neurons j , which have a synaptic connection strength w_{ij} and an impulse response $h(t, \tau)$:

$$S_{ij}(t) = w_{ij}^S I_j(t) * h(t, \tau_S), \quad (2.21)$$

where $*$ is the convolution operator, I_j is the spike-output of the presynaptic neuron j . The synaptic response $h(t, \tau)$ was modelled by a leaky integrator:

$$h(t, \tau) = \exp(-t/\tau) H(t), \quad (2.22)$$

where $H(t)$ denotes the Heaviside function:

$$H(t) = \begin{cases} 0 & t < 0 \\ 1 & t \geq 0 \end{cases}. \quad (2.23)$$

Thus, each connection performs an exponentially decaying summation of signals from presynaptic neurons. For layer-1 neurons, presynaptic signals correspond to the visual input.

Excitatory and inhibitory synapses have different time constants, τ_E and τ_I , respectively. Although the exact choice of the time constants is not crucial for the functioning of the network, a longer inhibitory time constant τ_I leads to better competition between layer-2 neurons because the longer integration time allows for a more robust estimation of the activity within layer-2.

Thus, the resulting membrane potential of neuron i , which drives the spike encoder, is

$$M_i(t) = \sum_j F_{ij}(t) - \sum_j I_{ij}(t). \quad (2.24)$$

In the spike encoder, the membrane potential $M_i(t)$ is compared to a dynamic threshold $\Theta_i(t)$. If $M_i(t)$ exceeds $\Theta_i(t)$, a spike is generated:

$$O_i(t) = H(M_i(t) - \Theta_i(t)). \quad (2.25)$$

The spike threshold has both a dynamic component, which is modelled as the impulse response of two leaky integrators, and a static component Θ_0 :

$$\Theta_i(t) = O_i(t) * ((V_{\Theta_a} \exp(-t/\tau_{\Theta_a}) + V_{\Theta_r} \exp(-t/\tau_{\Theta_r})) H(t)) + \Theta_0. \quad (2.26)$$

One leaky integrator $(V_{\Theta_r}, \tau_{\Theta_r})$ models the neuron's refractory period with a short time constant, the other $(V_{\Theta_a}, \tau_{\Theta_a})$ accounts for spike rate adaptation. In our model, only layer-2 neurons adapt ($V_{\Theta_a} \neq 0$).

Learning Rule

Changes in synaptic connection strengths depend on the relative timing of pre- and postsynaptic spikes. Each spike initiates a synaptic learning potential in the corresponding neuron:

$$L_i(t) = O_i(t) * (\exp(-t/\tau_L) H(t)). \quad (2.27)$$

The change in connection strength between a postsynaptic neuron i and a presynaptic neuron j depends on the product of the corresponding learning potentials:

$$\Delta w_{ij}(t) = L_i(t) L_j(t) - \delta_{\text{decay}}, \quad (2.28)$$

$$w_{ij}(t) = w_{ij}(t-1) + \Delta w_{ij}(t). \quad (2.29)$$

The term δ_{decay} causes all synaptic connection strengths to decline by a small amount in every time step. This causes the total synaptic connection strength of neurons which are inactive for a long time to drop to zero.

If the total connection strength to a postsynaptic neuron i is greater or equal than a maximum value A_{norm} , every synaptic weight to this neuron is divided by a common factor, so that the total connection strength is equal to A_{norm} . Thus, the total connection strength to a postsynaptic neuron i is always less than or equal to A_{norm} :

$$\sum_j w_{ij} \leq A_{\text{norm}}. \quad (2.30)$$

All network parameters are summarized in Table 2.1.

| layer-1 Parameters | | | |
|-------------------------|--------------------|-------------------|-------|
| τ_E | 1 ms | | |
| Θ_0 | 1.0 | | |
| τ_{Θ_r} | 2 ms | V_{Θ_r} | 2 |
| τ_{Θ_a} | 0 ms | V_{Θ_a} | 0 |
| layer-2 Parameters | | | |
| τ_E | 5 ms | τ_I | 20 ms |
| Θ_0 | 1.0 | w^I | 3.0 |
| τ_{Θ_r} | 20 ms | V_{Θ_r} | 2 |
| τ_{Θ_a} | 50 ms | V_{Θ_a} | 0.3 |
| Learning Parameters | | | |
| τ_L | 20 ms | V_L | 0.015 |
| δ_{decay} | 1×10^{-7} | A_{norm} | 10.0 |

Table 2.1: Network parameters

Input Stimuli

Input stimuli were one pixel wide dots with a movement direction towards the periphery. Stimulation phases (100 ms) were followed by brief pauses (20 ms) after which a new random stimulus position is chosen.

In the *main simulation* velocities v increased linearly with eccentricity E ($v(E) \propto E$), with a maximum value of $v = 0.25$ pixels per millisecond in the periphery (Figure 2.3).

Additionally, we performed two *supplemental simulations* to further investigate the influence of stimulus velocity on the properties of the learned RFs. First, we wanted to rule out the possibility that the learned inhomogeneous distribution of RF positions and sizes is mainly determined by the asymmetry in movement direction towards the periphery and not by the linear increase in velocity. Therefore, in an additional simulation, stimulus velocities were constant across the whole visual field ($v = 0.05$ px/ms).

Second, we wanted to account for the fact that an organism experiences a wide range of retinal velocities at each eccentricity due to different velocities of self-motion and different distances of objects in the environment. A realistic, eccentricity-dependent velocity distribution of static objects during self-motion along the direction of gaze would depend on the distribution of movement velocities during self-motion, the spatial distribution of objects in the environment, and their sizes, in order to account for possible occlusions. Furthermore, the velocity of self-motion probably depends on the distances of objects in front of the ob-

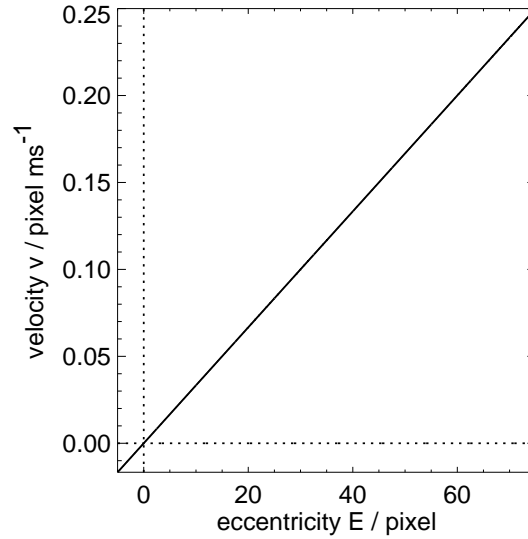


Figure 2.3: DEPENDENCE OF STIMULUS VELOCITY ON ECCENTRICITY. In the main simulation, stimulus velocity increases linearly with eccentricity. To avoid boundary effects, the network-fovea was shifted five pixels to the right.

server. For simplicity, we assumed that the distribution of velocities has the same shape at each position within the visual field, but is scaled linearly with eccentricity. For each stimulus presentation, a random velocity scaling factor S was chosen from a rectified Gaussian distribution centered at 0 (prior to rectification). Stimulus velocities were computed according to $v(E) = cSE$. The constant c was manually chosen to lead to learned RFs similar in size to RF sizes in the main simulation. Comparable results were obtained with different velocity distributions (e.g., uniform or power-law distributions).

In every time step ($\Delta t = 1$ ms), independent Gaussian white noise (GWN, $\sigma_N = 0.25$) was added to all excitatory synapses of layer-1 and layer-2.

To avoid boundary effects, the model fovea was shifted five pixels to the right. Thus, the 80 layer-1 neurons correspond to eccentricities from -5 to 74.

Analysis

After learning, we examined the connection matrix between layer-1 and layer-2 neurons. For convenience we refer to the connection strengths from layer-1 to a single layer-2 neuron as the *RF* of the corresponding layer-2 neuron. This neglects the nonlinear response properties of both layer-1 and layer-2 neurons, which, however, is not crucial for the current analysis.

For a given layer-2 neuron, its *RF center position* or eccentricity is defined as the eccentricity of the layer-1 neuron with the largest connection strength to this neuron. The *RF peak amplitude* or *peak sensitivity* of a layer-2 neuron is defined as the connection strength in the center of the RF. *RF size* of a layer-2 neuron is the number of layer-1 neurons after which connection strength is less than $1/e$ of the RF peak amplitude, where e is Euler's constant. For the fits in Figure 2.6, only RFs with sizes greater than 2 pixels were incorporated.

The *model magnification factor* was assessed by computing a histogram of the positions of the RF centers. The width of one bin in the histogram was chosen to be proportional to the RF size at the bin's center position. To avoid boundary effects, only neurons with RF center positions greater than or equal to 0 and less than 65 were considered in the analysis. Layer-2 neurons which had a maximum connection strength less than 0.01 after learning, were pruned and not considered in the analysis.

2.4.2 Results

Main Simulation

Receptive Field Distribution after Learning. Figure 2.4A shows the matrix of connection strengths from the first to the second layer after learning. RFs at small eccentricities are small with high peak amplitudes, RFs at large eccentricities are large with low peak amplitudes. This is a consequence of the spatial stimulus speed distribution. If a layer-2 neuron is activated, the connections from the layer-1 neurons which were activated before and those that are activated thereafter are strengthened. For fast moving stimuli, more layer-1 neurons are active in the near past and future than for slowly moving stimuli. Due to the additional constraint that the total presynaptic connection strength is less than or equal to a fixed value, RF peak amplitudes decrease with increasing RF sizes (compare Figure 2.5), with each RF having the maximum total presynaptic connection strength.

Figure 2.4B is computed from Figure 2.4A by sorting the RFs according to their center positions. More neurons have RF centers at small than at large eccentricities. This is due to the strong all-to-all inhibition between layer-2 neurons, which prevents the RFs of neighboring neurons from overlapping substantially. Consequently, only few neurons respond to a stimulus at a given position. This is further demonstrated in Figure 2.5, which shows the corresponding RF profiles. RFs are slightly asymmetric, as a result of the linearly increasing velocity and the relatively small network size.

Receptive Field Size Increases Linearly with Eccentricity. Figure 2.6A shows the RF size of the layer-2 neurons as a function of eccentricity. RF size increases linearly with

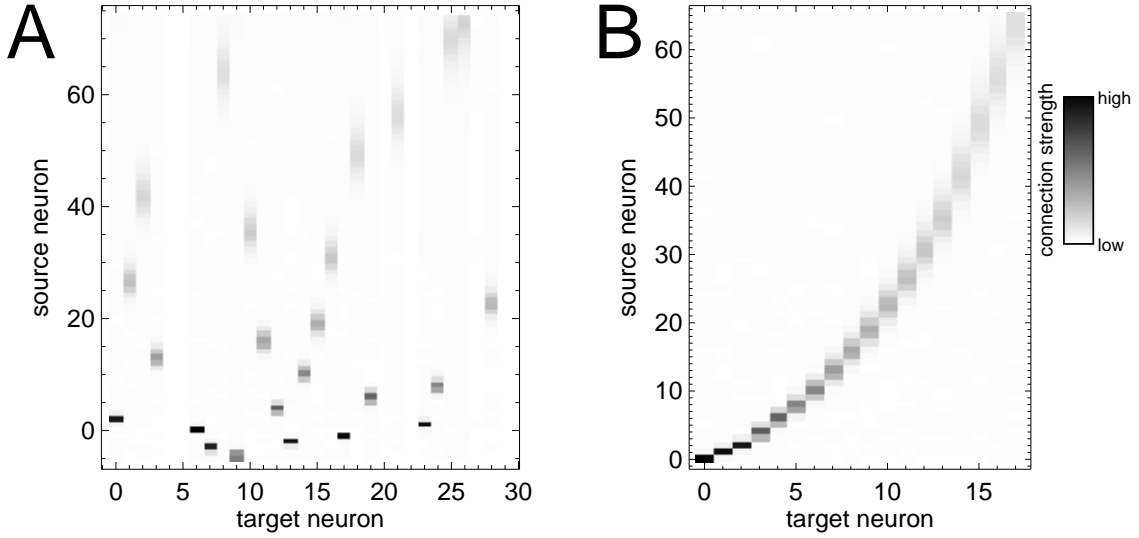


Figure 2.4: CONNECTION STRENGTHS FROM LAYER-1 TO LAYER-2 AFTER LEARNING. (A) Connection strengths from each layer-1 neuron (source) to every layer-2 neuron (target) after learning. Neurons with RFs at small eccentricities have small RFs with high center sensitivities while neurons with RFs at large eccentricities have larger RFs with lower center sensitivities. The large overlap of RFs visible at the top of the diagram is due to boundary effects and is not considered in the analysis. (B) RFs of layer-2 neurons, sorted according to the position of their RF centers. Only layer-2 neurons with RF centers at positions greater or equal than 0 and less than 65 and with maximum synaptic connection strengths greater than 0.01 are included (see Section 2.4.1).

increasing eccentricity as a consequence of the linearly increasing stimulus velocity.

Receptive Field Peak Amplitude Depends on Receptive Field Size. As can be seen in Figure 2.6B, RF peak amplitude A decreases exponentially with RF size r . The regression line has the form

$$A \propto r^{-c}, \quad (2.31)$$

with c close to one (here: $c \approx 0.97$), due to the normalization term in the learning rule, which ensures that the total connection strength is kept constant.

Magnification Factor Declines with Increasing Eccentricity. The model magnification factor M and inverse magnification factor M^{-1} are shown in Figure 2.7A,B. Qualitatively, the curves are similar to the empirical relationship (Equation 2.1). The non-zero value of M^{-1} in the fovea is a consequence of the strong inhibitory competition between layer-2 neurons, which prevents RFs of different neurons to overlap substantially.

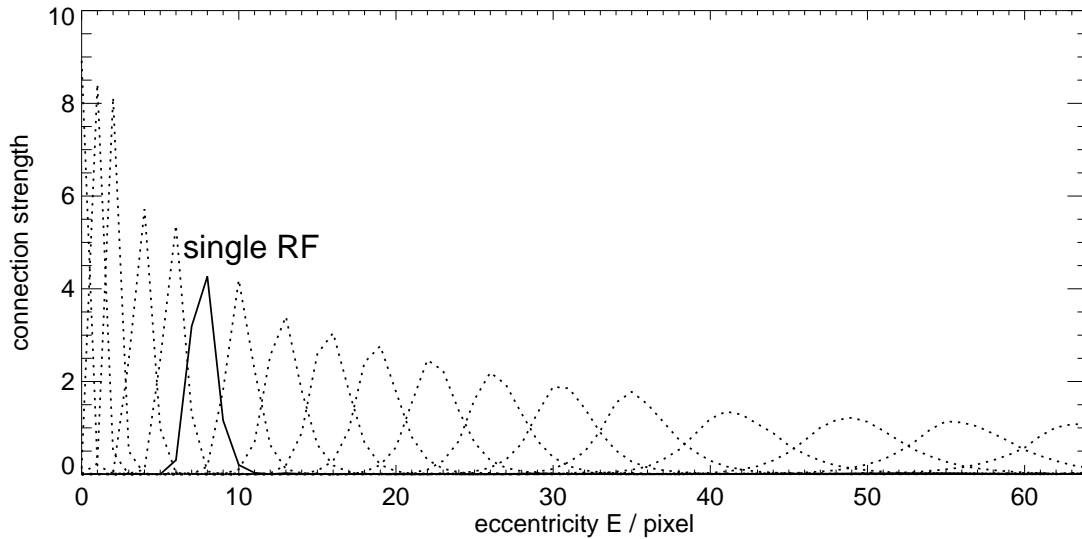


Figure 2.5: RF PROFILES OF LAYER-2 NEURONS FOR A SINGLE SIMULATION. Plotted are the connection strengths for every layer-2 neuron as a function of the corresponding layer-1 neurons (compare Figure 2.4). Note the increasing RF size and the decreasing center sensitivity with increasing eccentricity of the RF center.

Supplemental Simulations

Constant Stimulus Velocity Across the Whole Visual Field. In this simulation, stimulus velocity was constant across the whole visual field ($v = 0.05$ px/ms). Figures 2.8 and 2.9 show the distribution and the profiles of the learned RFs. Adjacent RFs have constant distances across the whole visual field and RF sizes do not depend on eccentricity. Thus, the inhomogeneous representation of the visual field in the main simulation is due to the increase in velocity with increasing eccentricity, and not a consequence of the asymmetry in stimulus movement direction.

Random Stimulus Velocities, Scaled Linearly with Eccentricity. The next simulation demonstrates that qualitatively similar results to those of the main simulation were obtained if stimulus velocity was not fixed for any given eccentricity, but was taken from a Gaussian distribution of velocities whose mean was increasing linearly with eccentricity (compare Section 2.4.1 for details).

Figures 2.10 and 2.11 show the RF structure after learning with random velocities. The results are comparable to the results from the main simulation. RF sizes increase with increasing eccentricity and magnification declines. However, learning took longer until a stable

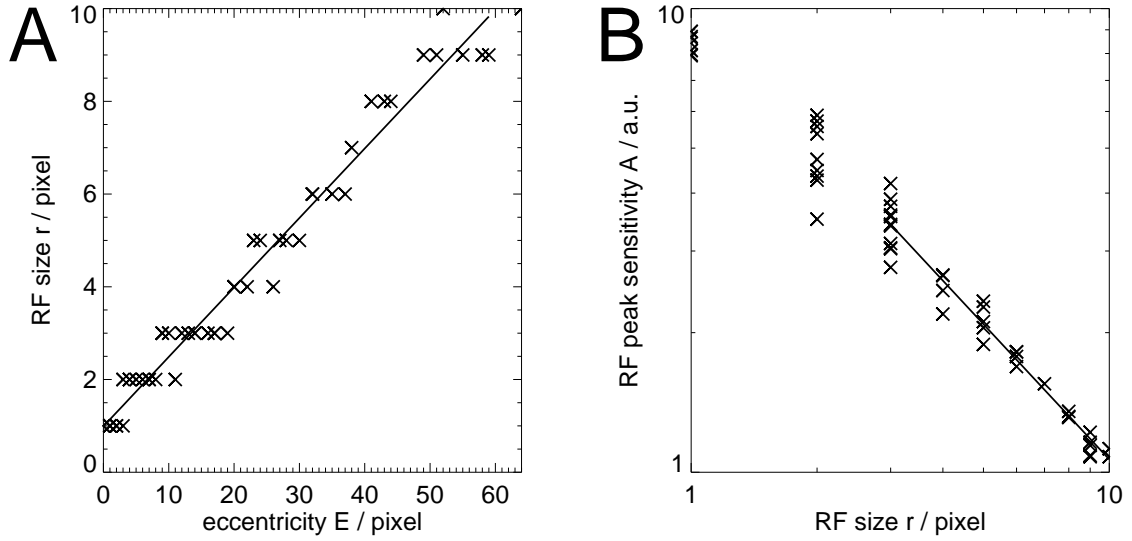


Figure 2.6: RF SIZE AND PEAK AMPLITUDE DEPEND ON ECCENTRICITY (POOLED DATA FROM $N = 3$ SIMULATIONS). (A) RF size r of all layer-2 neurons as a function of the eccentricity E . RF sizes increase linearly with eccentricity (least square fit: $r = 1.0 + 0.15E$). (B) Double-logarithmic plot of RF peak amplitude A as function of RF size r (least square fit: $A = 9.92r^{-0.97}$).

distributions of RF positions was obtained, and RFs are more rugged than in the case of the main simulation (Figures 2.4 and 2.5). The latter could be overcome by reducing the parameter V_L of the Hebbian learning rule, which determines the amplitude of changes in synaptic weights.

2.5 Discussion

2.5.1 Summary of Results

Our results demonstrate that cortical magnification is well adapted to represent flow fields generated during self-motion of an observer walking in the direction of gaze, if the distribution of stationary objects in the environment corresponds to an ellipsoid with the observer in its center. Additionally, a distribution of RF centers whose density is in qualitative agreement with primate cortical magnification (Dow et al., 1981; Van Essen et al., 1984; Adams and Horton, 2003) can be learned in a biologically plausible network model with Hebbian learning. The sizes of the learned RFs increase with increasing eccentricity while peak sensi-

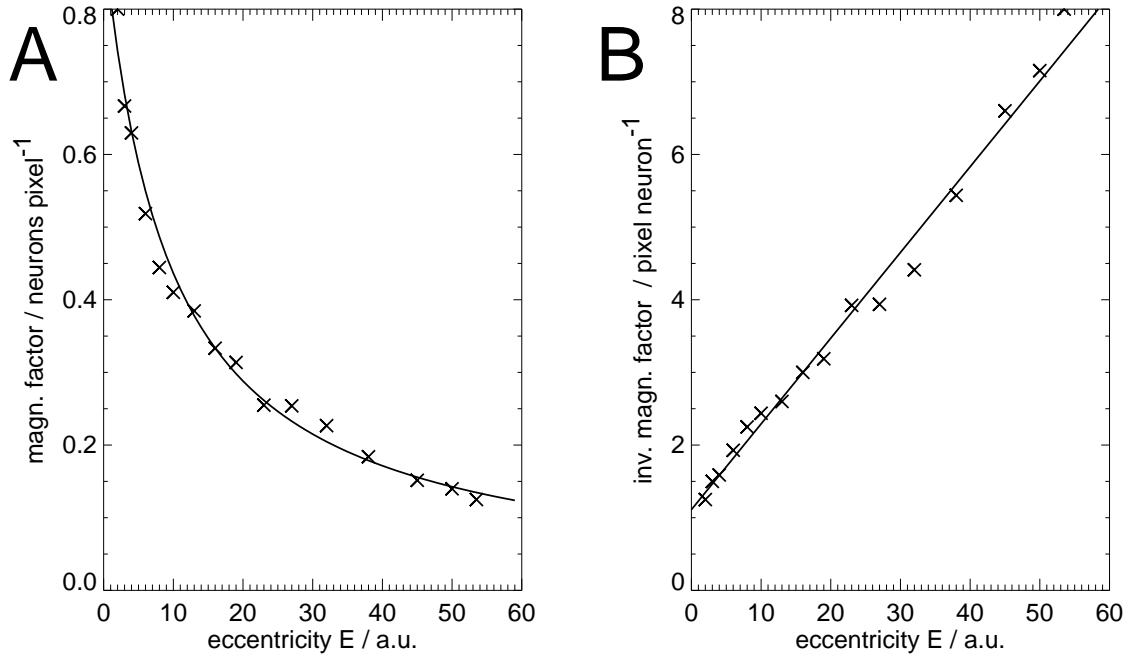


Figure 2.7: MAGNIFICATION FACTOR DERIVED FROM MODEL SIMULATIONS (POOLED DATA FROM $N = 3$ SIMULATIONS). (A) Magnification factor, computed from the RF centers of the layer-2 neurons. (B) Inverse magnification factor. The solid lines in (A) and (B) show the result of least squares fitting inverse cortical magnification ($M^{-1} = 1.11 + 0.12E$, with eccentricity E).

tivities decrease. Our results support the view that self-motion may have played an important role in the evolution of the visual system (Virsu and Hari, 1996).

Although in real visual systems the inhomogeneous retino-cortical mapping is to a high degree determined genetically, it has been shown that even in the adult brain changes in cortical organization can occur, for example in monkey (e.g., Heinen and Skavenski, 1991) and human (e.g., Baker et al., 2005). Thus, the mechanisms presented here may play a role in refining and stabilizing cortical magnification under natural viewing conditions.

2.5.2 Relating Optical Flow to Cortical Magnification

Virsu and Hari (1996) estimated the cortical magnification factor from linear self-motion of an observer in a world in which objects move on a sphere with the observer in its center. In contrast, our results show that the linear increase in inverse cortical magnification with eccentricity can be more accurately deduced from a flow field generated by a distribution

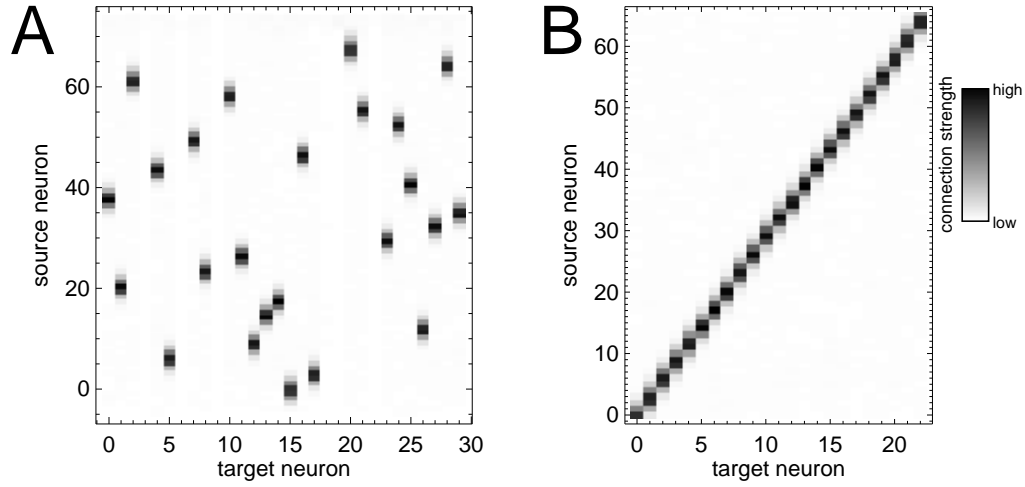


Figure 2.8: CONNECTION STRENGTHS FROM LAYER-1 TO LAYER-2 AFTER LEARNING WITH STIMULI OF CONSTANT VELOCITY ACROSS THE WHOLE VISUAL FIELD. (A) Connection strengths from each layer-1 neuron (source) to every layer-2 neuron (target) after learning. (B) RFs of layer-2 neurons, sorted according to the position of their RF centers. Only layer-2 neurons with RF centers at positions greater or equal than 0 and less than 65 and with maximum synaptic connection strength exceeding 0.01 are included (see Section 2.4.1). For constant stimulus velocity across the whole visual field, RF size and density do not depend on the position within the visual field.

of objects whose distances from the observer correspond to an ellipsoid (with a ratio of semiminor to semimajor axis of ≈ 0.8). The interpretation of our findings is as follows. If the arrangement of objects in the environment was independent of the direction of self-motion of an observer, the average distances of objects from the observer would correspond to a sphere. It is quite plausible, though, that during self-motion, an observer tends to keep larger distances to objects in the direction of motion – for example, when walking along paths or between trees in a forest – in order to minimize the danger of collisions. However, as can be seen in Figure 2.1, both circle and ellipse provide a good estimate for a linear increase in angular velocity for eccentricities up to 40° , which renders it difficult to confirm our results experimentally.

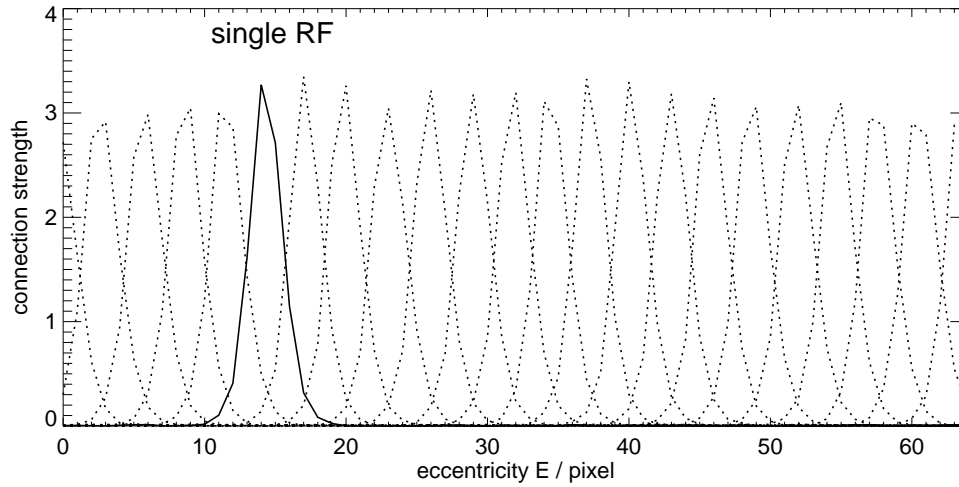


Figure 2.9: RF PROFILES OF LAYER-2 NEURONS AFTER LEARNING WITH CONSTANT STIMULUS VELOCITY ACROSS THE WHOLE VISUAL FIELD. Plotted are the connection strengths for every layer-2 neuron as a function of the corresponding layer-1 neurons. For constant stimulus velocity across the whole visual field, RF size and density do not depend on the position within the visual field. The slight differences in RF shape and RF peak sensitivity are not systematic and vary during learning.

2.5.3 Minimal Network Model

After training with moving stimuli, the network model developed a spatial distribution of RF centers whose density is in qualitative agreement with primate cortical magnification. The spatial distribution arises from correlation-based learning with a temporal Hebbian learning-rule and competitive interactions between layer-2 neurons via inhibitory connections. Hebbian learning adapts the RF sizes of the layer-2 neurons to the stimulus velocities at the corresponding eccentricities, while strong inhibitory competition ensures that RFs of distinct neurons do not overlap substantially.

RF Sizes Increase Linearly with Eccentricity

The linear increase in model RF size is in accordance with linearly increasing RF diameters of retinal, thalamic and primary visual cortical neurons in monkey (Hubel and Wiesel, 1974; Dow et al., 1981; Croner and Kaplan, 1995; Xu et al., 2002). How well do RF sizes in our model correspond to experimentally measured RF sizes? In monkey primary visual cortex, RF sizes are approximately 0.4° at 5° eccentricity (Hubel and Wiesel, 1974). If

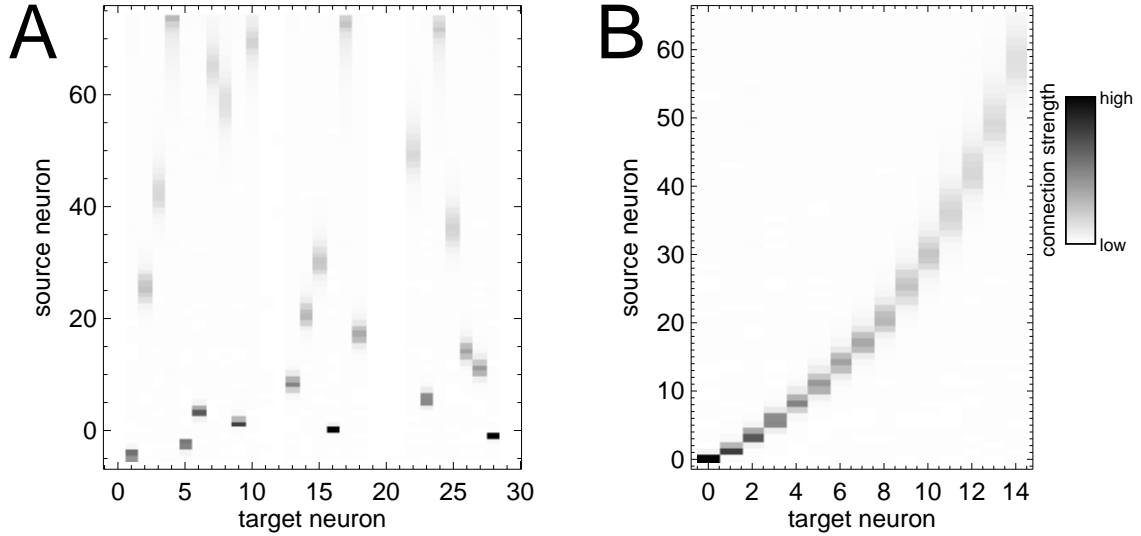


Figure 2.10: CONNECTION STRENGTHS FROM LAYER-1 TO LAYER-2 AFTER LEARNING WITH STIMULI MOVING AT RANDOM VELOCITIES. (A) Connection strengths from each layer-1 neuron (source) to every layer-2 neuron (target) after learning. (B) RFs of layer-2 neurons, sorted according to the position of their RF centers. Only layer-2 neurons with RF centers at positions greater or equal than 0 and less than 65 and with maximum synaptic connection strength exceeding 0.01 are included (see Section 2.4.1). The distribution of RFs is similar to the one obtained in the main simulation (Figure 2.4).

we assume that one pixel in our model corresponds to 0.08° , RF sizes are approximately 0.4° for a stimulus speed of $8^\circ/s$. If we further assume that the position of this RF corresponds to 5° eccentricity and that an observer moves with ≈ 1 m/s, then the required mean observer-object-distance would be less than 1 m, according to Equation 2.12. This seems to be fairly small for observer-object-distances during self-motion. However, model RF size is determined both by stimulus speed and the width of the temporal correlation window of the learning rule. Thus, a longer temporal correlation window would lead to larger RF sizes. For example, Földiák proposed possible neuronal mechanisms for correlating neuronal activity between neurons on the order of 100 ms (Földiák, 1997). Moreover, many other factors have not been considered here, such as the spatial structure of single objects, or head- and eye-movements, that could potentially influence overall RF size.

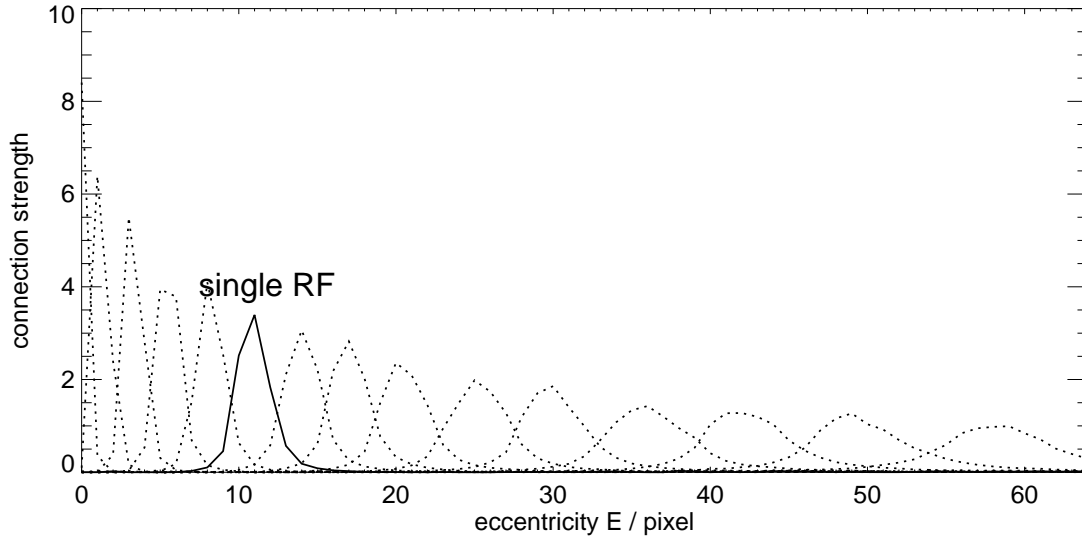


Figure 2.11: RF PROFILES OF LAYER-2 NEURONS AFTER LEARNING WITH STIMULI MOVING AT RANDOM VELOCITIES. Plotted are the connection strengths for every layer-2 neuron as a function of the corresponding layer-1 neurons. The distribution of RFs is similar to the one obtained in the main simulation (Figure 2.10).

Dependence of Contrast Sensitivity on Eccentricity

In our model, the sum of synaptic connection strengths to each neuron is restrained. This is in accordance with experimental results of human contrast sensitivity, which is similar at different eccentricities if visual stimuli are scaled in size, according to cortical magnification (Rovamo et al., 1978; Rovamo and Virsu, 1979). In our model, RF peak sensitivity A as a function of RF size r has the form $A \propto \frac{1}{r^c}$, with c theoretically equal to 1 (here: $c = 0.97$). For two-dimensional RFs we would expect c to have a value close to 2, which is the case for primate retinal ganglion cells (Croner and Kaplan, 1995). However, in neurons of the LGN of owl-monkeys ($c \approx 1.3$) (Xu et al., 2002) and retinal X- and Y-ganglion cells in cats ($c \approx 1.2$) (Linsenmeier et al., 1982), c was found to be considerably smaller. A reason for the differences between our model and these physiological measurements could be that we estimated the neurons' center-sensitivities by their afferent weights and did not take into account nonlinearities in the neurons' response properties and possible interactions between neurons.

Influence of Optical Flow on Spatial Visual Acuity During Learning

Another interesting aspect is the influence of the velocity of optical flow fields during learning on spatial visual resolution and acuity. It has been shown that spatial visual acuity is consistent with cortical magnification at different eccentricities (Daniel and Whitteridge, 1961; Virsu and Rovamo, 1978; Rovamo and Virsu, 1979). In our model, the decline in spatial resolution with increasing eccentricity is a direct consequence of the increasing velocity of optical flow with increasing eccentricity during self-motion along the direction of gaze. Hence, our model provides an example of how the *temporal* structure of the visual input may determine the *spatial* response properties of cortical neurons during learning.

Differences in Receptive Field Sizes of Visually Driven Neurons

The simulations demonstrate that if the network model is trained with stimuli of different velocities at the same eccentricity, the learned RF sizes depend on the range of stimulus velocities experienced during learning. This has interesting consequences for the interpretation of RF sizes of visually driven neurons. In our natural environment, we experience stimuli at a wide range of retinal velocities, due to self-motion, object-motion or body-, head- or eye-movements. Retinal velocities range from static views up to velocities too high to be resolved by the visual system. Our model suggests that the size of a neuron's RF may be determined by the spatio-temporal response properties of its afferent neurons. Evidence for this hypothesis comes from experiments which show a correlation between the upper cutoff velocity of neurons and their RF size in the primary visual cortex of cats (Leventhal and Hirsch, 1980) and monkeys (Orban et al., 1986).

2.5.4 Extensions to the Model

The aim of our study was to demonstrate a basic principle, using as few ingredients as necessary. Therefore, the current model leaves much space for extensions. We discuss possible extensions and ideas for further investigations.

Initial Network Connectivity

In our network model, we chose an all-to-all connectivity between layer-1 and layer-2 neurons, in order not to make any assumptions about the expected magnification to be learned. Therefore, the learned representation of the visual field in layer-2 is not retinotopic. Constraining the afferent input region of each layer-2 neuron would provide a raw retinotopic ar-

range of the layer-2 RFs. In addition, distance-dependent conduction delays were shown to lead to a retinotopic arrangement of RFs during learning (Saam and Eckhorn, 2000). This would further allow to confine the spatial range of the inhibitory interactions within layer-2 to a spatial region which is in accordance with the spatially restricted range of cortical lateral connections (Gilbert and Wiesel, 1979; Stettler et al., 2002). Another possibility would be to apply an anti-Hebbian learning rule to the self-organization of the inhibitory connections, which was shown to lead to a sparse distribution of RFs (Földiák, 1990; Falconbridge et al., 2006).

Extending the Model to Two Dimensions

Extending the current model under the assumption of rotational symmetry with respect to the direction of gaze would lead to radially elongated RFs, with elongations, increasing linearly with eccentricity. Although we are not aware of data showing radially elongated RFs in the primary visual cortex of monkeys, neurons with strikingly similar RFs have been described in area V4A of the visual cortex of monkeys (Pigarev et al., 2002). These RFs have comet-like shapes, with a preference for radially moving stimuli. It is possible that these RFs play a role for the encoding of ocularly fixated objects during self-motion, and may self-organize according to a similar principle like the one shown in this Chapter.

A two-dimensional network model would further allow to extend the variety of flow fields presented during learning. A next step would be to include rotational flow fields around the direction of gaze. These can be treated in a similar way to the expanding flow fields used in the current model. Training the model with pure rotational flow fields would lead to RFs with identical tangential angular extension across the whole visual field. This corresponds to RF sizes, increasing linearly in tangential direction¹ with increasing eccentricity. This transforms a retinal velocity-distribution, due to pure rotational flow-fields, to constant cortical velocities, independent of eccentricity. This is consistent with the two-dimensional mapping of visual space onto the primary visual cortex, which can be approximated mathematically by a log-polar transformation (e.g., Schwartz, 1977; Reitboeck and Altmann, 1984), and transforms retinal translations due to expansional and rotational flow fields to cortical translations along perpendicular directions.

¹For small angular differences $\Delta\phi$, the distance of two points of the same eccentricity r is proportional to $r\Delta\phi$

Realistic Flow Fields

A limitation of the current model is the simplifying assumption that the retino-cortical mapping is solely determined by linear self-motion along the direction of gaze. This neglects deviations of the direction of gaze from the direction of self-motion as well as head and eye movements (e.g., Lappe et al., 1999). An interesting extension to the current study would be the recording of movies with a mobile, head-mounted camera in combination with a mobile eye-tracking device, and the investigation of the velocity distribution of the corresponding flow fields. Additionally, it would be interesting to assess differences between results from these scenes and results from a camera mounted, for example, on a cat's head (Betsch et al., 2004). Systematic changes in the retinal velocity distribution across the visual field, depending on the average velocity of self-motion, the altitude of the eyes with respect to the ground, and the structure of the natural environment, could help to understand differences in the cortical magnification factors of different species.

2.5.5 Related Studies

Self-Organization of Hippocampal Receptive Fields

When rats move through their environment, a class of hippocampal neurons, so called *place cells*, are activated in a positionally and directionally selective fashion, which allows to estimate the location of the rat (O'Keefe and Dostrovsky, 1971). Mehta et al. (2000) found that the spatial shapes of the place cells' RFs were initially symmetric, but became asymmetric and directionally selective with increased experience of the rat in a given environment. They proposed a model to explain this experience-dependent, asymmetric shape of hippocampal place-fields, which relies on a similar principle like the network model proposed in this chapter. In contrast to our model, they used a temporally asymmetric Hebbian learning rule, i.e. weights were strengthened if a presynaptic neuron was activated before the postsynaptic neuron, and synaptic weights were weakened otherwise. Thus, for the situation of a rat moving repeatedly from one location to another (comparable to the situation in our model, where a stimulus moved repeatedly from small eccentricities towards larger eccentricities), RFs became skewed, and expanded towards the initial position of the rat. Furthermore, the RF centers shifted in the direction opposite to the direction of movement. Their results differ from the results in our model, obtained with a temporally symmetric Hebbian learning rule, where learned RFs have a symmetric shape, with RF positions remaining stable. By using a temporally asymmetric learning rule, we were not able to obtain a stable distribution

of RFs consistent with cortical magnification, due to the fact that RFs kept shifting towards the fovea. It remains to be investigated how the self-organization of afferent connections due to temporally asymmetric learning rules can be stabilized during repeated unidirectional stimulation by additional, biologically plausible mechanisms.

Temporal Coherence

In order to enable a network model to learn invariant object representations from continuous spatio-temporal image sequences, Földiák (1991) proposed a learning rule similar to the temporal Hebbian learning rule used in the current study. In its original formulation, this so-called trace learning rule is a modified Hebbian learning rule, where the change in synaptic weight is proportional to the product of the instantaneous presynaptic activity with a running average of the postsynaptic activity (the memory trace), although a presynaptic memory trace was mentioned to lead to similar results (Földiák, 1997; Rolls, 2000). The underlying idea of the trace learning rule is that transformed versions of the same object often occur close together in time, a principle called *temporal coherence*. The principle of temporal coherence forms the basis for a number of learning rules and mathematical algorithms to extract invariances from image sequences (e.g. Földiák, 1991; Becker, 1993; Wallis, 1996; Wallis and Rolls, 1997; Becker, 1999; Rolls and Milward, 2000; Körding and König, 2001; Stringer and Rolls, 2002; Wiskott and Sejnowski, 2002). To our knowledge, our study is the first to apply the principle of temporal coherence to the learning from flow-fields and to investigate the influence of retinal stimulus velocity on the sizes of the learned RFs.

Chapter 3

Spatial Statistics of Local Contour Elements in Real-World Scenes

3.1 Abstract

It has been proposed that primate cortical magnification provides a scale invariant representation of ocularly fixated objects with respect to changes in viewing distance. If the visual system makes use of this scale invariant representation, the mechanisms subserving the grouping of local contour elements into coherent objects should also be scale invariant across the visual field. Long-range horizontal connections, which preferably link neurons with like feature preferences, have been suggested to subserve contour grouping in visual cortical processing. With increasing eccentricity cortical RFs become larger and their spatial frequency preference shifts to lower values. Psychophysical evidence exists for an independence of the contour grouping mechanisms of the spatial scale for foveal stimuli. Hence, scaling fixated objects according to cortical magnification could, in principle, result in a comparable grouping performance in the periphery. Nevertheless, psychophysical experiments show that contour integration is impaired for targets at non-foveal locations, even if the targets are scaled according to cortical magnification. In order to better understand how the mechanisms responsible for contour grouping depend on the spatial scale of local, oriented contour elements, we investigated the spatial statistics of Gabor wavelet responses derived from real-world images with respect to the spatial wavelength of the wavelets. For the set of images and wavelets examined we find nearly scale-invariant collinear correlations only for wavelets of horizontal orientation. For vertical and oblique orientations, collinear correlations drop in coordinates normalized to the wavelengths of the wavelets relatively faster for

long-wavelength wavelets. Assuming that neurons in the primary visual cortex adapt their horizontal connectivity by correlation-based (Hebbian) learning mechanisms, this would result in cortically shorter collinear horizontal connections in the peripheral compared to the foveal representation for neurons with RF-sizes scaled according to cortical magnification. Our results provide evidence against a uniform mechanism of contour grouping across all spatial scales and across the visual field.

3.2 Introduction

In Chapter 2 we have shown that cortical magnification transforms an inhomogeneous *retinal* velocity distribution due to self-motion along the direction of gaze into constant *cortical* velocities across the whole visual field, if the average arrangement of objects in the environment corresponds to an ellipsoid with the observer in its center. This has the advantage that the cortical connectivity for the processing of self-motion can be identical across the whole visual field. However, in addition to the processing of self-motion, one of the most fundamental tasks of the visual system is to group local elements of a visual scene into coherent objects. Psychophysical, neurophysiological, anatomical, and theoretical studies provide evidence for mechanisms by which this grouping may be accomplished. However, it is not clear how these mechanisms depend on the position within the visual field. It has been proposed that cortical magnification provides a scale invariant representation of fixated objects with respect to changes in viewing distance (Schwartz, 1980; Reitboeck and Altmann, 1984). In order to make effective use of this cortical scale invariant representation, the contour grouping mechanisms should also be scale invariant across the visual field.

In the following we will review experimental and theoretical findings about possible mechanisms supporting contour grouping on early stages of visual processing.

3.2.1 Contour Grouping in Human Perception

The human visual system exploits a great number of grouping cues at multiple levels of processing which can be based on spatial and temporal properties within a visual scene. A prominent set of phenomenological rules was described by the Gestalt psychologists (Koffka, 1935; Wertheimer, 1923). Some of these so called *Gestalt Rules* (proximity, similarity, and good continuation) are illustrated in Figure 3.1.

These empirical principles were later refined in psychophysical experiments (e.g. Field et al., 1993; Polat and Sagi, 1993, 1994; McIlhagga and Mullen, 1996; Dakin and Hess,

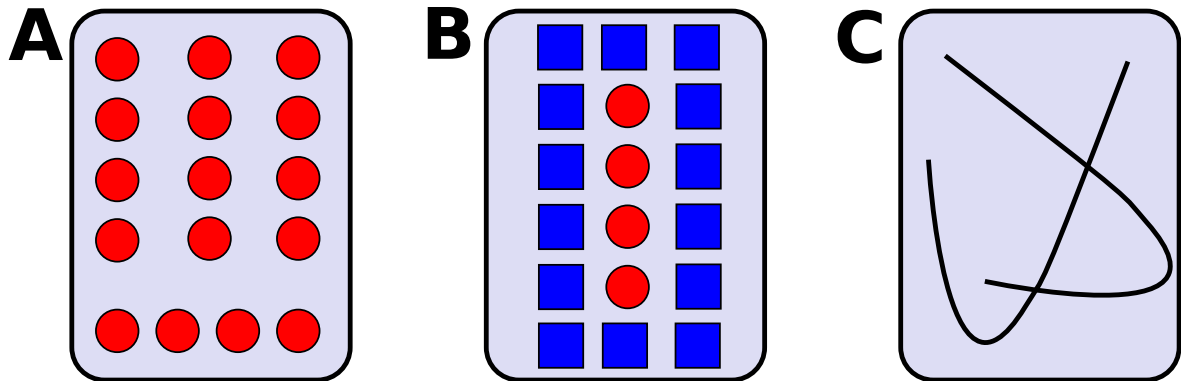


Figure 3.1: GESTALT RULES AS AN EXAMPLE OF BASIC GROUPING RULES IN HUMAN PERCEPTION. (A) Grouping by proximity. There is a tendency to perceive elements near to each other as belonging to the same object. (B) Grouping by similarity. Local elements are perceived to belong together if they are similar. (C) Grouping by good continuation. Local elements are grouped together if they form a smooth curve. The Gestalt rule of good continuation plays an important role in contour integration.

1998). Field et al. (1993) carried out a series of seminal experiments in which human subjects had to identify a continuous path of Gabor elements with similar orientations, which were embedded in a background of randomly oriented Gabor elements. It turned out that the relative orientation of neighboring Gabor elements within a path had a large impact on the detection performance. Performance degraded with increasing difference in orientation of successive Gabor elements. These results have been formalized by the term association field (e.g., Field et al., 1993; Hess and Dakin, 1999), which quantitatively describes the tendency of local contour elements to be perceptually bound together as a function of their relative position, orientation, and spatial frequency.

3.2.2 Spatial Statistics of Contours in Real-World Scenes

If the visual grouping mechanisms arose to subserve the perception of visual objects, they should be well adapted to the statistical co-occurrence of edges and contours in real-world scenes. The idea that the visual system is structured in a way to provide an efficient representation of the incoming signals goes back to Attneave (1954) and Barlow (1961), who proposed that information theory could provide a link between the statistics of the environment and neural responses through the concept of efficient coding. Brunswik and Kamiya (1953) suggested that there should be a quantitative relationship between the basic Gestalt principles and the statistics of the visual world.

Real-world images have characteristic statistical properties that distinguish them from random noise distributions (e.g., Field, 1987; Ruderman and Bialek, 1994; Krüger, 1998; Zetzsche and Röhrbein, 2001). For example, Field (1987) showed that the spatial power-spectrum of the intensity-values of real-world images decreases according to a power law for nearly 3 octaves of scaling and therefore is scale-invariant. Several studies have demonstrated that the statistics of local contour elements in real-world scenes correspond to the Gestalt principle of collinearity (Krüger, 1998), or more general *cocircularity* (Sigman et al., 2001; Geisler et al., 2001), and can predict human contour grouping performance (Geisler et al., 2001).

3.2.3 Neurophysiology and Anatomy

The response properties of neurons on early stages of visual processing are commonly classified by their classical receptive field (cRF) (Hubel and Wiesel, 1962). In the primary visual cortex of cats and monkeys most neurons respond selectively to bars of specific orientations in their cRF. However, physiological studies have shown that the response of a neuron to a stimulus within its cRF can be modulated by stimuli outside the cRF, a phenomenon called *contextual modulation* (e.g., Maffei and Fiorentini, 1976; von der Heydt et al., 1984; Gilbert and Wiesel, 1990; Gilbert, 1992; Knierim and van Essen, 1992; Kapadia et al., 1995; Sillito et al., 1995). These experiments demonstrate that the response of a neuron to an optimally oriented stimulus in its cRF can, for example, be enhanced by collinearly arranged stimuli outside the cRF, while the response can be either enhanced or diminished by other geometrical arrangements of contextual stimuli.

It has been suggested that these contextual modulations are either mediated by long-range horizontal connections in the primary visual cortex of cats and monkeys, which were shown to preferentially link neurons with similar orientation preferences up to cortical distances of a few millimeters (monkey: Sincich and Blasdel, 2001; Angelucci et al., 2002; Stettler et al., 2002, cat: Ts'o et al., 1986; Schmidt et al., 1997; Gilbert and Wiesel, 1989, 1990, tree shrew: Bosking et al., 1997), or by feedback from higher visual areas (e.g. Angelucci et al., 2002). Although it has been shown in cats and monkeys that feedback connections from higher cortical areas can modulate the responses of V1 neurons (Mignard and Malpeli, 1991; Salin and Bullier, 1995; Hupé et al., 1998, 2001), it is not clear if they preferably connect neurons with similar orientation preferences (Angelucci et al., 2002) or provide orientation-unspecific feedback (Stettler et al., 2002).

3.2.4 Ontogenetic Development of Grouping Mechanisms

There is experimental evidence that contour-grouping mechanisms develop after birth in an activity-dependent fashion. Children younger than 9 months cannot make use of the basic Gestalt principles (Spelke et al., 1993). Similarly, in monkeys it has been demonstrated that contour grouping develops several months after birth (Kiorpes and Bassin, 2003). In humans, the patchiness of the long-range lateral connections, which is typical in adults, develops at about eight weeks after eye opening (Burkhalter et al., 1993; Katz and Callaway, 1992). Several studies have shown that the ordered formation of long-range horizontal connections happens in an input-dependent fashion in the primary visual cortex of cats (Callaway and Katz, 1990, 1991; Löwel and Singer, 1992; Kasamatsu et al., 1998; Trachtenberg and Stryker, 2001) and ferrets (Ruthazer and Stryker, 1996). For instance, kittens raised without patterned visual experience in one eye, as a consequence of suturing the lid of one eye, develop non-specific lateral interactions for that eye (Kasamatsu et al., 1998). If inputs from both eyes are decorrelated during development by artificially induced strabism, lateral connectivity develops mainly between cell groups activated by the same eye (Löwel and Singer, 1992).

Taken together, these experimental findings suggest that the initial development of cortical circuits and their later refinement depends critically on the spatio-temporal structure of the visual input, and that certain statistical regularities in the visual environment are reflected in the cortical connectivity.

3.2.5 Models of Contour Grouping

In model studies it has been shown that intra-areal horizontal connections within the primary visual cortex as well as feedback connections from higher visual areas can support the grouping of contour elements, consistent with the basic Gestalt principles (e.g., intra-areal: Eckhorn et al., 1990; Ostkamp, 1996; Yen and Finkel, 1998; Li, 1999; Hansen et al., 2001, feedback: Grossberg et al., 1997; Neumann and Sepp, 1999; Hansen et al., 2001). The connectivity in these models is fixed and determined in advance, based on theoretical or biologically motivated considerations. However, it has been demonstrated that long-range horizontal connections, linking neurons with similar feature preferences, can be learned through input-driven self-organization with artificial or real-world scenes through Hebbian learning mechanisms (Prodöhl et al., 2003; Grossberg and Williamson, 2001; Choe and Miikkulainen, 2004) and sparse coding approaches (Hoyer and Hyvärinen, 2002).

3.2.6 Dependence of Contour Grouping Mechanisms on Retinal Eccentricity

Relatively little is known about how the mechanisms subserving contour grouping depend on the neurons' preferred spatial frequencies and cRF-positions within the visual field. Several psychophysical studies have demonstrated that collinear facilitation in the fovea is independent of the spatial scale of the contour elements (Polat and Sagi, 1993; Hess and Dakin, 1997; Dakin and Hess, 1998; Woods et al., 2002).

With increasing eccentricity, cRFs of neurons in the primary visual cortex become larger and their peak spatial frequency preference shifts to lower values (e.g., De Valois et al., 1982). The scale independence of perceptual collinear facilitation in the fovea suggests that collinear facilitation performance could be comparable in the periphery, if stimuli are scaled according to cortical magnification. However, performance decreases in many subjects when stimuli are presented at nonfoveal locations (e.g., Williams and Hess, 1998; Zenger-Landolt and Koch, 1996; Hess and Dakin, 1997; Shani and Sagi, 2005). Xing and Heeger (2000) found that surround suppression is markedly stronger and less orientation specific in the periphery in comparison to the fovea, while the effect of surround facilitation is diminished or even absent. Importantly, this could not be accounted for by the cortical magnification factor. In psychophysical experiments Shani and Sagi (2005) demonstrated reduced facilitation for collinearly arranged Gabor wavelets at eccentricities as small as $1^\circ - 2^\circ$. Facilitation did not even increase if the stimuli were scaled according to the cortical magnification factor. However, facilitation performance could be increased when attention was directed from the fovea to the peripheral stimulus location. Similarly, Giorgi et al. (2004) found weak collinear facilitation for peripheral Gabor targets up to eccentricities of 6° , using a temporal, but not a spatial, two-alternative forced-choice paradigm. The latter findings underline the possible role of attention in modulating collinear facilitation.

Neurophysiological and anatomical studies in cats and monkeys demonstrate that long-range lateral connections in primary visual cortex are not restricted to the foveal representation, but extend extra-foveally up to retinal eccentricities of 10° . However, no systematic changes in lateral connectivity with eccentricity have been reported (monkey: Sincich and Blasdel, 2001; Angelucci et al., 2002; Stettler et al., 2002, cat: Ts'o et al., 1986; Schmidt et al., 1997; Gilbert and Wiesel, 1989, 1990, tree shrew: Bosking et al., 1997).

The above findings suggest that the lateral connectivity, subserving the grouping of local contour elements, could be identical in the fovea and in the periphery; with other factors, like attentional mechanisms, modulating the effect of collinear facilitation (Ito and Gilbert,

1999; Freeman et al., 2001; Giorgi et al., 2004; Shani and Sagi, 2005). However, the lack, or at least strong decrease, of collinear facilitation for non-foveal targets could be due to a different pattern of lateral connectivity in the fovea compared to the periphery.

3.2.7 Aim of the Current Study

The size and the spatial frequency preference of primary cortical cRFs change with ocular eccentricity. We wanted to know how the statistics of local oriented contour elements in real-world scenes depend on the spatial filter properties of cortical neurons at different eccentricities. Therefore, we examined the statistics of Gabor wavelet responses in real-world scenes with regard to wavelets of different orientations and spatial scales.

To our knowledge, no data exists about the statistics of local contour elements in real-world scenes at different spatial scales. In previous studies, oriented edge elements have been extracted using fixed-scale spatial filters. Krüger (1998) used oriented Gabor filters of a fixed scale to extract local contour elements. Sigman et al. (2001) employed quadrature pairs of fixed-scale steerable filters as a measure of the local oriented energy. Geisler et al. (2001) used a two-stage filtering process. In a first step, edge locations were identified as the zero-crossing pixels in the response of a nonoriented log-Gabor function. In a second step, local orientation energy was measured using quadrature pairs of oriented log-Gabor filters. They note that a preliminary analysis at a 2 octaves higher spatial scale yielded similar results, but they show no quantitative comparison.

3.3 Methods

3.3.1 Real-World Scenes

Real-world scenes were taken from a database of freely available still images (van Hateren and Van der Schaaf, 1998). The image set used consisted of 1800 black and white pictures, each $1536 \text{ pixel} \times 1024 \text{ pixel}$ in size, with an amplitude resolution of 12 bits, and an angular resolution of approximately 1 min of arc per pixel¹. In order to compare the statistics of local contour elements for different types of environments, we categorized a subset of the images according to the categories *plants* ($N = 255$), *buildings* ($n = 96$), and *forest* ($N = 112$). Figure 3.2 shows typical images from these different hand-chosen semantical categories.

¹Visit <http://hlab.phys.rug.nl/imlib/index.html> for more information.

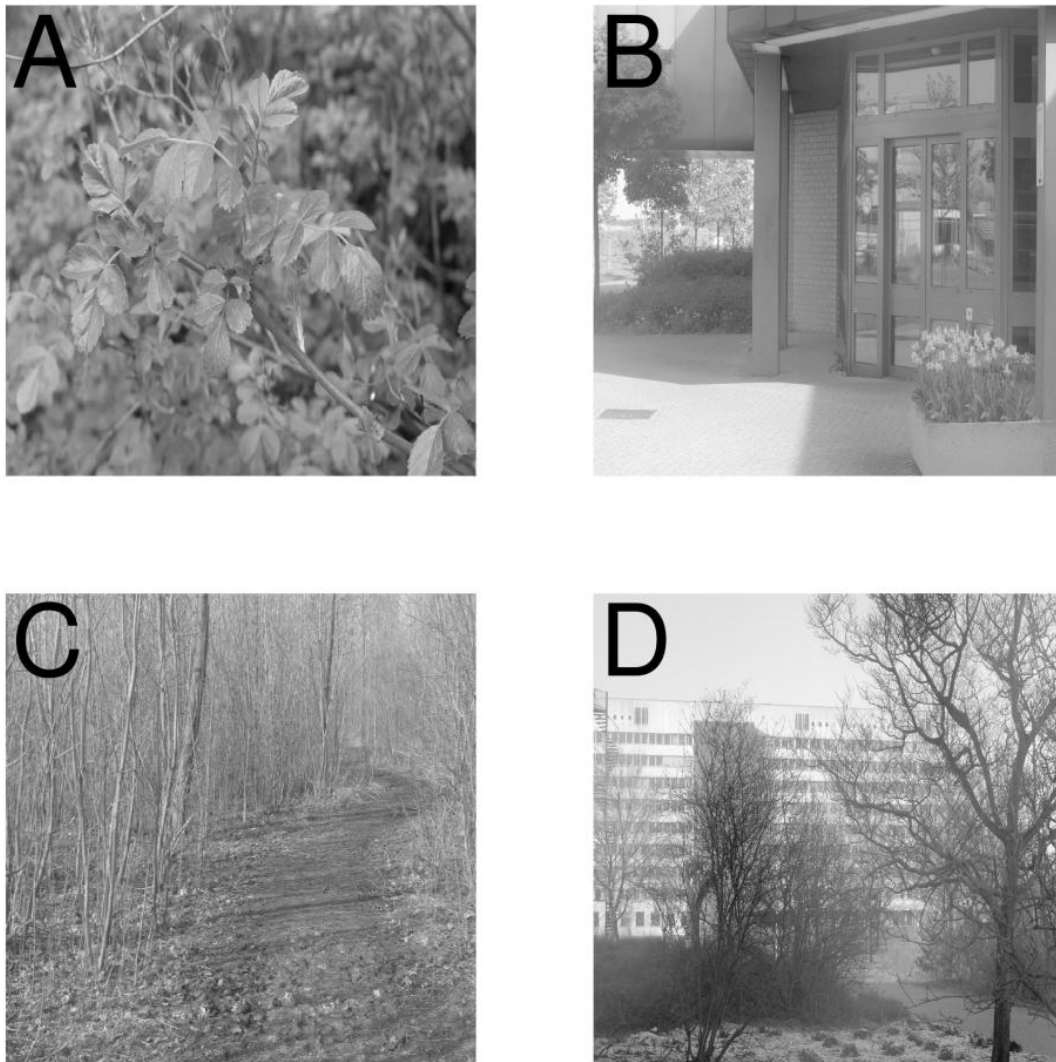


Figure 3.2: SAMPLE IMAGES FROM A DATABASE OF 1800 DIFFERENT IMAGES. Shown are images from 3 hand-chosen categories and an uncategorized image: (A) close-up photographs of plants, (B) buildings, (C) forest, and (D) uncategorized image. For better visibility, the logarithm of the image intensities is shown.

3.3.2 Extraction of Local Contour Elements

Gabor Wavelets as Spatial Filters

We used Gabor wavelets (Gabor, 1946) of constant spatial frequency bandwidth as a linear model for the spatial transfer function of cortical simple cells. This is consistent with neurophysiological findings (Marčelja, 1980; Pollen and Ronner, 1981; De Valois et al., 1982; Kulikowski and Vidyasagar, 1986; Jones and Palmer, 1987; De Valois and De Valois, 1988) and theoretical considerations, which demonstrate that spatial filters, similar to Gabor wavelets, can be learned in an unsupervised fashion from the statistics of natural images by applying constraints either concerning the sparseness of the neural representation (Olshausen and Field, 1996), or the independence of the resulting filters (Bell and Sejnowski, 1997; van Hateren and Ruderman, 1998).

A Gabor wavelet is a pixel-wise product of a Gaussian with a plane wave and can be parametrized by 5 parameters: A , σ_x , σ_y , λ , ϕ , and α . A is the amplitude of the wavelet, σ_x and σ_y characterize the Gaussian envelope function parallel and perpendicular to the wave vector of the plane wave, λ and ϕ are the wavelength and spatial phase of the plane wave, and α is the orientation of the wavelet.

$$G(x, y, \lambda, \sigma_x, \sigma_y, \alpha, \phi) = A \exp \left(-\frac{x'^2}{2\sigma_x^2} - \frac{y'^2}{2\sigma_y^2} \right) \cos \left(\frac{2\pi}{\lambda} y' - \phi \right) \quad (3.1)$$

with

$$x' = x \cos \alpha + y \sin \alpha \quad (3.2)$$

and

$$y' = y \cos \alpha - x \sin \alpha. \quad (3.3)$$

For our analysis we used Gabor wavelets of 4 different wavelengths (5, 10, 20, and 40 pixels, corresponding to 12, 6, 3, and 1.5 cycles per degree) and of four different orientations (0° , 45° , 90° , 135°), which resulted in a total of 16 different Gabor wavelets. To ensure a constant spatial frequency bandwidth for all wavelets, σ_y was chosen proportional to λ :

$$\sigma_y = \frac{2.5}{2\pi} \lambda. \quad (3.4)$$

In order to obtain a narrow orientation characteristic for the Gabor wavelets, the Gaussian envelope function was chosen to be oriented, with $\sigma_x = 1.5\sigma_y$, i.e. stretched perpendicular to the wave vector of the wave function. The wavelets had a size of four times the wavelet's wavelength in both x- and y-directions. Finally, we subtracted the mean of every Gabor

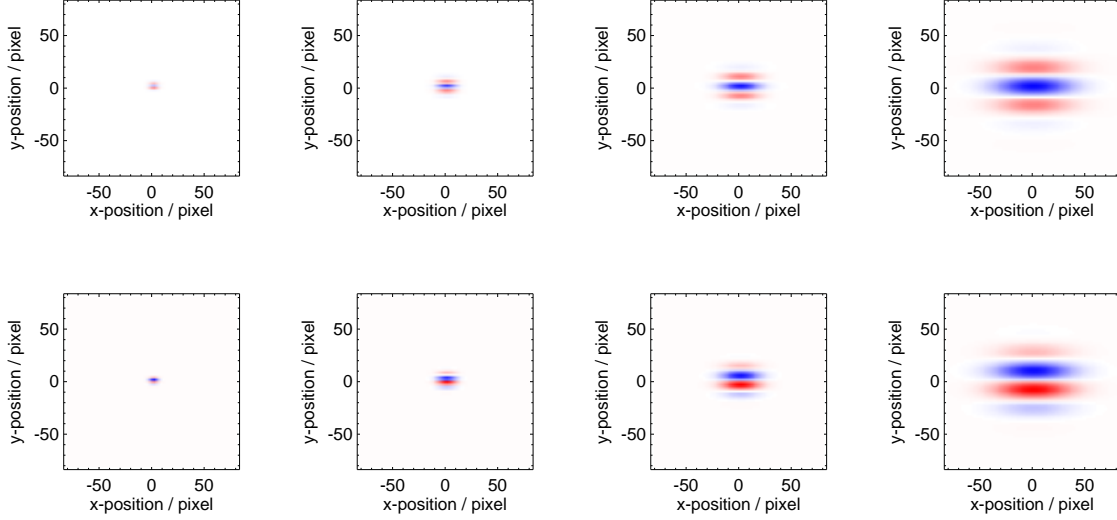


Figure 3.3: EXAMPLES OF GABOR WAVELETS USED TO EXTRACT LOCAL CONTOUR ELEMENTS. Shown are eight Gabor wavelets of orientation 0° , with four different wavelengths of the wave function (5, 10, 20, 40 px, respectively), with a wavefunction of phase 0° (top row) and of phase 90° (bottom row).

wavelet and normalized the sum of the absolute values to 1 in order to obtain identical maximum responses for the wavelets of all wavelengths. Figure 3.3 shows eight example wavelets of orientation 0° for 4 different wavelengths and two different spatial phases.

Spatial Complex Cell Filters

Contour elements were extracted by convoluting each image with a Gabor wavelet of a given orientation, wavelength and spatial phase. To mimic the spatial response characteristic of cortical complex cells, the squares of the convolution of two Gabor wavelets with the same orientation and wavelength, but shifted by 90° in phase (Adelson and Bergen, 1985; Spitzer and Hochstein, 1988), were added:

$$R_1(\lambda, \alpha) = |G(\lambda, \sigma_x, \sigma_y, \alpha, 0) * I|^2 + |G(\lambda, \sigma_x, \sigma_y, \alpha, \frac{\pi}{2}) * I|^2, \quad (3.5)$$

where $*$ is the convolution operator. To reduce the amount of necessary computation, we determined the convolution only for 150×150 different positions with horizontal and vertical distances of 4 pixels each, corresponding to an image region of $\approx 10^\circ$.

Normalization of Wavelet Responses

In order to sharpen the orientation characteristics of the wavelet responses, a thresholding and normalization procedure was applied to the filtered images. Similar approaches were used in comparable studies (Krüger, 1998; Sigman et al., 2001; Geisler et al., 2001). In a first step, we applied a threshold θ in order to discard small wavelet responses:

$$R_2(\lambda, \alpha) = \max \{R_1(\lambda, \alpha) - \theta, 0\}. \quad (3.6)$$

In a second step, we normalized the total response strength for every single pixel in the image by dividing the wavelet response for a single orientation i through the sum of the wavelet responses of all orientations of the same wavelength.

$$R_3(x, y, \lambda, i) = \frac{R_2(x, y, \lambda, i)}{C + \sum_j R_2(x, y, \lambda, j)} \quad (3.7)$$

The constant C had a small value in comparison to the values of R_2 , and ensured that the denominator was always $\neq 0$. This normalized the responses R_3 to the interval $[0, 1]$, where 1 corresponds to the situation of a single wavelet response being $\neq 0$ with all others being 0.

Finally, we applied a second threshold ($\theta_2 = 0.5$) to the normalized values, and discarded all wavelet responses which had a value less than θ_2 :

$$R(x, y, \lambda, i) = \max \{R_3(x, y, \lambda, i) - \theta_2, 0\}. \quad (3.8)$$

Although the main purpose of the thresholding procedure is of computational nature, it is similar to the operations performed by cortical neurons. Thresholding corresponds to the firing thresholds of cortical neurons and the normalization is similar to shunting inhibition, which has a divisive effect on the neurons' membrane potentials (e.g., Borg-Graham et al., 1996, 1998).

Figure 3.4 shows the resulting preprocessed wavelet responses for the four different wavelet wavelengths for an example image.

3.3.3 Data Analysis

In the current study we were mainly interested in the second order statistics of collinearly arranged contour elements of the same spatial scale. Therefore we computed the correlations between Gabor wavelets of the same orientation α and the same wavelength λ . The autocorrelation function of a single filtered image i is computed according to

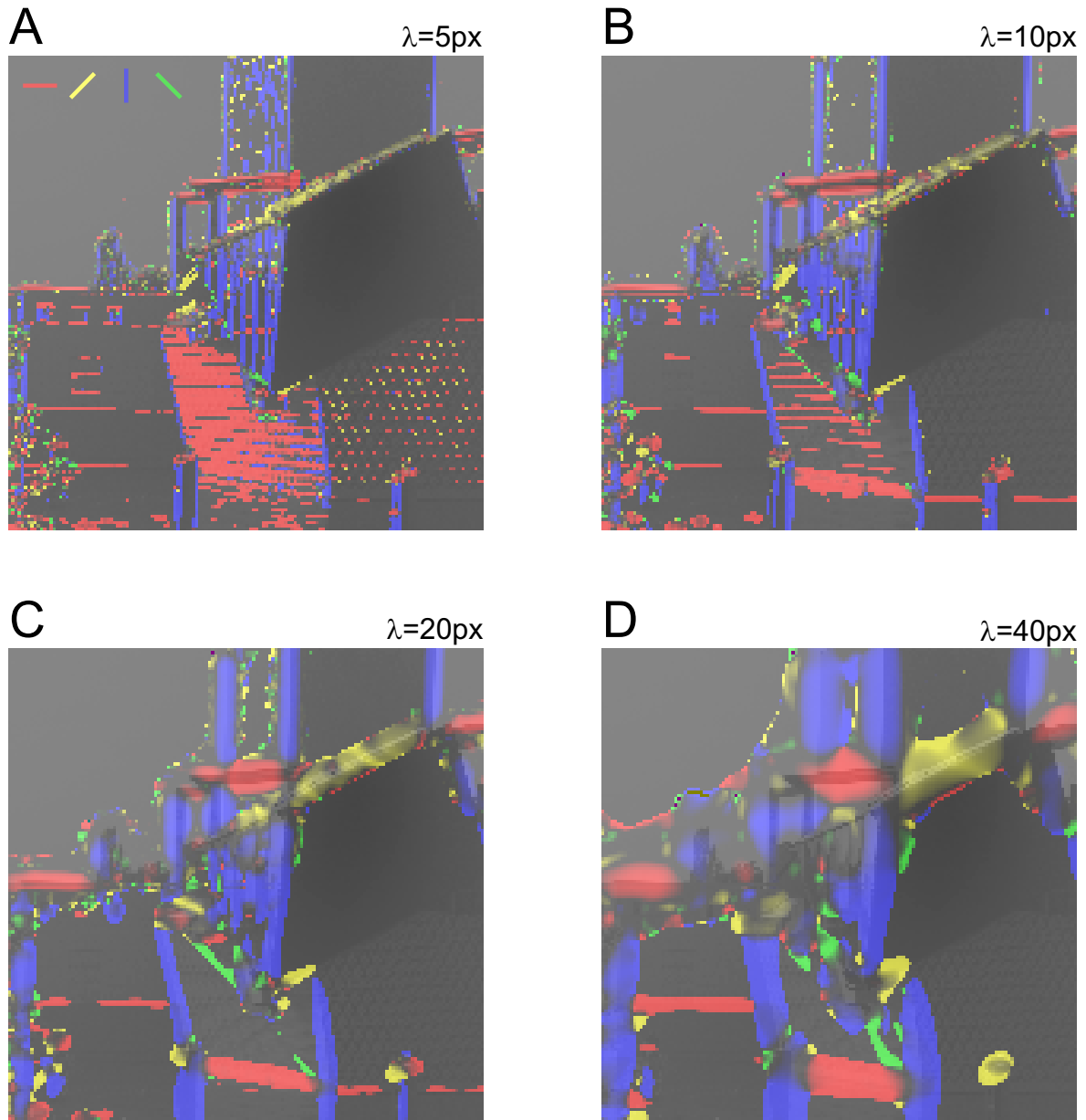


Figure 3.4: NORMALIZED RESPONSES FOR WAVELETS OF DIFFERENT SPATIAL SCALES. Shown are the normalized wavelet-responses for the four different filter-sizes: (A) $\lambda = 5\text{ px}$, (B) $\lambda = 10\text{ px}$, (C) $\lambda = 20\text{ px}$, and (D) $\lambda = 40\text{ px}$. The different colors correspond to the four different orientations 0° (red), 45° (yellow), 90° (blue), and 135° (green).

$$C_i(\Delta x, \Delta y) = \frac{\sum_{x,y} (R(x, y) - \bar{R})(R(x + \Delta x, y + \Delta y) - \bar{R})}{\sum_{x,y} \frac{1}{150 \cdot 150}}$$

The term $\sum_{x,y} \frac{1}{150 \cdot 150}$ is the overlap of the shifted image-patches and compensates reduced correlation-values for large values of $(\Delta x, \Delta y)$ due to the finite patch-size. Correlations were computed for values of Δx and Δy in the range from -160 px to 160 px.

The mean autocorrelation function for a given Gabor wavelet, averaged over all images, was computed according to

$$C(\Delta x, \Delta y) = \frac{1}{N} \sum_{i=1}^N C_i(\Delta x, \Delta y)$$

To compare the correlation functions for filters of different orientations and wavelengths, the autocorrelation functions were normalized such that

$$C(0, 0) = 1. \quad (3.9)$$

3.4 Results

3.4.1 Average Normalized Wavelet Responses

Figure 3.5 shows the normalized wavelet responses for the 16 different Gabor wavelets, averaged across all image locations and images. The average responses for wavelets of horizontal and vertical orientations are larger than the responses for wavelets of oblique orientations for all wavelengths examined. Furthermore, wavelet response strength varies in a qualitatively similar fashion with orientation for wavelets of different wavelengths, with slightly more pronounced differences for wavelets of large wavelengths. Figure 3.5B shows the response strength, averaged across all wavelengths, in dependence on the orientation of the wavelets.

However, the results depend on the stimulus set analyzed. If only a subset of the images which contain buildings is considered, one obtains the distribution of response strengths shown in Figure 3.6. The difference between the response strengths for wavelets of cardinal and oblique orientation is even more pronounced than for the case of pooling over all images. This seems to be mainly caused by the edges of the buildings, which, in the stimulus set examined, are often aligned parallel to the horizontal or the vertical axis.

In contrast, a subset of images which mainly consists of close-up views of plants leads to similar response strengths for wavelets of all orientations (Figure 3.7), with slightly larger responses for vertically oriented wavelets.

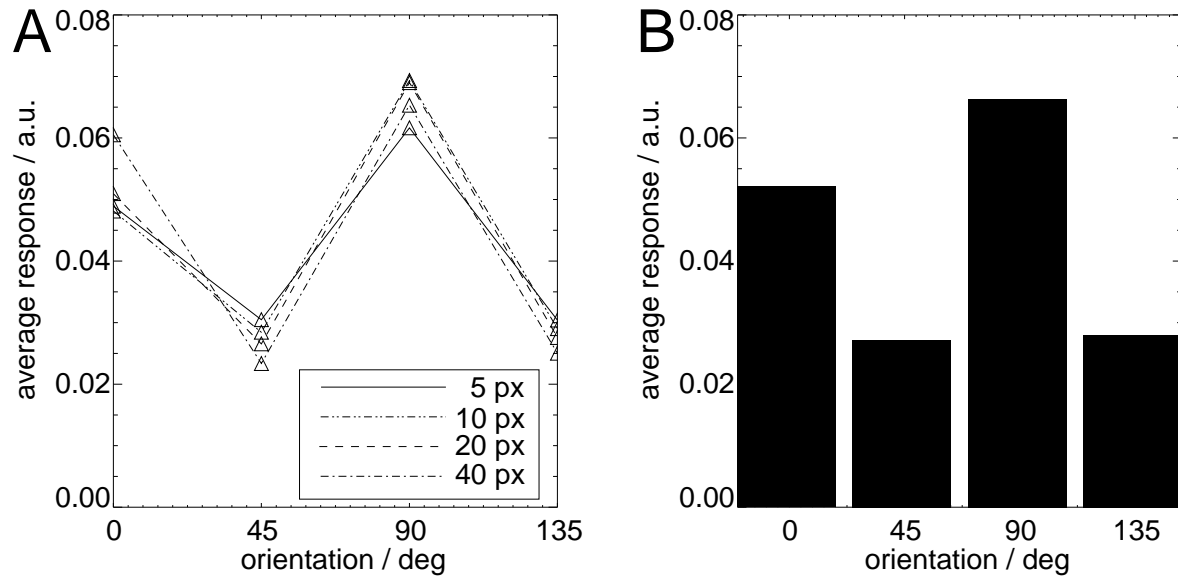


Figure 3.5: AVERAGE NORMALIZED WAVELET RESPONSES FOR WAVELETS OF DIFFERENT WAVELENGTHS AND ORIENTATIONS, COMPUTED FROM ALL 1800 IMAGES. (A) Dependence of the average normalized wavelet responses on orientation and wavelength, and (B) averaged across all wavelengths. Note the larger responses for wavelets of horizontal and vertical orientation and the similar responses for wavelets of the same orientation but different wavelengths.

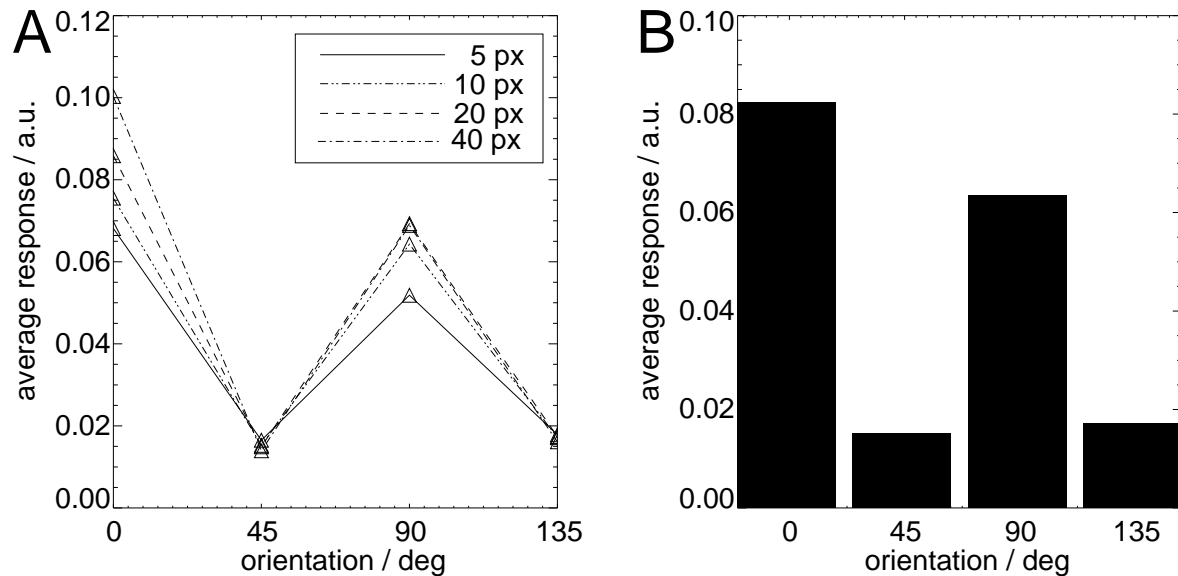


Figure 3.6: AVERAGE NORMALIZED WAVELET RESPONSES FOR WAVELETS OF DIFFERENT WAVELENGTHS AND ORIENTATIONS, COMPUTED FROM IMAGES WITH BUILDINGS. Compare Figure 3.5.

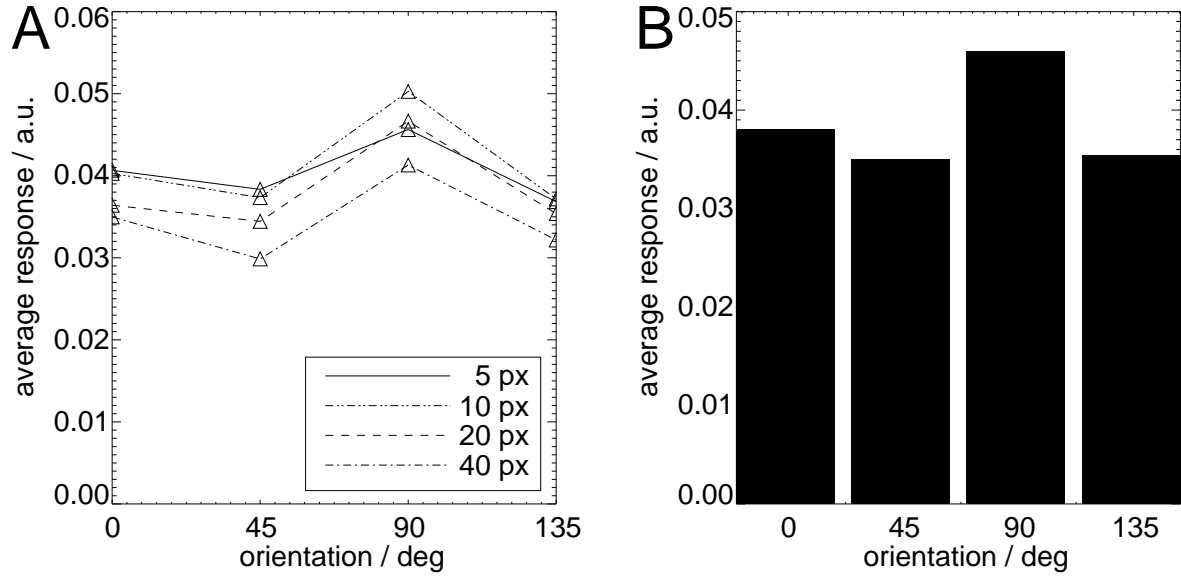


Figure 3.7: AVERAGE NORMALIZED WAVELET RESPONSES FOR WAVELETS OF DIFFERENT WAVELENGTHS AND ORIENTATIONS, COMPUTED FROM IMAGES WITH CLOSE-UP PHOTOGRAPHS OF PLANTS. Compare Figure 3.5.

For images depicting trees and forest-scenes, response strength is highest for wavelets of vertical orientation (Figure 3.8), most probably caused by the dominant trunks of the trees. Interestingly, for the smallest wavelets used, there are similar responses for wavelets of all orientations. This could be due to the fact that the small structures in the forest scenes are similar to the above mentioned class of plants in close-up view.

Taken together, differences in the average response strengths of wavelets of different orientations depend strongly on the image set analyzed. Our results indicate further that the relative response strengths for wavelets of different orientations depend only weakly on the wavelength of the wavelets. Thus, for the range of wavelengths examined, the relative contribution of wavelet responses of different orientations is nearly independent of the spatial scale of the wavelets. It is, however, important to note that the wavelength of the largest wavelets used (40 px) corresponds to a visual angle of less than one degree.

3.4.2 Two-Dimensional Autocorrelation Matrices

Figure 3.9 shows the two-dimensional autocorrelation matrices for wavelets of four different orientations and four different wavelengths. The correlation profile between wavelets of the same orientation is elongated along the collinear direction. Collinear correlations are

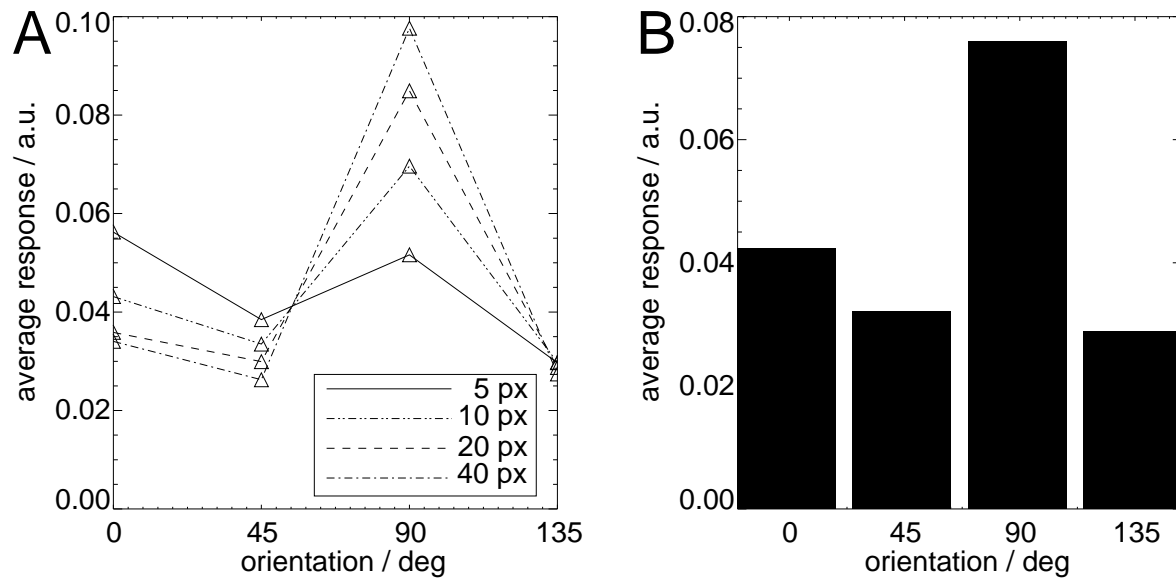


Figure 3.8: AVERAGE NORMALIZED WAVELET RESPONSES FOR WAVELETS OF DIFFERENT WAVELENGTHS AND ORIENTATIONS, COMPUTED FROM IMAGES WITH FOREST-SCENES. Compare Figure 3.5.

more far-reaching for wavelets of cardinal orientations in comparison to wavelets of oblique orientations. Furthermore, correlation declines more steeply with distance for wavelets of short wavelengths in comparison to wavelets of the same orientation but longer wavelength.

3.4.3 Collinear Correlations

Figures 3.10A,B show the distance-dependent collinear correlation strengths for the wavelets of horizontal orientation. One can see that for any given distance of wavelets correlation is stronger the larger the wavelength of the corresponding wavelets.

A better understanding of the decline in correlation strength is achieved by normalizing the distance of the wavelets to their wavelength. This is shown in Figures 3.10C,D. Correlation strengths for pairs of wavelets of different wavelengths are similar at the same relative distance. Thus, for wavelets of horizontal orientation, collinear correlation is nearly scale invariant for the wavelets of different wavelengths.

However, this is only the case for the wavelets of horizontal orientation, but not for the three other orientations examined (Figure 3.11). There is a general trend for correlations to decline more steeply with increasing distance for wavelets with larger wavelengths. It is further notable that collinear correlations decline faster for wavelengths of oblique orienta-

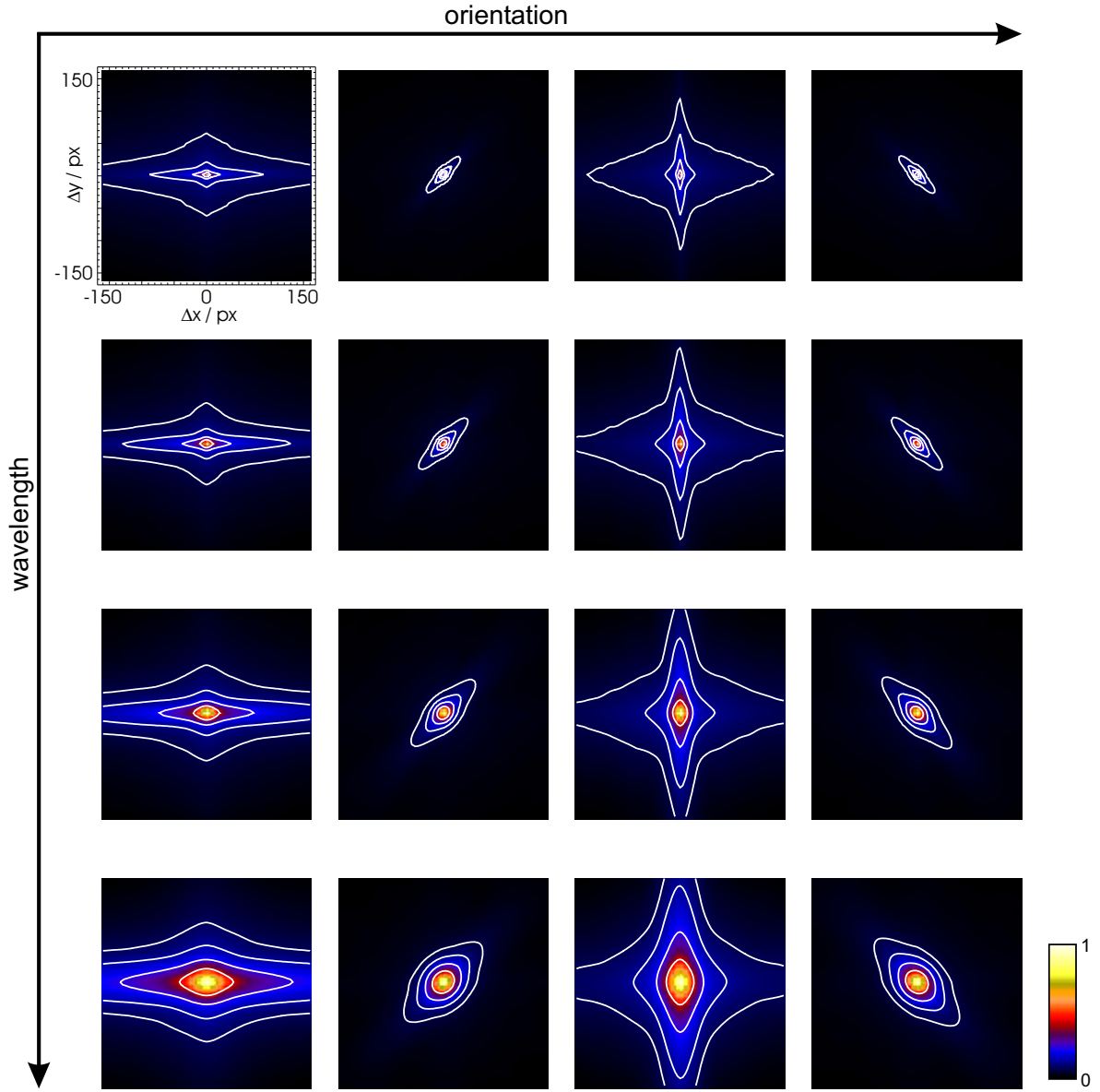


Figure 3.9: TWO-DIMENSIONAL AUTOCORRELATION MATRICES FOR WAVELETS OF DIFFERENT WAVELENGTHS AND ORIENTATIONS. The contours indicate correlation strengths of 0.4, 0.2, 0.1, and 0.05, respectively. From left to right: 0° , 45° , 90° , 135° . From top to bottom: $\lambda = 5$ px, $\lambda = 10$ px, $\lambda = 20$ px, and $\lambda = 40$ px. Note the elongation of the correlation profiles along the collinear direction with respect to the orientation of the wavelets. The correlation profiles of wavelets of the same wavelength but different orientations are in general not rotation invariant. Correlations along the collinear direction as well as in the perpendicular direction are more long-range for wavelets of horizontal and vertical orientations in comparison to wavelets of oblique orientations.

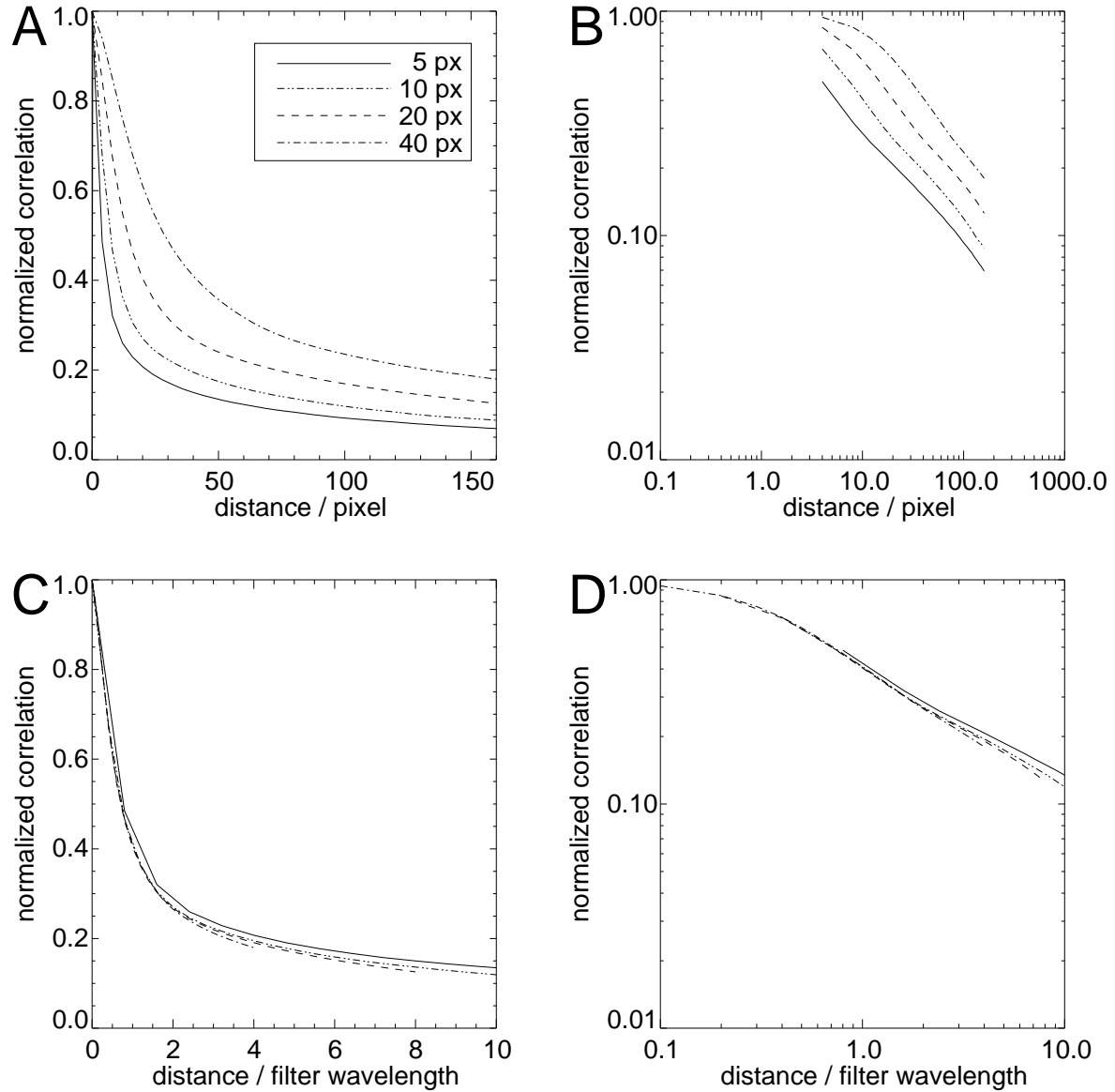


Figure 3.10: COLLINEAR CORRELATION FOR WAVELETS OF HORIZONTAL ORIENTATION (0°). Normalized Correlation (A) in linear coordinates, (B) in logarithmic coordinates, (C) in linear coordinates, with distances normalized to the wavelets' wavelengths, and (D) like in (C), but in logarithmic coordinates. Collinear correlation decreases more steeply with distance for wavelets of short wavelengths in comparison to wavelets of long wavelengths (A-B). However, if distances are normalized with respect to the wavelets' wavelengths, the decline in correlation with increasing distance becomes similar for wavelets of different wavelengths (C-D).

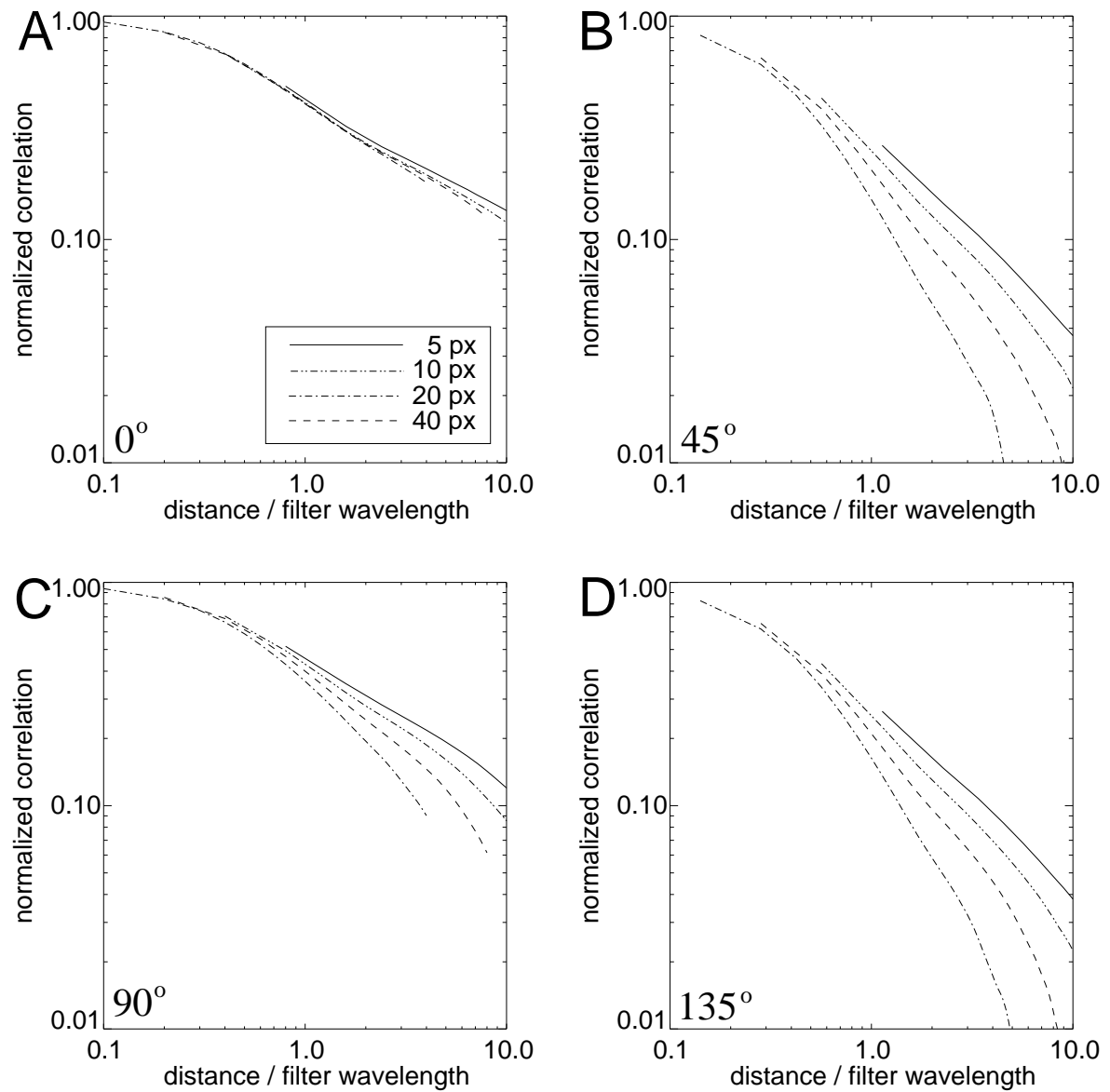


Figure 3.11: CORRELATION STRENGTH AT DISTANCES NORMALIZED TO THE WAVELETS' WAVELENGTHS. (A) 0° , (B) 45° , (C) 90° , and (D) 135° . Note the steeper decline in correlation with increasing distance for wavelets of large wavelengths compared to wavelets of shorter wavelengths.

tions in comparison to correlations for wavelets of the same wavelengths, oriented along the cardinal orientations.

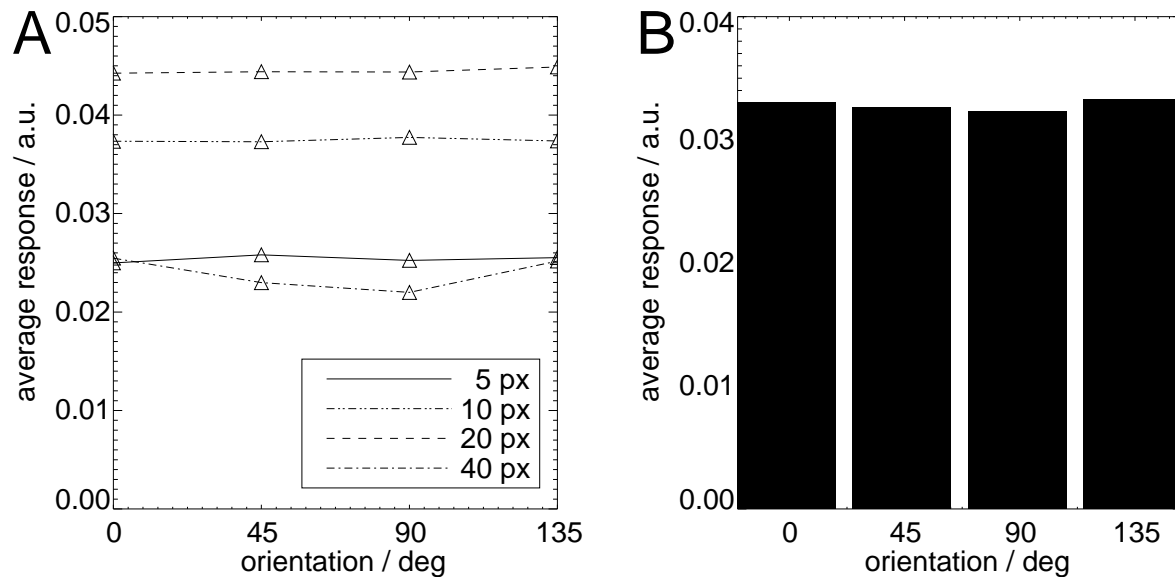


Figure 3.12: AVERAGE WAVELET RESPONSES FOR THE CASE OF SHUFFLED IMAGES. The average responses for wavelets of the same wavelength do not depend on the orientation of the wavelets.

3.4.4 Shuffled Images

In order to rule out the possibility that the increased wavelet responses for horizontally and vertically oriented wavelets and the increased correlation along the collinear direction are trivially determined by the shape of the spatial filters used, we computed the average wavelet responses and the two-dimensional autocorrelation matrices for the wavelet responses obtained from a set of 1000 images, with the intensity values of the images shuffled across space. The average wavelet response strengths are shown in Figure 3.12. As one can see, response strengths are similar for the different wavelet orientations. Thus, the strong wavelet responses for horizontal and vertical contours in real-world scenes are a consequence of the spatial structure of the scenes, and not artifacts of the shape of the spatial filters used.

The two-dimensional autocorrelation matrices for the wavelet responses obtained from the set of shuffled images are shown in Figure 3.13. The autocorrelation profiles merely resemble the oriented Gaussian envelope functions of the wavelets. Figure 3.14 shows the correlation along the collinear orientation for the filters of all orientations and wavelengths. Correlation is essentially zero for relative differences greater than two times the wavelength of the wavelets. Wavelets of different wavelengths display scale-invariant behavior, as expected from the scale invariance of the wavelets. Furthermore, there is no difference in collinear correlation for wavelets of different orientations.

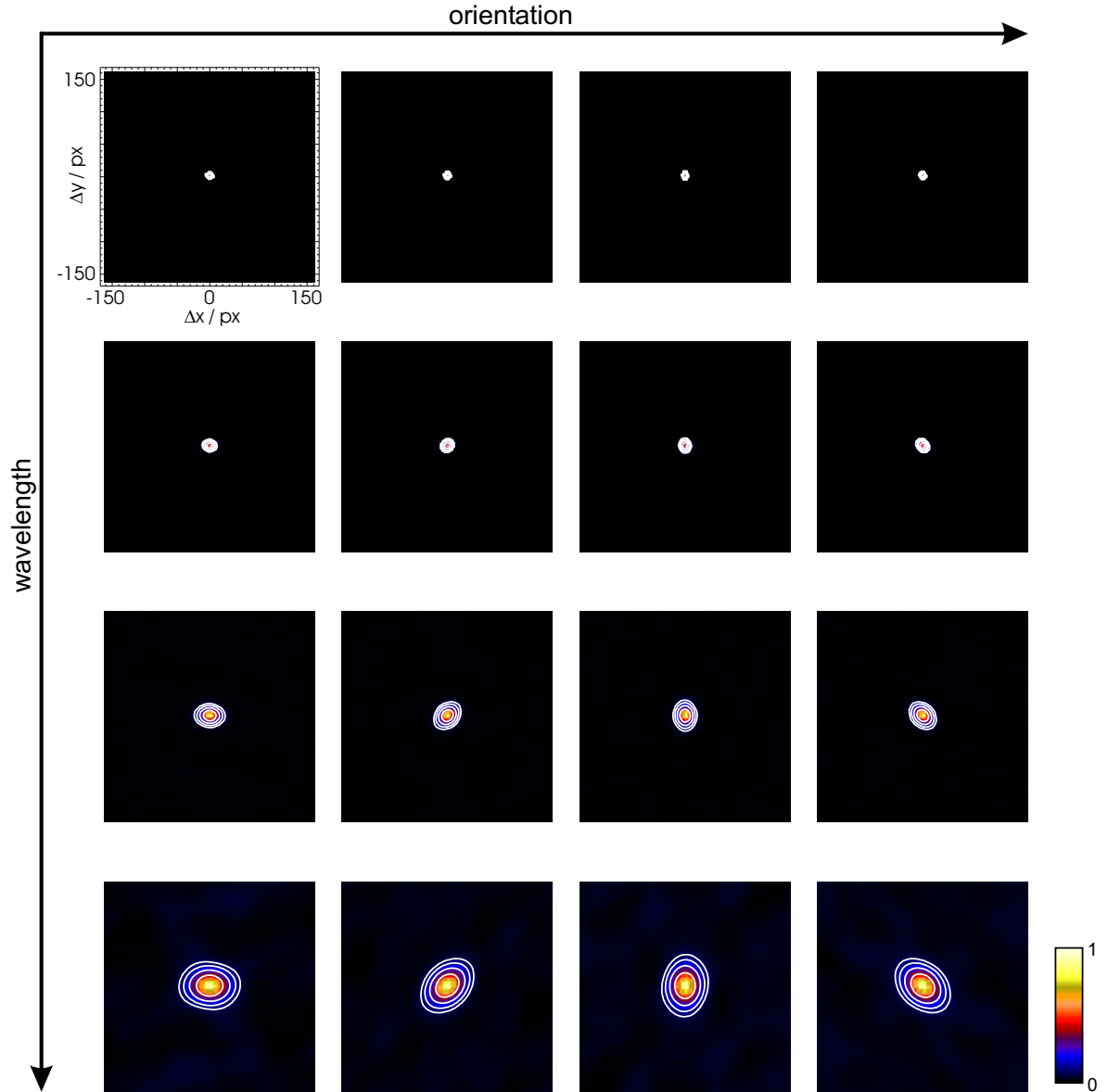


Figure 3.13: TWO-DIMENSIONAL AUTOCORRELATION MATRICES FOR SHUFFLED IMAGES. The contours indicate correlation strengths of 0.4, 0.2, 0.1, and 0.05, respectively. From left to right: 0° , 45° , 90° , 135° . From top to bottom: $\lambda = 5 \text{ px}$, $\lambda = 10 \text{ px}$, $\lambda = 20 \text{ px}$, and $\lambda = 40 \text{ px}$.

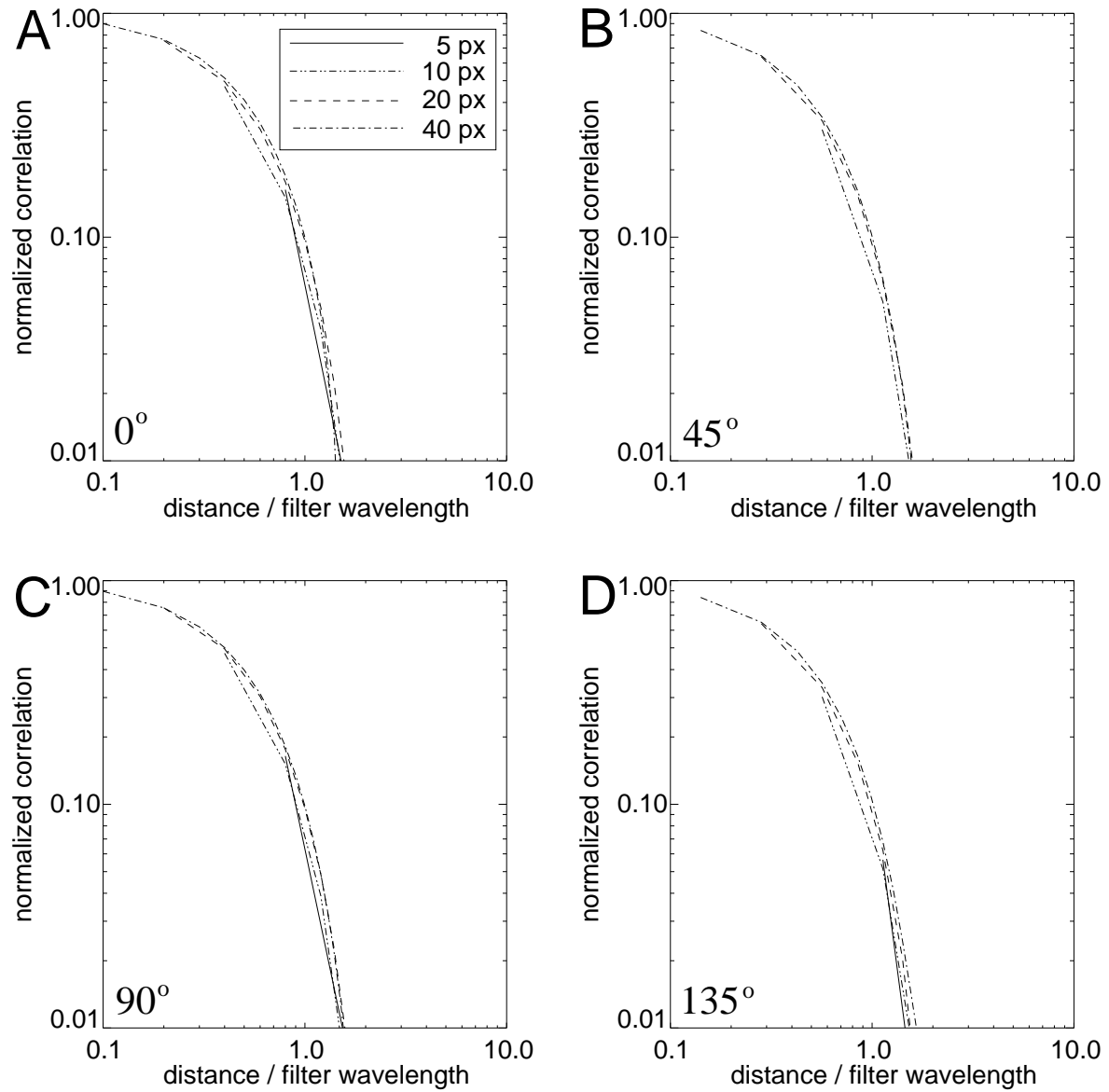


Figure 3.14: COLLINEAR CORRELATIONS FOR SHUFFLED IMAGES. (A) 0° , (B) 45° , (C) 90° , and (D) 135° . For shuffled images, collinear correlations are scale- and rotation-invariant. Compare Figure 3.11.

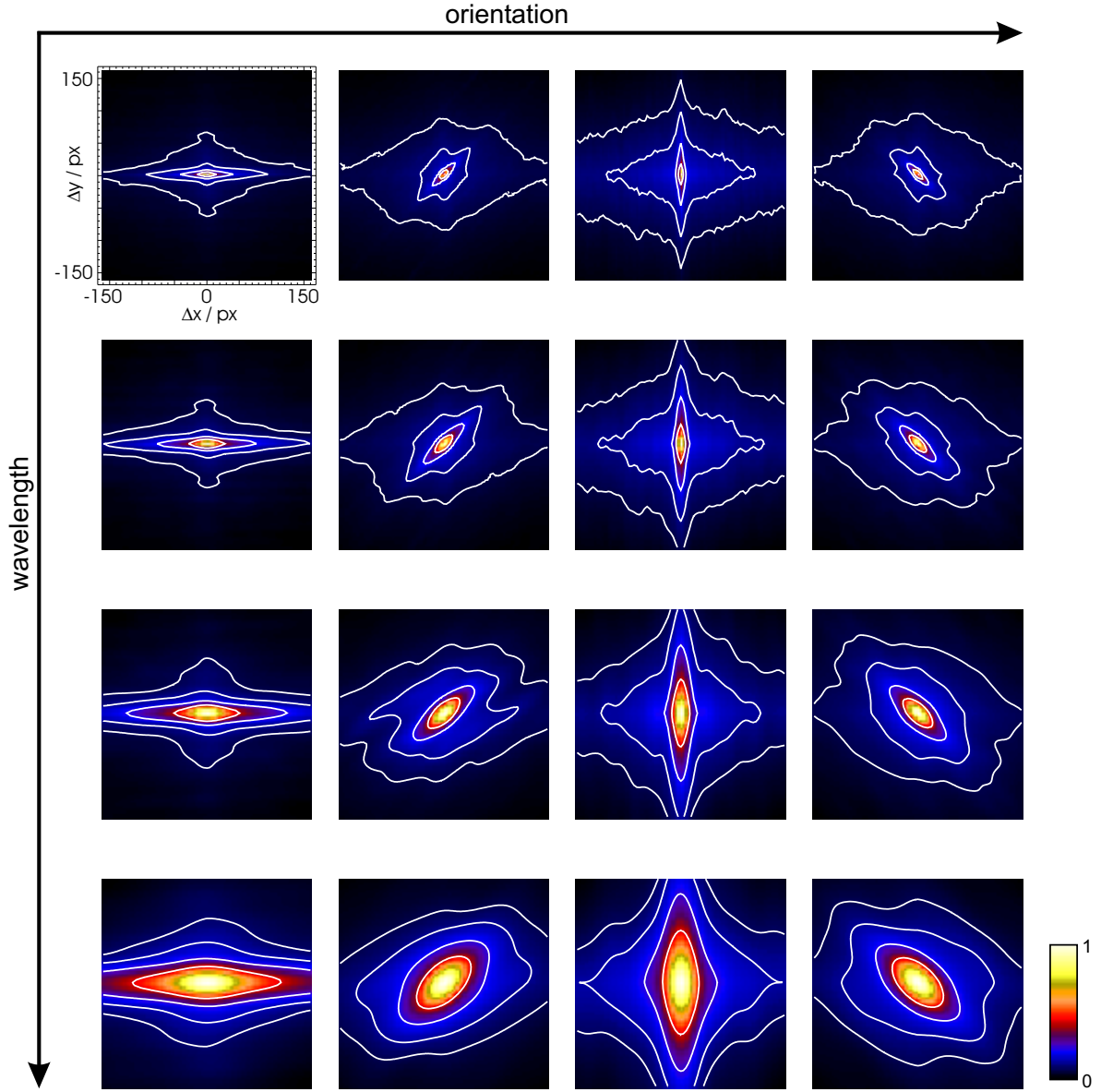


Figure 3.15: TWO-DIMENSIONAL AUTOCORRELATION MATRICES FOR NON-NORMALIZED WAVELET RESPONSES. The contours indicate correlation-levels of 0.4, 0.2, 0.1, and 0.05, respectively. From left to right: 0° , 45° , 90° , 135° . From top to bottom: $\lambda = 5$ px, $\lambda = 10$ px, $\lambda = 20$ px, and $\lambda = 40$ px.

3.4.5 Non-Normalized Wavelet Responses

In order to estimate the influence of the thresholding and normalization procedure on the correlations, we computed the autocorrelation functions for the non-normalized wavelet responses R_1 . This is shown in Figure 3.15. There is an increased correlation in the collinear

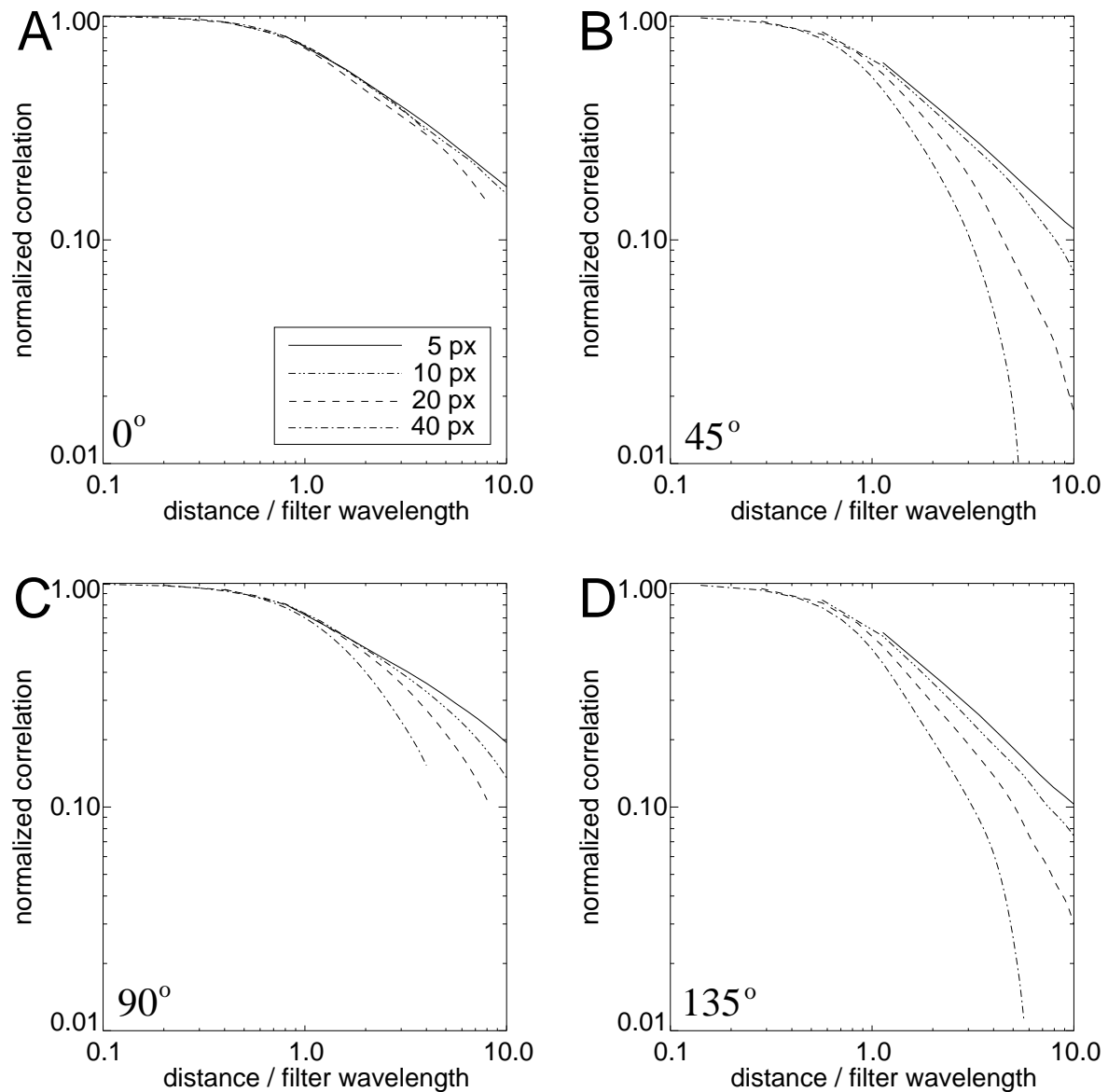


Figure 3.16: COLLINEAR CORRELATIONS OF THE NON-NORMALIZED WAVELET RESPONSES. Compare Figure 3.11.

direction, but the effect is generally not as clearly visible as for the normalized wavelet responses (Figure 3.9).

However, as can be seen in Figure 3.16, collinear correlations depend in a similar way on the orientation and wavelength of the wavelets as for the normalized wavelet responses, and decrease more steeply with increasing distance for wavelets of large wavelengths.

3.5 Discussion

The spatial response properties of neurons in the primary visual cortex of cats and monkeys can be described by Gabor wavelets of different orientations and wavelengths for cortical simple cells, or, in the case of cortical complex cells, as a nonlinear superposition thereof (Adelson and Bergen, 1985). We investigated how the statistics of Gabor wavelet responses, extracted from real-world images, change with both the orientation and the spatial scale of the wavelets.

3.5.1 Summary of Results

We have shown that the average normalized strength of wavelet responses depends both on their orientation and the semantical content of the real-world scenes, but that the relative response strengths for different wavelet orientations do not qualitatively change with the scale of the wavelets used. However, differences between cardinal and obliquely oriented wavelets are slightly more pronounced for wavelets of large wavelengths.

Collinear correlations between wavelets of the same orientation are in general not scale invariant. In retinal coordinates, correlations are more long-range for wavelets of larger wavelengths. However, transformed to distances, normalized by the wavelength of the wavelets, correlations are more short-range for wavelets of larger wavelengths. Furthermore, collinear correlations are not invariant with respect to the orientations of the wavelets. Collinear correlations between wavelets of oblique orientations are more short-range than collinear correlations between wavelets of cardinal orientations of the same wavelength.

3.5.2 Anisotropy of Normalized Wavelet Responses

We found an anisotropy in the averaged normalized wavelet-responses dependent on the orientation of local contour elements and on the semantical scene-category analyzed. The orientation-anisotropy is consistent with an effect described in psychophysical and neurophysiological measurements as the *oblique effect*. In humans and animals, the perception of horizontally and vertically oriented contours is superior to the perception of contours of oblique orientations. This has been documented in psychophysical measurements of contrast sensitivity, orientation discrimination and recognition rate (e.g., Appelle, 1972; Heeley et al., 1997; Krebs et al., 2000). A possible neural substrate for the oblique effect could be an overrepresentation of neurons selective for horizontal and vertical contours, which has been demonstrated in single cell recordings in cats (e.g., Orban and Kennedy, 1981; Leventhal

and Hirsch, 1980; Bauer et al., 1990; Li et al., 2003), monkeys (e.g., Mansfield and Ronner, 1978) and ferrets (Coppola et al., 1998b). In optical imaging studies in cats it has further been shown that horizontally and vertically oriented stimuli evoke stronger responses in comparison to obliquely oriented stimuli (Dragoi et al., 2001). Vertically and horizontally oriented stimuli cause larger visually evoked potentials in comparison to obliquely oriented stimuli in cats (Bonds, 1982) and monkeys (Mansfield and Ronner, 1978; Bonds et al., 1987), and result in faster and larger evoked potentials in humans (Arakawa et al., 2000). An anisotropy with respect to horizontal and vertical orientations has also been demonstrated as early as in retinal ganglion cells, whose dendrites are preferentially arranged along the vertical and horizontal meridian (Wässle et al., 1975).

Less is known about the dependence of the oblique effect on the spatial scale of oriented stimuli and their position within the visual field. In the macaque visual cortex there is a predominance of neurons which respond to high spatial frequencies and prefer cardinal orientations, while there is no such effect for neurons with low spatial frequency preference (De Valois et al., 1982; Li et al., 2003). Another study found that neurons selective for middle to low spatial frequencies even prefer oblique orientations (Nelson et al., 1984). Evidence exists that the overrepresentation of contours of different orientations depends on the position within the visual field: While in the striate cortex of cats horizontal and vertical orientations are overrepresented in the central visual field, in the periphery there is an overrepresentation of radial orientations in the upper layers and of concentric orientations in the lower layers (Bauer et al., 1990).

The oblique effect may have its cause in the statistical properties of natural scenes. The predominance of contours oriented along the cardinal axes is a robust phenomenon in the statistics of real-world scenes (e.g., Coppola et al., 1998a; Hancock et al., 1992; Van der Schaaf and Hateren, 1996; Keil and Cristóbal, 2000; Betsch et al., 2004). The bias towards horizontal and vertical contour orientations is most probably due to the horizontal surface of the earth on the one hand, and gravity on the other hand, which causes plants to develop supports parallel to the direction of the gravity vector and horizontal surfaces to effectively absorb sunlight (Coppola et al., 1998a). However, the quantitative relations between cardinal and oblique orientations depend on the semantical content of the examined real-world scenes (e.g., Coppola et al., 1998a; Keil and Cristóbal, 2000). For example, natural scenes with plants and no man-made objects show a more uniform distribution of orientations than do scenes with man-made objects (Coppola et al., 1998a), which is consistent with our results (Figure 3.7).

3.5.3 Scale Invariance of Contour Integration

We have demonstrated that correlation strength along the axis of orientation declines faster with distance for wavelets of large wavelengths compared to wavelets of short wavelengths. If collinear horizontal connections self-organize according to the spatial statistics of the natural environment, our results imply that the effect of collinear facilitation should be weaker between neurons with a preference for low spatial frequencies compared to facilitation between neurons at the same relative distance with a preference for high spatial frequencies.

However, several psychophysical studies have demonstrated an independence of collinear facilitation on the spatial scale of the targets, at least in the foveal representation of the visual field (Polat and Sagi, 1993; Hess and Dakin, 1997; Woods et al., 2002). Our results cannot account for the independence of collinear facilitation on spatial scale in the fovea.

A possible reason for this discrepancy could be the specific shape of the spatial filters used in the current study, or the particular choice of the real-world scenes, manually selected by a human observer. Another possibility for this discrepancy could be that neurons with cRFs of large wavelengths have a larger cRF overlap in the fovea than neurons with cRFs of small wavelengths, which would result in an effectively stronger lateral coupling and a better signal-to-noise ratio between neurons of large wavelengths. However, we are not aware of experimental data subserving this hypothesis. Furthermore, it is possible that learning of long-range horizontal connections is influenced by scale-combination processes between neurons of different spatial frequency preferences. It has been demonstrated that the detection of straight paths of Gabor elements is possible even for paths composed of alternating Gabor elements of different spatial frequencies for differences in spatial frequency up to ≈ 1.3 octaves (Dakin and Hess, 1998). Thus, the investigation of spatial correlations between wavelet-responses of different spatial scales would be a valuable extension of the current study.

3.5.4 Dependence of Spatial Scene Statistics on Eccentricity

With increasing eccentricity, the peak spatial frequency preference of neurons in the primary visual cortex shifts to lower values (De Valois et al., 1982), while at the same time cortical magnification declines (e.g., Dow et al., 1981; Van Essen et al., 1984; Slotnick et al., 2001). If collinear horizontal connections self-organize according to the spatial statistics of the natural environment, our results imply that the length of these connections is not scale invariant with respect to the spatial filter properties of the corresponding RFs at different eccentricities: Lateral connections between neurons with small RFs in the fovea should be

longer in range in cortical coordinates than lateral connections between neurons with larger RFs in the periphery, scaled in accordance with cortical magnification. This could lead to a decreased grouping performance for collinearly arranged elements in the periphery, even if stimuli are scaled according to cortical magnification. However, our results can not explain the nearly absent collinear facilitation even for stimuli at small retinal eccentricities (e.g., Zenger-Landolt and Koch, 1996; Shani and Sagi, 2005).

The extrapolation of our results to the image statistics at different eccentricities depends on the assumption that the spatio-temporal statistics of the environment, as projected on the retina, is constant across the whole visual field. This, however, is not strictly the case (Reinagel and Zador, 1999; Krieger et al., 2000). Vision is an active process. Nearly all animals with visual systems actively control their gaze with their eyes, head, or body movements. In fact, this active gaze control is the most important mechanism in order to direct attention to interesting parts of visual scenes. On average, high spatial frequency content, edge density, and contrast are highest at the point of fixation (Mannan et al., 1996, 1997; Reinagel and Zador, 1999). Furthermore, spatial correlations at the center of gaze are on average lower in comparison to the correlations across the whole visual field. Thus, it is possible that the spatial statistics of peripheral contours in real-world scenes differ from the spatial statistics in the fovea under natural viewing conditions.

Another reason for the psychophysically decreased collinear facilitation with increasing eccentricity could be a change in the temporal response characteristics of neurons with increasing eccentricity. With increasing eccentricity, the ratio of parvocellular to magnocellular inputs from the LGN to the primary visual cortex decreases from 35:1 in the fovea to 5:1 at 15° eccentricity (Azzopardi et al., 1999). If contour integration is mainly accomplished by parvocellular neurons mediating fine, slowly changing details within visual scenes, this decrease could account for a reduced performance with increasing eccentricity.

These points cannot be answered on the basis of the set of real-world images used in this study. A possibility to further study the influence of spatial and temporal inhomogeneities at different positions within the visual field could be the use of a mobile eye-tracker device to record movies of visual scenes as seen by freely moving observers and analyze both the change in spatial and temporal statistics across the visual field. Furthermore, this could reveal interesting differences in the cortical connectivity of different species, depending on posture, movement speed, and the characteristic properties of different environments.

In addition, attentional mechanisms seem to play a role in modulating collinear facilitation (e.g., Ito and Gilbert, 1999; Freeman et al., 2001; Giorgi et al., 2004; Shani and Sagi, 2005), which implies that collinear facilitation performance can not solely be predicted by

the lateral connectivity.

Chapter 4

Self-Organization of Lateral Connections

Stimulus Velocity Influences Self-Organization of Lateral Connections in a Network Model of Pulse-Coding Neurons with Hebbian Learning

4.1 Abstract

In the primary visual cortex, horizontal connections between neurons of similar feature preference are supposed to mediate contextual influences from outside the classical receptive field (cRF). This provides a mechanism which could support the perceptual grouping and segregation of local *spatial* features in visual scenes into coherent visual objects. Additionally, it has been suggested that asymmetric horizontal connections may enhance the selectivity of neurons for the direction of stimulus movement, thus providing a mechanism for the coding of *spatio-temporal* stimulus attributes. What factors determine the shape of the lateral connectivity during learning? We investigated the influence of stimulus velocity and the conduction velocity of the lateral connections on the self-organization of lateral connections in a single-layer network model of pulse-coding neurons with a temporal Hebbian learning rule. We show that stimulus velocities much lower than the conduction velocity of the lateral connections favor the development of lateral connections which are well adapted to the spatial structure of the visual input. High stimulus velocities lead to lateral connections which support the coding of the spatio-temporal structure of the visual input. Considering the different temporal response characteristics of magnocellular (temporal bandpass) and parvocellular (temporal lowpass) neurons, we discuss possible influences of these two retino-cortical pathways on the encoding of object-motion and object-form in the cortical dorsal and ventral pathways, respectively. Additionally, our results may help in understanding the decreased

collinear facilitation and path detection performance for peripheral compared to foveal stimuli which has been found in psychophysical experiments.

4.2 Introduction

Lateral connections between neurons of similar feature preference may serve as a possible neuronal substrate for mediating contextual influences and supporting the grouping of local *spatial* image features within a visual scene into coherent objects (experiment: e.g., Gilbert and Wiesel, 1989, 1990; Bosking et al., 1997; Schmidt et al., 1997; Stettler et al., 2002, model: e.g., Eckhorn et al., 1990; Ostkamp, 1996; Yen and Finkel, 1998; Li, 1999; Neumann and Sepp, 1999; Hansen et al., 2001). In model studies it has been demonstrated that lateral connections can self-organize according to the spatial statistics of artificial or real-world scenes by Hebbian learning mechanisms (e.g., Grossberg and Williamson, 2001; Prodhöhl et al., 2003; Choe and Miikkulainen, 2004). In addition to the grouping of spatial features within a visual scene, lateral connections may enhance the selectivity of cortical neurons for the direction of stimulus movement, although the actual mechanisms, leading to direction selectivity are still a matter of debate (e.g., Feidler et al., 1997; Wimbauer et al., 1997; Livingstone, 1998; Clifford and Ibbotson, 2003). In model studies it has been demonstrated that asymmetric lateral connections, linking neurons along the direction of motion, lead to direction selective response properties (e.g., Mineiro and Zipser, 1998; Shon et al., 2004). The required lateral connectivity can be learned by Hebbian mechanisms from directed motion stimuli (e.g., Jastorff and Giese, 2004; Shon et al., 2004; Wenisch et al., 2005). We investigated which properties of the network and the visual input determine the shape of the lateral connectivity during learning.

4.2.1 Conduction Velocities of Lateral Connections

Interactions between neurons are mediated by action potentials which travel with finite velocity along axons. The conduction velocity depends on the axon's diameter and its myelination (e.g., Rushton, 1951; Waxman and Bennett, 1972). Another factor limiting the velocity of the spread of activation between neurons is the neural activation time, which may vary substantially depending on the activation state of the neurons. Typical values of conduction velocities along horizontal connections range from 0.1-0.6 m/s in cats (Komatsu et al., 1988; Hirsch and Gilbert, 1991) and rats (Murakoshi et al., 1993; Nowak and Bullier, 1998), which is consistent with the lateral spread of synaptic activity in monkeys, as revealed by optical

imaging studies (Grinvald et al., 1994; Sloviter et al., 2002).

4.2.2 Parallel Retinal and Cortical Processing Streams

Throughout the visual system sensory information is processed along parallel pathways of neurons with different spatio-temporal response properties.

The two major retino-cortical processing streams are the magnocellular (M) and parvocellular (P) pathways originating in the retinal ganglion cells. The cRFs of M-neurons in the LGN are by a factor of 2–3 larger than the cRFs of P-neurons at the same eccentricity (e.g., Xu et al., 2002). While the temporal response characteristics of P-neurons resemble a temporal lowpass filter, M-neurons display temporal response properties resembling a temporal bandpass filter (e.g., Hicks et al., 1983; Kaplan and Bernadete, 2001). Additionally, M-neurons exhibit steeper contrast gain functions than do P-neurons at the same eccentricity (Kaplan and Shapley, 1986). P-neurons encode most of the chromatic information within a visual scene due to the spectral opponency of their cRF center and surround, while M-neurons are virtually insensitive to color and respond primarily to luminance stimuli (e.g., De Monasterio, 1978). In the LGN of monkeys, the proportion of P- to M-neurons at a given eccentricity is not constant across the visual field, but declines with increasing eccentricity from 35:1 in the fovea to 5:1 at 15° eccentricity (Azzopardi et al., 1999).

Lesions of the parvocellular layers of the LGN (P-lesions) cause a 3- to 4-fold reduction in spatial acuity in monkeys while magnocellular lesions (M-lesions) do not effect acuity (Merigan et al., 1991a,b). Luminance and chromatic contrast sensitivities for static gratings of high spatial frequency are reduced for P-lesions, but not for M-lesions. However, luminance contrast sensitivity for low spatial frequency gratings, modulated at a temporal frequency of 10 Hz, is reduced by both P- and M-lesions.

It has been suggested that the P- and M-pathways are dedicated to different visual tasks: The P-pathway dominates chromatic vision, acuity, and contrast detection at low temporal and high spatial frequencies, pointing out its role in the analysis of form and color, while the M-pathway dominates contrast detection at higher temporal and lower spatial frequencies, suggesting its role in motion analysis (e.g., Merigan et al., 1991b; Kaplan and Bernadete, 2001).

Cortically, information is processed along at least two pathways: The dorsal pathway, which originates in V1 and leads to the posterior parietal cortex, and the ventral stream, leading from V1 to the inferior temporal cortical areas (Ungerleider and Mishkin, 1982; Felleman and Van Essen, 1991; Goodale et al., 1991). There is experimental evidence that

these two pathways serve different visual functions, namely the processing of color and shape information in the ventral pathway (e.g., Ungerleider and Mishkin, 1982; Goodale et al., 1991, 1994; Perrett et al., 1982; Desimone et al., 1984; Tanaka, 1993; Logothetis et al., 1995; Rolls, 2000; Quiroga et al., 2005), and position and motion information in the dorsal pathway (e.g., Andersen et al., 1997; Duhamel et al., 1997; Bremmer et al., 2000, 2001).

It seems plausible that the different spatio-temporal response properties of neurons along retino-cortical M- and P-pathway may favor different characteristic coding strategies within both cortical pathways during learning, despite the fact that the mapping of the M- and P-projections onto the cortical dorsal and ventral pathway is not complete (e.g., Ferrera et al., 1994; Yabuta et al., 2001; Sincich and Horton, 2003).

4.2.3 Goal of the Model

We assumed that the development of the lateral connections subserving the coding of both spatial and temporal properties of visual scenes relies on activity-dependent, Hebbian learning mechanisms. Therefore, we asked which factors determine the structure of the resulting lateral connectivity during learning. We investigated the influence of stimulus velocity and the conduction velocity of lateral connections on the self-organization of lateral connections in a single-layer network model of pulse-coding neurons due to a Hebbian learning rule. We demonstrate that stimulus velocities much lower than the conduction velocity of the lateral connections favor the development of connections adapted to the spatial structure of the visual input. High stimulus velocities lead to lateral connections supporting the coding of the spatio-temporal structure of the visual input. We discuss possible influences of the different temporal filter properties of neurons of the retino-cortical M- and P-pathways on the coding of spatial (form) and spatio-temporal (motion) stimulus attributes along the cortical dorsal and ventral pathway, respectively.

4.3 Methods

4.3.1 Network Architecture

Model Neuron

We used pulse coding neurons with realistic synaptic potentials and a dynamic threshold (Eckhorn et al., 1990), similar to the ones used in Chapter 2¹. The input stage of a neuron i consists of synapses $S_{ij}(t)$ to presynaptic neurons j , which have a synaptic connection strength w_{ij}^S and an impulse response $h(t, \tau)$:

$$S_{ij}(t) = w_{ij}^S I_j(t - \Delta_{ij}) * h(t, \tau_S), \quad (4.1)$$

where $*$ is the convolution operator, I_j is the spike-output of the presynaptic neuron j . Δ_{ij} is the conduction delay between neuron i and neuron j .

The synaptic response $h(t, \tau)$ was modelled as a leaky integrator:

$$h(t, \tau) = \exp(-t/\tau) H(t), \quad (4.2)$$

where $H(t)$ denotes the Heaviside function:

$$H(t) = \begin{cases} 0 & t < 0 \\ 1 & t \geq 0 \end{cases}. \quad (4.3)$$

Thus, each connection performs an exponentially decaying summation of signals from presynaptic neurons.

The model neurons have three types of different synapses, excitatory feeding F , inhibitory feeding I , and linking L synapses. The resulting membrane potential of neuron i , which drives the spike encoder, is

$$M_i(t) = \sum_j F_{ij}(t) \cdot \left(1 + \sum_j L_{ij}(t) \right) - \sum_j I_{ij}(t) + I_{\text{noise}}(t), \quad (4.4)$$

with $I_{\text{noise}}(t)$ being normally distributed noise with standard deviation σ_{noise} , added independently to every membrane potential in each time step.

While excitatory (inhibitory) feeding inputs have an additive (subtractive) influence on the membrane potential, the signals of the linking synapses act multiplicatively on the excitatory feeding-inputs. In V1, long-range lateral connections are mainly found between neurons

¹The description of the model neurons has some common parts with the description in Chapter 2. We decided to maintain this duplication in order to preserve the self-containedness of the different chapters.

of the upper layers, where the synapses are dominated by NMDA-type channels (Fox et al., 1989), which have been reported to act on the afferent input in a modulatory fashion (Fox and Daw, 1992). Modulatory linking-connections ensure that the cRFs of single neurons are not altered by the lateral connectivity (Eckhorn et al., 1990).

In the spike encoder, the membrane potential $M_i(t)$ is compared to a dynamic threshold $\Theta_i(t)$. If $M_i(t)$ exceeds $\Theta_i(t)$, a spike is generated:

$$O_i(t) = H(M_i(t) - \Theta_i(t)). \quad (4.5)$$

The spike threshold has both a dynamic component, which is modelled as the impulse response of a single leaky integrator, and a static component Θ_0 :

$$\Theta_i(t) = O_i(t) * (V_\Theta \exp(-t/\tau_\Theta)) H(t) + \Theta_0. \quad (4.6)$$

All network parameters are summarized in Table 4.1.

Network Topology

The network-model consists of a single layer of pulse-coding neurons, arranged on a 21×21 Cartesian grid (Figure 4.1). In order to avoid boundary effects, toroidal boundary conditions were applied. Each neuron provides input to neighboring neurons via lateral inhibitory feeding-synapses. Inhibitory synaptic connection strengths decay according to a Gaussian function (amplitude G_I , width σ_I). This form of inhibition was chosen for convenience, in order to keep the network as simple as possible. The main purpose of the inhibition in the current network is to counteract the effect of strong excitatory and modulatory inputs. In a more realistic scenario, excitatory neurons would act inhibitory on other excitatory neurons only via inhibitory interneurons.

Neurons receive excitatory input via their feeding-synapses, representing the afferent visual input. Although we did not model the cRFs explicitly, the neurons can be thought of as having retinotopically arranged, equally spaced cRFs of identical orientation and direction preferences, i.e., each neuron is sensitive to an oriented stimulus at a certain position within the visual field, moving in a direction perpendicular to its orientation.

Additionally, neurons can form lateral linking connections with all other neurons. The development of these connections is due to Hebbian learning (see Section 4.3.3).

In the first set of simulations we modelled infinite conduction velocities for both the modulatory and inhibitory feeding connections. In the remaining simulations, modulatory linking and inhibitory feeding conduction velocities were set to 0.1 g.u./ms.

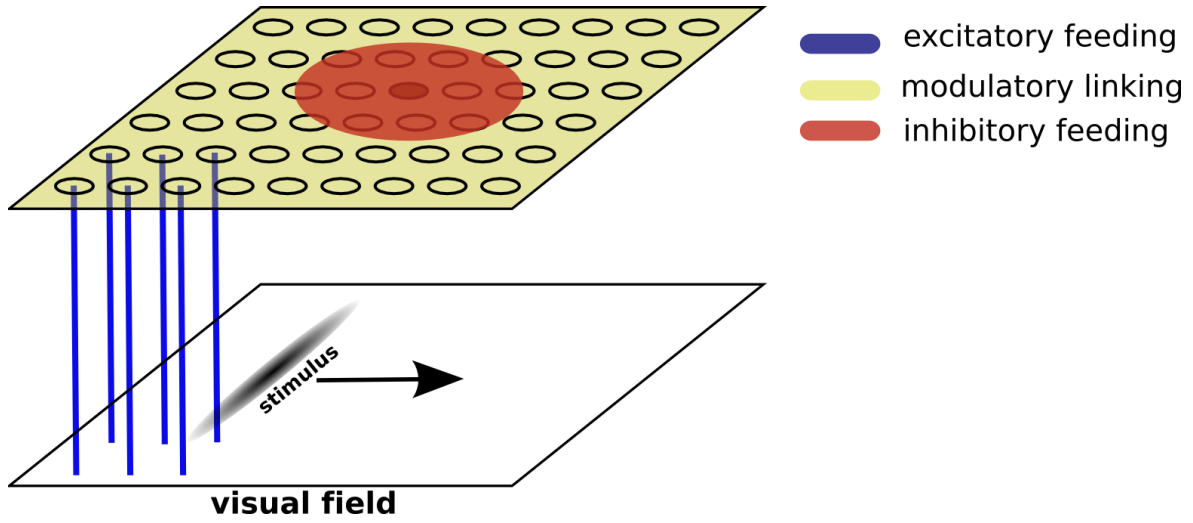


Figure 4.1: MODEL ARCHITECTURE AND INPUT STIMULI. The network consists of a single layer of spiking neurons. Every neuron receives input signals from a corresponding region of the visual field. Neurons interact via inhibitory feeding-connections and lateral linking connections. The latter were subject to Hebbian learning. Initially, the synaptic connection strengths of the lateral linking connections were zero. Input stimuli were oriented Gaussian bars of simulated light intensity of fixed orientation, moving in a direction perpendicular to their orientation-axis.

4.3.2 Input Stimuli

Input stimuli were elongated Gaussian bars of simulated light intensity with vertical orientation. A Gaussian bar, centered at position (x_c, y_c) and orientation α is described by the equation

$$G(x, y) = \exp \left(-\frac{(x - x_c)^2}{2\sigma_a^2} - \frac{(y - y_c)^2}{2\sigma_b^2} \right).$$

The width- and length-constants were chosen as $\sigma_a = 0.5$ and $\sigma_b = 3.0$ grid units (g.u.).

The bars were presented at random positions within the visual field and moved perpendicularly to their length axis with fixed velocities of $v = 0.0$ (0.05, 0.1) g.u./ms, or with random velocities, taken from different velocity-distributions (compare Section 4.4.3).

Each presentation phase lasted for 100 ms, followed by a pause of 100 ms, after which a new random position was chosen. The pause of 100 ms was not critical for the qualitative shape of the learned lateral connections, but it improved the smoothness of the learned connectivity. Without a pause between successive stimulus presentations, the slow lateral conduction velocities of 0.1 g.u./ms caused learning events between spikes of neurons activated

by the current stimulus, and spikes of neurons activated by a prior stimulus presentation. This effect is due to the small network size and the restricted set of stimuli.

4.3.3 Self Organization

Synaptic coupling strengths between horizontal connections were updated according to a temporal Hebbian learning rule. Each presynaptic spike initiates a synaptic learning potential

$$L_{ij}(t) = O_i(t - \Delta_{ij}) * (\exp(-t/\tau_l)H(t)). \quad (4.7)$$

The learning potential was modelled as a leaky integrator with time constant τ_l . Every time the postsynaptic neuron i spikes, the connection strengths between all presynaptic neurons j and the postsynaptic neuron are changed according to the current value of the learning potentials:

$$\Delta w_{ij}(t) = \gamma O_i(t) L_{ij}(t), \quad (4.8)$$

$$w_{ij}(t) = w_{ij}(t-1) + \Delta w_{ij}(t). \quad (4.9)$$

Hebbian learning rules are inherently unstable: Correlated activity leads to stronger synaptic connection strengths which in turn lead to correlated activity between the corresponding neurons. In order to prevent the synaptic connection strengths from growing without bounds, we applied a normalization procedure in every time step. If the total connection strength to a postsynaptic neuron i was greater or equal than a maximum value A_{norm} , every weight to this neuron was divided by a common factor, so that the total connection strength was equal to A_{norm} . Thus, the total connection strength to a postsynaptic neuron i was always less than or equal to A_{norm} :

$$\sum_j w_{ij} \leq A_{\text{norm}}. \quad (4.10)$$

The learning parameters are summarized in Table 4.1.

4.3.4 Data Analysis

In order to quantify the fraction of the total synaptic connection strength between neurons with collinearly aligned cRFs, we defined a *collinearity index* CI as the sum of the synaptic connection strengths from a single neuron j to neurons with collinearly aligned cRFs, divided by the total synaptic connection strength from this neuron to all other neurons:

| Neuron Parameters | | | |
|-------------------------|-------|------------|-------------------|
| τ_F | 10 ms | τ_L | 10 ms |
| τ_I | 10 ms | Θ_0 | 1.0 |
| τ_Θ | 5 ms | V_Θ | 5 |
| σ_{noise} | 0.2 | | |
| Network Parameters | | | |
| G_I | 0.005 | σ_I | 5 g.u. |
| Learning Parameters | | | |
| τ_l | 15 ms | γ | $2 \cdot 10^{-4}$ |
| A_{norm} | 0.5 | | |

Table 4.1: NEURON, NETWORK AND LEARNING PARAMETERS

$$CI = \left\langle \frac{\sum_{i||j} w_{ij}}{\sum_i w_{ij}} \right\rangle_j, \quad (4.11)$$

where the relation $i||j$ holds for all neurons i and j with collinearly aligned CRFs. $\langle \rangle_j$ denotes the average over all neurons j . The collinearity index has a value of one for lateral connections only between neurons with collinearly aligned cRFs, and has a value of zero for lateral connections not connecting neurons with collinearly aligned cRFs at all.

4.4 Results

4.4.1 No Lateral Conduction Delays

In the first set of simulations the conduction delays of the lateral connections were set to zero, which corresponds to infinitely high conduction velocities. Three different simulations were carried out, with three different stimulus velocities (0.0, 0.05, and 0.1 g.u./ms). Figures 4.2A,B,C show the average lateral connection strengths from a single neuron to the surrounding neurons for the three different simulations.

After training the network with static stimuli, the lateral connections are adapted according to the spatial shape of the bar, with strong reciprocal connections mainly between neurons along the orientation axis of the bar (Figure 4.2A).

For higher stimulus velocities, the connection profiles are broader with an asymmetry towards the direction of the bar-movement (Figures 4.2B,C). Less of the total connection

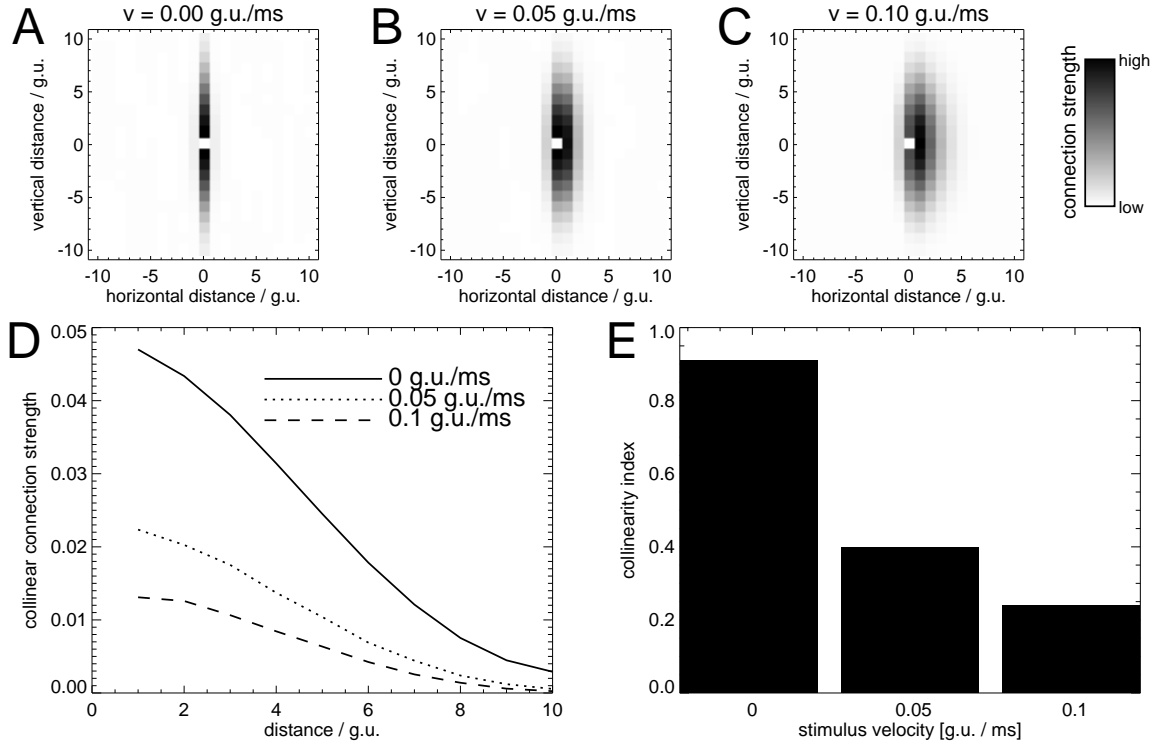


Figure 4.2: LATERAL CONNECTIVITY AFTER LEARNING WITHOUT LATERAL CONDUCTION DELAYS. (A-C) show the average lateral synaptic connection strengths of a neuron (centered) to its surrounding neurons after training with stimuli moving at different velocities (0.0, 0.05, and 0.1 g.u./ms). The intensities are scaled independently for each diagram, with white for low and black for high synaptic connection strengths. After training with static stimuli, lateral connections are mainly learned between neurons along the vertical orientation-axis of the bar. For moving stimuli, the lateral connection profile becomes asymmetric towards the direction of stimulus movement. (D) Average lateral connection strengths along the collinear direction for the three different stimulus velocities. The higher the stimulus velocity during learning, the smaller are the collinear connection strengths between neurons with collinearly aligned cRFs. (E) Collinearity index for simulations with different stimulus velocities during learning. After learning with static stimuli, nearly 90% of the total connection strength is due to connections between neurons with collinearly aligned cRFs. For faster stimulus movements, the collinearity index declines due to connections formed between neurons whose cRFs are not collinearly aligned.

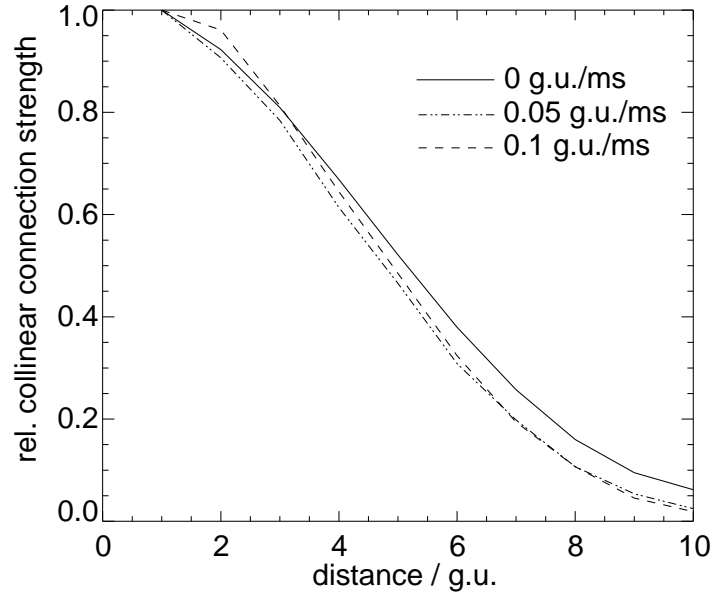


Figure 4.3: RELATIVE DECLINE IN COLLINEAR CONNECTION STRENGTH AFTER LEARNING WITHOUT LATERAL CONDUCTION DELAYS. Shown are the lateral synaptic connection strengths along the collinear direction, normalized to the collinear connection strength for neurons with a relative distance of 1 grid unit. The shapes of the normalized collinear connection profiles are similar for all three stimulus velocities (compare Figure 4.2D).

strength is concentrated along the collinear direction.

Figure 4.2D shows the decline in lateral connection strength with increasing distance along the collinear direction. This is further quantified in Figure 4.2E which shows the collinearity indices for the three different simulations. Note that although the absolute connection strengths along the collinear direction decline with increasing stimulus velocity, the relative shape of the decline does not change qualitatively (Figure 4.3).

The “broadening” of the lateral connectivity profile towards the direction of stimulus movement is caused by the temporal extent of the Hebbian learning window. This is demonstrated in Figure 4.4, which shows the results from a set of simulations where the decay constant of the presynaptic learning potential τ_l was set to a small value of 1 ms. In this case, there are only small changes in the shape of the learned lateral connectivity with increasing stimulus velocity.

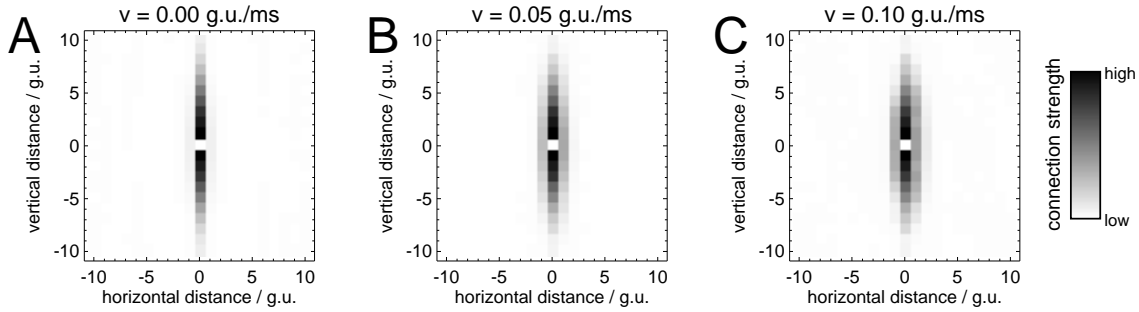


Figure 4.4: LATERAL CONNECTIVITY AFTER LEARNING WITHOUT LATERAL CONDUCTION DELAYS AND A SHORT LEARNING WINDOW. (A-C) show the average lateral synaptic connection strengths from a neuron (centered) to its surrounding neurons due to input stimuli moving at different velocities (0.0, 0.05, and 0.1 g.u./ms). For the depicted case of learning with a short learning window ($\tau_l = 1$ ms), changes in lateral connectivity with increasing stimulus velocity are smaller than in the case of a longer learning window (compare Figure 4.2).

4.4.2 Finite Lateral Conduction Velocity

In the next set of simulations, lateral conduction velocities were set to 0.1 g.u./ms, thus being identical to the highest stimulus velocity applied during learning.

For static stimulation, lateral connections are learned along the direction of orientation of the bar (Figure 4.5A). A comparison of Figure 4.5D with Figure 4.2D reveals that collinear coupling is shorter in range for learning with static stimuli and finite conduction velocities than in the situation of static stimuli and infinite conduction velocities. This effect depends strongly on the duration of stimulus presentation: Imagine two neurons i and j at a relative distance d , activated simultaneously by a static stimulus. Due to the finite conduction velocity v , a spike needs the time $t = d/v$ to travel from neuron i to neuron j . With a lateral conduction velocity of $v = 0.1$ g.u./ms and a distance $d = 10$ g.u., a spike needs 100 ms to travel from neuron i to neuron j . Thus, if the duration of the stimulus presentation is less than 100 ms, simultaneous activation of neurons i and j will never lead to a coincidence of pre- and postsynaptic spikes. A strengthening of the corresponding synaptic weights is only possible due to the finite temporal extent of the Hebbian learning window. In the current simulation, the maximum lateral coupling range is restricted to a distance of approximately 10 g.u., due to the fixed stimulus duration of 100 ms and the lateral conduction velocity of 0.1 g.u./ms. Longer stimulus presentation times would lead to longer collinear connec-

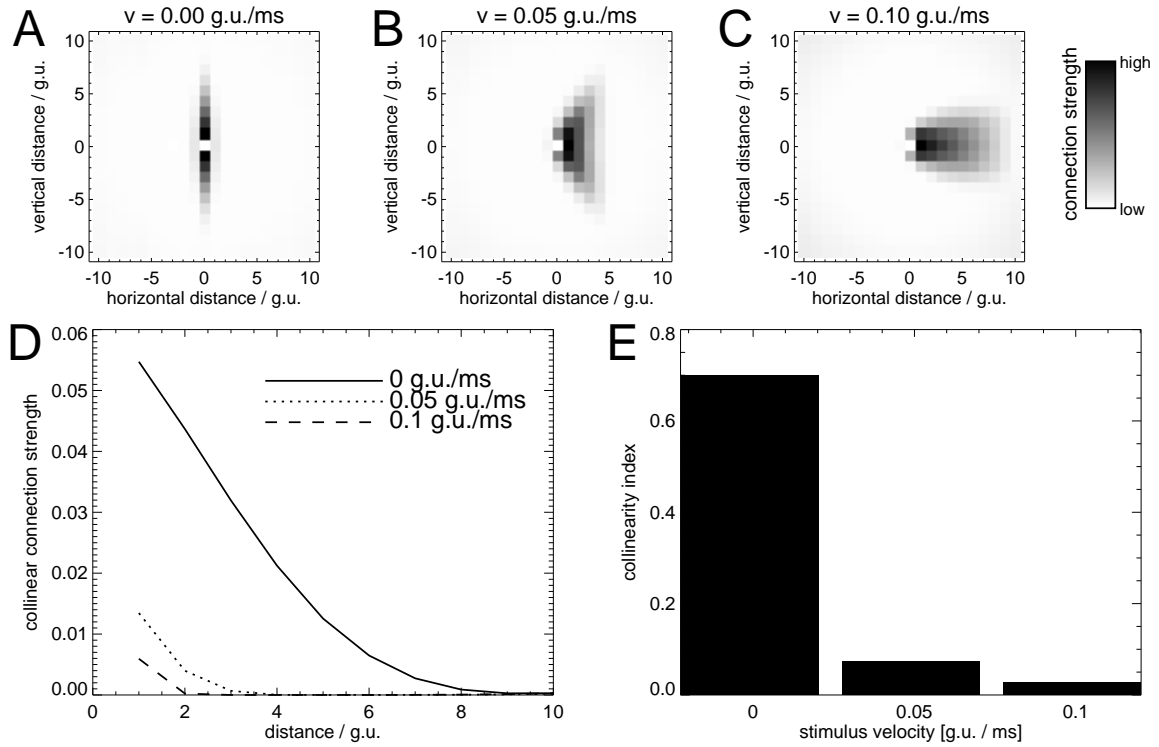


Figure 4.5: LATERAL CONNECTIVITY AFTER LEARNING WITH FINITE LATERAL CONDUCTION VELOCITIES. (A)-(C) show the average lateral synaptic connection strengths of a neuron (centered) to its surrounding neurons after training with stimuli moving at different velocities (0.0, 0.05, and 0.1 g.u./ms). The intensities are scaled independently for each diagram, with white for low and black for high synaptic connection strengths. For static stimulus presentations lateral connections are learned between neurons along the orientation-axis of the bar. For moving stimuli, each neuron forms connections with other neurons at positions shifted towards the direction of stimulus-movement. For stimulus velocities equal to the conduction velocity of the lateral connections, neurons form predominantly connections with neurons along the direction of stimulus movement. (D) Average strength of lateral connections along the collinear direction for the three different stimulus velocities. The higher the velocity of stimulus movement, the faster collinear connection strengths decline with increasing distance of source- and target-neuron. (E) Collinearity indices for the corresponding simulations. After learning with static stimuli, 70% of the total connection strength is due to connections between neurons with collinearly aligned cRFs. For higher stimulus velocities, the collinearity index declines due to the connections formed predominantly between neurons whose cRFs are not collinearly aligned.

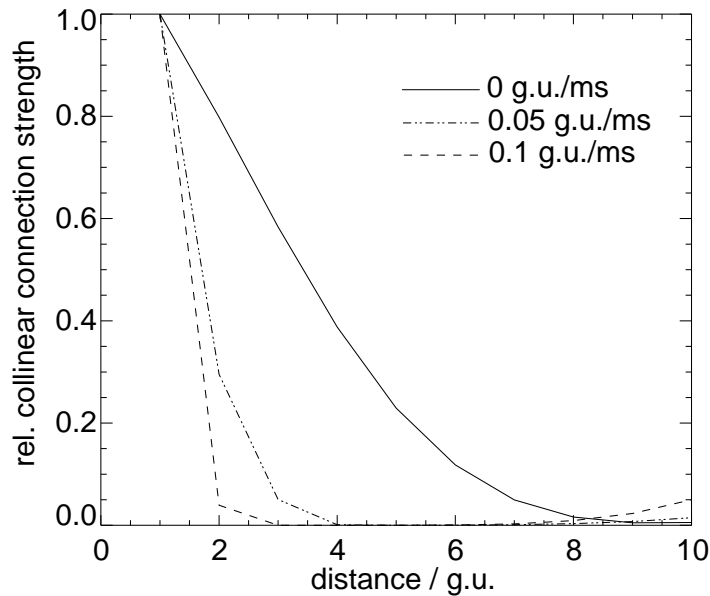


Figure 4.6: RELATIVE DECLINE IN COLLINEAR CONNECTION STRENGTH AFTER LEARNING WITH SLOW LATERAL CONDUCTION VELOCITIES. Shown are the lateral connection strengths along the collinear direction, normalized to the collinear connection strength for neurons with a relative distance of 1 grid unit. Relative collinear connection strengths decline faster with increasing distance after learning with high stimulus velocities in comparison to learning with low stimulus velocities.

tions, comparable to those in the case of infinite conduction velocities. Note also the lower collinearity index after static stimulation in the case of finite conduction velocities (Figure 4.5E) in comparison to the case of infinite conduction velocities (Figure 4.2E). This is mainly due to spurious correlations between the spikes of neurons activated by a stimulus and spikes caused by preceding stimulus presentations, traveling along the axons for more than 140 ms.

For higher stimulus velocities, lateral connections develop asymmetrically between neurons aligned towards the direction of stimulus movement. For a stimulus velocity of 0.1 g.u./ms (Figure 4.5C), the stimulus velocity equals the lateral conduction velocity. In this case, lateral connections are formed mainly in the direction of stimulus movement, but not along the orientation of the bar.

Figure 4.6 shows the relative decline in collinear connection strength for the three different stimulus velocities. Unlike in the case of zero conduction delays (Figure 4.3), collinear connection strengths decline more steeply with increasing distance for high stimulus velocities than for low stimulus velocities.

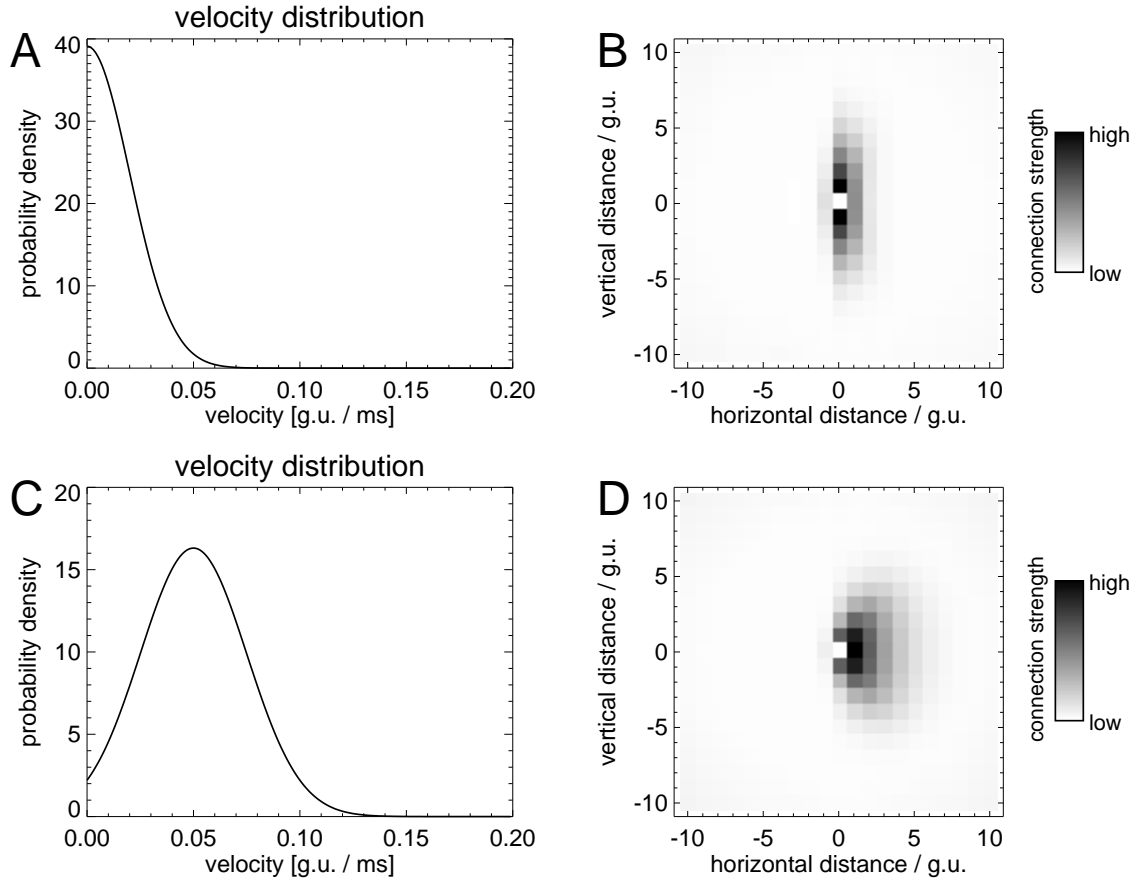


Figure 4.7: LATERAL CONNECTIVITY AFTER LEARNING WITH VARIABLE STIMULUS VELOCITIES. Upper Row: (A) Stimulus velocities were taken from the positive-valued part of a Gaussian distribution, centered at 0 g.u./ms with standard deviation of 0.02 g.u./ms. (B) The average lateral connectivity after learning according to the velocity distribution depicted in (A). Lower Row: (C) Stimulus velocities were taken from the positive-valued part of a Gaussian distribution, centered at 0.05 g.u./ms with standard deviation of 0.025 g.u./ms. (D) Average lateral connectivity after learning according to the velocity distribution depicted in (C).

4.4.3 Random Stimulus Velocities during Learning

During normal viewing, retinal stimulus velocities are not fixed, but cover a range from static views up to velocities too fast to be resolved by cortical neurons. To account for this situation, we varied the movement velocity of the Gaussian bar for each presentation phase. In one simulation, stimulus velocities were chosen from a Gaussian distribution, centered at $v_c = 0$ g.u./ms, with a standard deviation of $\sigma_v = 0.02$ g.u./ms (Figure 4.7A). In another

simulation, the Gaussian distribution was centered at $v_c = 0.05$ g.u./ms with a standard deviation of $\sigma_v = 0.025$ g.u./ms (Figure 4.7C). Negative velocity values corresponding to movements in the opposite direction were discarded.

The resulting lateral connectivity is shown in Figures 4.7B,D. The results are similar to the results obtained with fixed stimulus velocities (Figure 4.5): For a velocity distribution which contains mainly low velocities, lateral connections connect mainly neurons with cRFs aligned along the direction of orientation of the bar. For a velocity distribution which contains higher stimulus velocities, lateral connections target predominantly neurons with cRFs towards the direction of stimulus motion.

4.5 Discussion

4.5.1 Summary of Results

We have investigated the influence of the temporal properties of the visual input and the conduction velocity of the horizontal connections on the self-organization of the lateral connectivity in a network model of pulse-coding neurons. By training the network with moving Gaussian light bars of different velocities, we have shown that the learned lateral connectivity depends on both the velocity of the input stimuli and the conduction velocity of the horizontal connections during learning. For stimuli moving slowly compared to the velocity of the horizontal connections, the learned lateral connections are reciprocal and well adapted to the spatial properties of the stimuli. For fast moving stimuli, lateral connections are asymmetric with respect to the direction of stimulus motion.

In the case of *infinite lateral conduction velocities*, the asymmetry in the lateral connectivity towards the direction of stimulus movement is due to the finite temporal extent of the asymmetric Hebbian learning window. In the current model, absolute collinear connection strengths are lower for higher stimulus velocities due to the synaptic weight normalization procedure. However, the relative collinear decline in connection strengths with increasing distance is similar after learning with different stimulus velocities (Figure 4.3). Thus, if the normalization procedure would be replaced by a mechanism which restricts the weights of the single lateral connections rather than the total presynaptic weight of a given neuron, we expect collinear lateral connections to have comparable synaptic strengths after learning with stimuli of different velocities. Hence, even if the learned lateral connectivity is asymmetric towards the direction of stimulus motion, it retains some specificity for the spatial structure of the visual input.

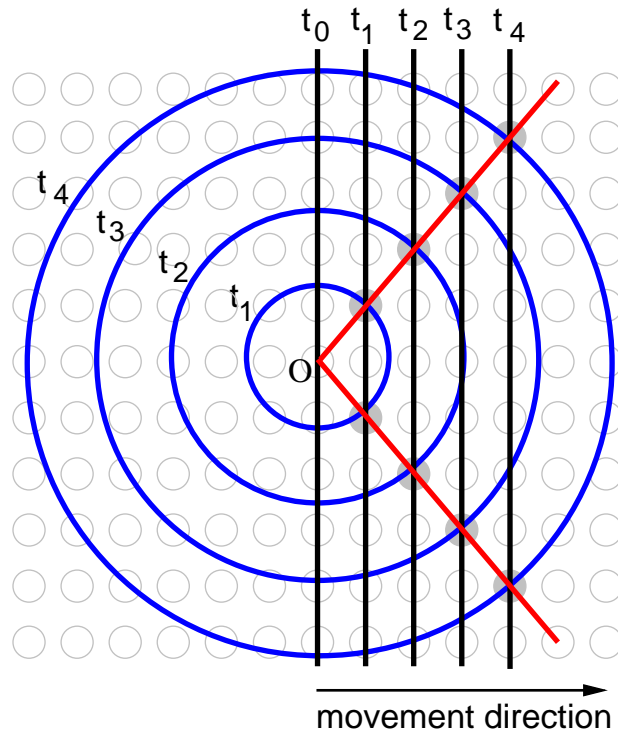


Figure 4.8: COINCIDENCE OF AFFERENT AND LATERAL SIGNALS IN A NETWORK WITH FINITE CONDUCTION VELOCITIES. The figure demonstrates how the learned connection structure can be interpreted. A bar-stimulus moves with constant velocity to the right, as indicated by the black bars. A spike emitted at time t_0 by a neuron at position O travels with constant velocity along the axon. The travelled distances at different times are indicated by the blue circles. Coincidence of this spike with direct activations by the stimulus at later times (t_1, t_2, t_3, t_4) can only occur at the intersection of the activation profile of the bar with the corresponding circle, as indicated by the red lines. For bars moving with a velocity equal to the lateral conduction velocity, coincidences of pre- and postsynaptic activations occur along the direction of motion.

In the case of *finite lateral conduction velocities*, the asymmetry in lateral connectivity towards the direction of motion is more pronounced for stimulus velocities similar to the lateral conduction velocity. Collinear lateral connections decline faster with distance the higher the velocity of the stimuli during learning. For stimulus velocities equal to the lateral conduction velocity, lateral connections are learned along the direction of stimulus movement, but not along the axis of orientation of the bar stimulus. The results can be interpreted in that the lateral connectivity learned with static stimuli consists of two blades along the axis of orientation. With increasing stimulus velocity these blades turn towards the movement

direction of the stimulus. If stimulus velocity equals the velocity of the lateral connections, the blades are parallel to the direction of motion (Figure 4.8). The lateral connectivity depicted in Figure 4.5B, which resembles a filled triangle, can be understood if one considers the additional influence of the temporal Hebbian learning window, which leads to an increase in synaptic connection strengths even if the presynaptic activation precedes the postsynaptic spike (compare Figure 4.2).

Comparable results were obtained if stimulus velocities during learning were chosen randomly according to a fixed distribution of velocities. For a distribution of stimulus velocities restrained to low velocities in comparison to the lateral conduction velocities, the learned lateral connectivity is well adapted to the spatial structure of the input. A distribution of higher stimulus velocities causes lateral connections to be learned between neurons with cRFs aligned towards the direction of stimulus movement.

For neurons of similar velocity preferences, the results show that slowly conducting horizontal connections, with conduction velocities similar to the velocities in the input, self-organize according to the coding of stimulus movement direction, enhancing responses to stimuli moving in the direction of the connections. Fast conducting horizontal connections self-organize according to the spatial properties within the visual input.

For lateral connections of fixed, finite conduction velocities, the results can be interpreted in terms of the velocity preference of presynaptic neurons. For neurons sensitive to stimulus velocities considerably lower than the lateral conduction velocities, the static correlations in the input play a dominant role in shaping the pattern of the lateral connectivity. Neurons sensitive to stimulus velocities similar to the lateral conduction velocities develop lateral connections according to the spatio-temporal correlations within the input.

In the following, we will relate these results to known experimental data and discuss different coding strategies along M- and P- dominated cortical pathways.

4.5.2 Network Scaling

Assuming lateral conduction velocities on the order of ≈ 0.1 m/s, consistent with the lateral spread of activity (monkey: Grinvald et al., 1994, cat: Bringuier et al., 1999), and a primate cortical magnification factor of $M(E) \approx 8.85 \cdot (0.87 + E)^{-1}$ mm/ $^\circ$ (Adams and Horton, 2003), we obtain lateral conduction velocities of $\approx 10^\circ$ /s for the center of the visual field, and velocities of $\approx 120^\circ$ /s at an eccentricity of 10° . Although relatively fast, the lateral conduction velocities are of the same magnitude as the retinal velocities of the visual input. As we have demonstrated, there is a considerable effect of stimulus movement on the learning

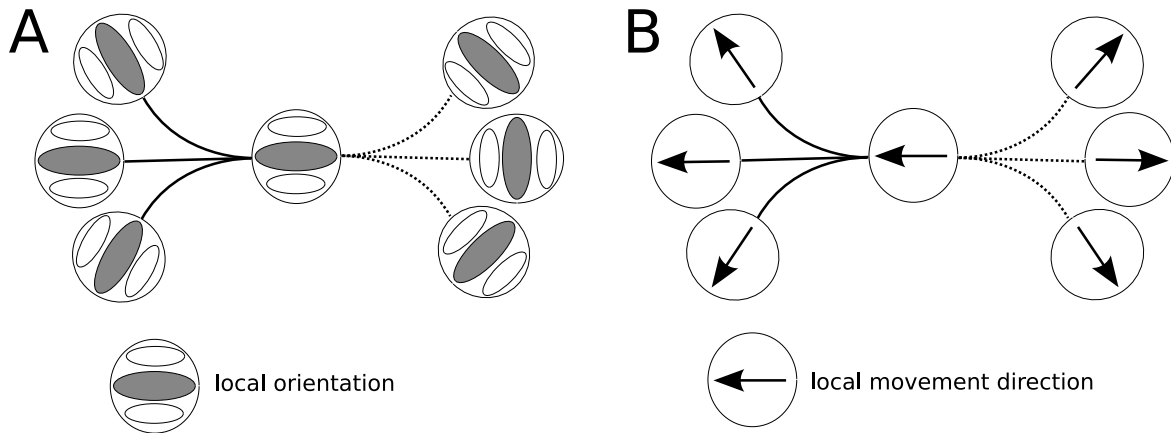


Figure 4.9: PERCEPTUAL ASSOCIATION FIELDS FOR ORIENTATION- AND MOTION-DEFINED GROUPING. (A) Association field for static, orientation-defined contours. The enhancement between neighboring contour-elements is strongest if they form a smooth contour (solid lines) and weak if they do not (dotted lines). Adapted from (Field et al., 1993). (B) Association field for motion-defined contours. The enhancement of neighboring contour-elements is strongest if their motion-directions are similar and form a smooth contour. Adapted from (Ledgeway et al., 2005).

of the lateral connectivity, even for stimulus velocities slower than the velocity of the lateral connections (Figure 4.7). Therefore, it seems plausible that stimulus motion may have an effect on the self-organization of lateral connections in the primary visual cortex during natural viewing conditions.

4.5.3 Grouping Mechanisms for Static and Motion-Defined Contours

Our results are consistent with recent psychophysical experiments, investigating the grouping performance of static and motion-defined contours (static: e.g., Field et al., 1993, motion: Ledgeway and Hess, 2002; Ledgeway et al., 2005). For static, orientation-defined contours, detection is best if the orientations of local contour-elements are aligned along the axis of the contour (Figure 4.9A). The grouping process could be supported by horizontal connections between neurons with cRFs aligned collinearly with respect to their orientation preferences. For motion-defined contours, however, detection performance is best if the local motion vectors of the local contour-elements are oriented along the contour. The results of Ledgeway and Hess (2002) suggest an association field for motion-defined contours like the one depicted in Figure 4.9B. Translating this motion-defined association field into lateral con-

nectivity corresponds well to the coupling profiles learned in our model with fast-moving stimuli, where lateral connections link neurons along the direction of motion.

Taken together, we suggest that the lateral connectivity for the grouping of static contours could be provided by neurons with low velocity-preference, supposedly receiving mainly P-input. The required lateral connectivity for the grouping of motion-defined contours could be provided by neurons with higher preferred stimulus velocities, possibly receiving mainly M-input. Thus, our results highlight the possible role of the retino-cortical M- and P-pathways on the self-organization according to spatio-temporal (motion) and spatial (form) properties of the visual input along the cortical dorsal and ventral pathway, respectively.

4.5.4 Grouping Mechanisms at Different Eccentricities

With increasing eccentricity, the psychophysical contour grouping performance (e.g., Hess and Dakin, 1997, 1999) and collinear facilitation (e.g., Giorgi et al., 2004; Shani and Sagi, 2005), as measured in contrast discrimination experiments, declines. Our simulations suggest that the decrease in the ratio of P- to M-inputs to V1 with increasing retinal eccentricity (e.g., Malpeli et al., 1996; Azzopardi et al., 1999) may play a role in the decrease in collinear facilitation with increasing eccentricity. Due to the increasing contribution of the M-pathway in providing input to cortical neurons at larger eccentricities, it seems possible that lateral connections self-organize according to the spatio-temporal structure of the visual input at the expense of the spatial structure (compare Figure 4.7). The spatial statistics of real-world scenes are dominated by horizontal and vertical contours (Coppola et al., 1998a; Hancock et al., 1992; Van der Schaaf and Hateren, 1996; Keil and Cristóbal, 2000; Betsch et al., 2004). Thus, we expect lateral connections between neurons which are selective for low stimulus velocities to predominantly target neurons with collinearly aligned cRFs along these cardinal directions. The distribution of retinal velocities during self-motion of an observer is dominated by radial (expansion) and tangential (rotation) velocity components. Therefore, we expect the lateral connections between neurons selective for high stimulus velocities to be arranged predominantly along these oblique directions, perpendicular to the axis of their orientation preferences. Indirect evidence for the plausibility of this hypothesis comes from the study of the orientation preferences of neurons in the primary visual cortex of cats (Bauer et al., 1990): While neurons of horizontal and vertical orientation preference are over-represented in the central visual field, they found an over-representation of neurons with radial and concentric orientation preferences in the peripheral visual field. Thus, it seems plausible that the response properties of cortical neurons in the central and periph-

eral visual field are specialized for different tasks, namely the encoding of spatial structure and motion, respectively. This is consistent with the finding that cortical areas along the ventral pathway of monkeys, associated with the encoding of object form, receive mainly input from the foveal portion of the visual field. Areas along the dorsal pathway, concerned with the encoding of motion and spatial coordination, receive predominantly input from the peripheral portion of the visual field (review: Gattass et al., 2005). Thus, it seems plausible that lateral connections could serve different functional roles in the fovea compared to the periphery. Our study demonstrates that the different patterns of lateral connectivity can self-organize according to the temporal response characteristics of the corresponding neurons. However, current experimental data on the structure of lateral connectivity reveal no systematic changes with eccentricity or with respect to the prominent thalamic input of the corresponding neurons (monkey: Sincich and Blasdel, 2001; Angelucci et al., 2002; Stettler et al., 2002, cat: Ts'o et al., 1986; Schmidt et al., 1997; Gilbert and Wiesel, 1989, 1990, tree shrew: Bosking et al., 1997).

4.5.5 Conclusion

Our results demonstrate that the temporal response properties of cortical neurons may have a considerable impact on the self-organization of the horizontal connectivity under natural viewing conditions, favoring either the coding of spatial (during fixation) or spatio-temporal (during observer- or object-motion) characteristics of the visual input. Our model makes predictions about changes in lateral connectivity depending on the temporal response characteristics of the corresponding cortical neurons with respect to the conduction velocities of horizontal connections. Due to the declining ratio of P- to M-input to the visual cortex with increasing retinal eccentricity this should result in a different pattern of lateral connectivity for the foveal in comparison to the peripheral representation of the visual field.

Chapter 5

Conclusion and Outlook

In the primary visual cortex of primates, relatively more space is devoted to the representation of the central visual field in comparison to the representation of the peripheral visual field (e.g., Daniel and Whitteridge, 1961). Furthermore, the ratio of parvocellular (P) to magnocellular (M) inputs to the primary visual cortex declines with increasing eccentricity (Azzopardi et al., 1999; Connolly and Van Essen, 1984; Malpeli et al., 1996). In this thesis we investigated to which visual situations this inhomogeneous mapping of visual space is well adapted and studied possible functional consequences for visual processing at central and peripheral locations of the visual field.

Summing up, our results indicate that self-motion may have played an important role in determining the global retino-cortical mapping. We have shown that the inhomogeneous retino-cortical mapping can be refined and stabilized by Hebbian learning mechanisms in ontogenesis under natural viewing conditions.

The spatially inhomogeneous retino-cortical mapping has the advantage that the neuronal modules, concerned with the processing of self-motion along the direction of gaze, can be identical in their spatial and temporal properties across the representation of the visual field. In contrast, our investigation of the spatial statistics of local oriented Gabor wavelet responses at different spatial scales, obtained from real-world scenes, provides evidence against uniform mechanisms of contour grouping across the visual field.

Furthermore, we have demonstrated that the development of lateral connections between neurons in the primary visual cortex may depend on the spatio-temporal response properties of their afferent inputs. Neurons sensitive to slow changes within the visual input may develop lateral connections well adapted to the spatial characteristics of the visual input (form), while neurons sensitive to higher temporal frequency components within the visual input may lead to lateral connections well adapted to the spatio-temporal characteristics of

the visual input (motion). With respect to the different temporal response characteristics of neurons along the retino-cortical parvocellular and magnocellular pathways, we have suggested that neurons receiving mainly parvocellular input may support the coding of spatial stimulus attributes (object-form) while neurons receiving mainly magnocellular input may subserve the coding of spatio-temporal stimulus attributes (object motion) along the cortical ventral and dorsal pathways, respectively. Due to the larger ratio of parvocellular to magnocellular neurons in the fovea in comparison to the periphery, these results suggest that foveal and peripheral cortical processing may have become specialized for different characteristics of the visual input: The foveal representation, which receives predominantly parvocellular input, may be well adapted to the spatial representation of fixated objects. The peripheral representation, with its increasing ratio of magnocellular input, may be better adapted to the processing of motion.

5.1 Specific Results

- We have assumed that cortical magnification is such that cortical activations, caused by stationary objects during self-motion along the direction of gaze, travel on average with constant speed across the cortical surface, independent of retinal eccentricity. This would have the important advantage that the cortical mechanisms, concerned with the processing of self-motion, can be identical in their spatial and temporal properties across the representation of the whole visual field. This is the case if the distribution of objects corresponds to an ellipsoid with the observer in its center.
- An RF distribution, consistent with cortical magnification, can be learned in a network model of pulse coding neurons with Hebbian learning, when trained with flow-fields similar to those during self-motion along the direction of gaze. RF sizes increase linearly with eccentricity, and RF peak sensitivities decrease with increasing eccentricity, consistent with experimental results.
- The spatial statistics of oriented Gabor wavelet responses extracted from real-world scenes are not invariant with respect to the spatial scale of the wavelets. Collinear correlations drop in coordinates normalized to the wavelength of the wavelets relatively faster for wavelets of long wavelengths. Furthermore, collinear correlations between wavelets of different orientations are not rotation invariant, with collinear correlations between wavelets of oblique orientations declining more steeply with increasing eccentricity than collinear correlations between wavelets of cardinal orientations.

- The self-organization of lateral connections of finite conduction velocities due to a temporal Hebbian learning rule depends on the temporal properties of the visual input. By training a one-layer network of spiking neurons with moving Gaussian bars of different velocities, we have shown that static or slowly-moving bars lead to horizontal connections reciprocally linking neurons along the direction of orientation of the bars, thus subserving the coding of spatial stimulus attributes. For fast moving stimuli with velocities comparable to the lateral axonal conduction velocity, the learned lateral connectivity is asymmetric towards the direction of bar movement, thus subserving the coding of the movement direction of visual stimuli. We have discussed these results with respect to the different temporal response characteristics of neurons along the retino-cortical parvocellular and magnocellular pathways. Neurons receiving mainly parvocellular input may subserve the coding of spatial stimulus attributes (object form) while neurons receiving mainly magnocellular input may subserve the coding of spatio-temporal stimulus attributes (object motion). Considering the decreasing ratio of parvocellular to magnocellular inputs to the primary visual cortex with increasing eccentricity (e.g., Azzopardi et al., 1999), this could further account for the psychophysically measured decrease in contour grouping performance for peripheral stimuli (e.g, Hess and Dakin, 1999).

5.2 Proposals for Future Research

Theoretical models, aimed at the understanding of the visual system, are worthless if they cannot be verified or falsified experimentally. Our investigations provide testable predictions which may be verified or rejected by future work.

5.2.1 Retinal Velocity Distribution During Self-Motion

According to the spatial retino-cortical mapping, we expect that average retinal stimulus velocities, due to self-motion of an observer, increase linearly with increasing eccentricity (Chapter 2). It is difficult to test this hypothesis based solely on theoretical considerations because of the unknown distribution of objects relative to the observer, deviations of the direction of gaze from the direction of self-motion, and the unknown distribution of movement velocities; which is most probably dependent on the distribution of objects around the observer. To our knowledge, no data exist about the average retinal velocity distribution across the whole visual field of a human observer during self-motion within natural environments.

5.2.2 Spatial Statistics of Contour Elements Across the Whole Visual Field

In Chapter 3 we have assumed that the spatial statistics of natural scenes are constant across the whole visual field. As we have discussed, this is not strictly the case (Reinagel and Zador, 1999; Krieger et al., 2000). On average, high spatial frequency content, edge density, and contrast are highest at the point of fixation (Mannan et al., 1996, 1997; Reinagel and Zador, 1999), and spatial correlations at the center of gaze are on average lower in comparison to the correlations across the whole visual field. The influence of these inhomogeneities on the spatial statistics of local contour elements at different eccentricities remains to be investigated.

5.2.3 Lateral Connections in the Primary Visual Cortex

Concerning the structure of lateral connections in the primary visual cortex it would be interesting to study possible changes in lateral connectivity between neurons in dependence on their spatial frequency preference. Our results from Chapter 3 suggest that lateral connections should be shorter in visual coordinates, normalized to the neurons' preferred spatial wavelengths, between neurons selective for low spatial frequencies in comparison to neurons selective for high spatial frequencies.

It would further be interesting to assess possible changes in lateral connectivity with respect to the predominant retino-cortical input (magnocellular or parvocellular) of the corresponding neurons. We expect that horizontal connections differ in their pattern of connectivity for cortical patches in V1, dominated by either magnocellular or parvocellular inputs from the LGN (Chapter 4). Our results suggest that lateral connections between neurons selective for low stimulus velocities, presumably dominated by parvocellular input, reciprocally connect mainly neurons with collinearly arranged cRFs. In contrast, lateral connections between neurons selective for high stimulus velocities, receiving predominantly magnocellular input, should be between neurons with cRFs aligned towards the axis of their direction preference. We are not aware of studies which investigated the lateral connectivity of neurons in the primary visual cortex of monkeys with respect to the velocity preferences of the corresponding neurons or their predominant retino-cortical inputs.

Bibliography

- Adams DL, Horton JC. A precise retinotopic map of primate striate cortex generated from the representation of angioscotomas. *J Neurosci*, 23(9):3771–3789, May 2003.
- Adelson EH, Bergen JR. Spatiotemporal energy models for the perception of motion. *J Opt Soc Am A*, 2:284–299, 1985.
- Andersen RA, Snyder LH, Bradley DC, Xing J. Multimodal representation of space in the posterior parietal cortex and its use in planning movements. *Annu Rev Neurosci*, 20:303–330, 1997.
- Angelucci A, Levitt JB, Walton EJS, Hupe JM, Bullier J, Lund JS. Circuits for local and global signal integration in primary visual cortex. *J Neurosci*, 22:8633–8646, 2002.
- Appelle S. Perception and discrimination as a function of stimulus orientation: the "oblique effect" in man and animals. *Psychol Bull.*, 78(4):266–278, 1972.
- Arakawa K, Tobimatsu S, Kurita-Tashima S, Nakayama M, Kira JI, Kato M. Effects of stimulus orientation on spatial frequency function of the visual evoked potential. *Exp Brain Res*, 131:121–125, 2000.
- Attneave F. Some informational aspects of visual perception. *Psychol Rev*, 61:183–193, 1954.
- Azzopardi P, Cowey A. Models of ganglion cell topography in the retina of macaque monkeys and their application to sensory cortical scaling. *Neuroscience*, 72(3):617–625, 1996.
- Azzopardi P, Jones KE, Cowey A. Uneven mapping of magnocellular and parvocellular projections from the lateral geniculate nucleus to the striate cortex in the macaque monkey. *Vision Res*, 39:2179–2189, 1999.
- Baker CI, Peli E, Knouf N, Kanwisher NG. Reorganization of visual processing in macular degeneration. *J Neurosci*, 25(3):614–618, 2005.
- Barlow HB. Summation and inhibition in the frog's retina. *J Physiol*, 119:69–88, 1953.
- Barlow HB. Possible principles underlying the transformation of sensory messages. In Rosenblith W, editor, *Sensory communication*, pages 217–234. Cambridge, MA: MIT Press, 1961.

- Bauer R, Leferink J, Eckhorn R, Jordan W. Complementary global maps for orientation coding in upper and lower layers of the cat striate cortex and their possible functions. *J Comp Neurol*, 305:282–288, 1990.
- Becker S. Learning to categorize objects using temporal coherence. In Hanson SJ, Cowan JD, Giles CL, editors, *Advances in Neural Information Processing Systems 5*, pages 361–368. San Francisco, CA. Morgan Kaufmann, 1993.
- Becker S. Implicit learning in 3D object recognition: the importance of temporal context. *Neural Comput*, 11(2):347–374, 1999.
- Bell AJ, Sejnowski TJ. The "independent component" of natural scenes are edge filters. *Vision Res*, 37(23):3327–3338, 1997.
- Betsch BY, Einhäuser W, Körding KP, König P. The world from a cat's perspective – statistics of natural videos. *Biol Cybern*, 90:41–50, 2004.
- Bi Gq, Poo Mm. Synaptic modifications in cultured hippocampal neurons: Dependence on spike timing, synaptic strength, and postsynaptic cell type. *J Neurosci*, 18(24):10464–10472, 1998.
- Bi Gq, Poo Mm. Synaptic modification by correlated activity: Hebb's postulate revisited. *Annu Rev Neurosci*, 24:139–166, 2001.
- Blakemore C, Cooper GF. Development of the brain depends on the visual environment. *Nature*, 228:477–478, 1970.
- Bliss TV, Lomo T. Long-lasting potentiation of synaptic transmission in the dentate area of the anaesthetized rabbit following stimulation of the perforant path. *J Physiol*, 232(2): 331–356, 1973.
- Bonds AB. An "oblique effect" in the visual evoked potential of the cat. *Exp Brain Res*, 46 (1):151–154, 1982.
- Bonds AB, Casagrande VA, Norton TT, DeBruyn EJ. Visual resolution and sensitivity in a nocturnal primate (galago) measured with visual evoked potentials. *Vision Res*, 27(6): 845–857, 1987.
- Borg-Graham L, Monier C, Fregnac Y. Voltage-clamp measurement of visually-evoked conductances with whole-cell patch recordings in primary visual cortex. *J Physiol Paris*, 90 (3–4):185–188, 1996.
- Borg-Graham LJ, Monier C, Fregnac Y. Visual input evokes transient and strong shunting inhibition in visual cortical neurons. *Nature*, 393(6683):369–373, 1998.
- Bosking WH, Zhang Y, Schofield B, Fitzpatrick D. Orientation selectivity and the arrangement of horizontal connections in tree shrew striate cortex. *J Neurosci*, 17(6):2112–2127, 1997.

- Braitenberg V, Schüz A. *Anatomy of the Cortex: Statistics and Geometry*. Springer Verlag, 1991.
- Bremmer F, Duhamel F, Ben Hamed JR, Graf W. Stages of self-motion processing in primate posterior parietal cortex. *Ann N Y Acad Sci*, 871:272–281, 2000.
- Bremmer F, Schlack A, Duhamel JR, Graf W, Fink GR. Space coding in primate posterior parietal cortex. *Neuroimage*, 1:S46–51, 2001.
- Bremmer F. Navigation in space – the role of the macaque ventral intraparietal area. *J Physiol*, 566(1):29–35, 2005.
- Bringuier V, Chavane F, Glaeser L, Fregnac Y. Horizontal propagation of visual activity in the synaptic integration field of area 17 neurons. *Science*, 283:695–699, 1999.
- Brunswik E, Kamiya J. Ecological cue-validity of 'proximity' and other gestalt factors. *Am J Psychol*, 66:20–32, 1953.
- Burkhalter A, Bernardo KL, Charles V. Development of local circuits in human visual cortex. *J Neurosci*, 13(5):1916–1931, 1993.
- Cajal SR. The croonian lecture: la fine structure des centers nerveux. *Proc R Soc London Ser B*, 55:444–467, 1894.
- Callaway EM, Katz LC. Emergence and refinement of clustered horizontal connections in cat striate cortex. *J Neurosci*, 10:1134–1153, 1990.
- Callaway EM, Katz LC. Effects of binocular deprivation on the development of clustered horizontal connections in cat striate cortex. *P Natl Acad Sci USA*, 88:745–749, 1991.
- Choe Y, Miikkulainen R. Contour integration and segmentation with self-organized lateral connections. *Biol Cybern*, 90:75–88, 2004.
- Clifford CWG, Ibbotson MR. Fundamental mechanisms of visual motion detection: Models, cells and functions. *Prog Neurobiol*, 68:409–437, 2003.
- Connolly M, Van Essen D. The representation of the visual field in parvocellular and magnocellular layers of the lateral geniculate nucleus in the macaque monkey. *J Comp Neurol*, 226(4):544–564, 1984.
- Coppola DM, Purves HR, McCoy AN, Purves D. The distribution of oriented contours in the real world. *P Natl Acad Sci USA*, 95:4002–4006, 1998a.
- Coppola DM, White LE, Fitzpatrick D, Purves D. Unequal representation of cardinal and oblique contours in ferret visual cortex. *P Natl Acad Sci USA*, 95(5):2621–2623, 1998b.
- Croner LJ, Kaplan E. Receptive fields of P and M ganglion cells across the primate retina. *Vision Res*, 35(1):7–24, 1995.

- Dacey D, Packer OS, Diller L, Brainard D, Peterson B, Lee B. Center surround receptive field structure of cone bipolar cells in primate retina. *Vision Res*, 40(14):1801–1811, 2000.
- Dacey DM, Petersen MR. Dendritic field size and morphology of midget and parasol ganglion cells of the human retina. *P Natl Acad Sci USA*, 89(20):9966–9670, 1992.
- Dakin SC, Hess RF. Spatial-frequency tuning of visual contour integration. *J Opt Soc Am A*, 15(6):1486–1499, 1998.
- Daniel PM, Whitteridge D. The representation of the visual field on the cerebral cortex in monkeys. *J Physiol*, 159:203–221, 1961.
- Daw NW, Fox K, Sato H, Czepita D. Critical period for monocular deprivation in the cat visual cortex. *J Neurophysiol*, 67(1):197–202, 1992.
- De Monasterio FM. Properties of concentrically organized X and Y ganglion cells of macaque retina. *J Neurophysiol*, 41(6):1394–1417, 1978.
- De Monasterio FM, Gouras P. Functional properties of ganglion cells of the rhesus monkey retina. *J Physiol*, 251(1):167–195, 1975.
- De Valois RL, Albrecht DG, Thorell LG. Spatial frequency selectivity of cells in macaque visual cortex. *Vision Res*, 22:545–559, 1982.
- De Valois RL, De Valois KK. *Spatial Vision*. Oxford Press, 1988.
- De Valois RL, De Valois KK. A multi-stage color model. *Vision Res*, 33(8):1053–1065, 1993.
- Derrington AM, Lennie P. Spatial and temporal contrast sensitivities of neurones in lateral geniculate nucleus of macaque. *J Physiol*, 357(1):219–240, 1984.
- Desimone R, Albright TD, Gross CG, Bruce C. Stimulus-selective properties of inferior temporal neurons in the macaque. *J Neurosci*, 4:2051–2062, 1984.
- Dow BM, Snyder AZ, Vautin RG, Bauer R. Magnification factor and receptive field size in foveal striate cortex of the monkey. *Exp Brain Res*, 44:213–228, 1981.
- Dragoi V, Turcu CM, Sur M. Stability of cortical responses and the statistics of natural scenes. *Neuron*, 32:1181–1192, 2001.
- Duffy CJ. Optic flow analysis for self-motion perception. *Int. Rev. Neurobiol.*, 44:199–218, 2000.
- Duhamel JR, Bremmer F, BenHamed S, Graf W. Spatial invariance of visual receptive fields in parietal cortex neurons. *Nature*, 389:845–484, 1997.

- Eckhorn R, Reitboeck HJ, Arndt M, Dicke P. Feature linking via synchronization among distributed assemblies: Simulations of results from cat visual cortex. *Neural Comput*, 2(3):293–307, 1990.
- Egelhaaf M, Borst A. A look into the cockpit of the fly: Visual orientation, algorithms, and identified neurons. *J Neurosci*, 13:4563–4574, 1993.
- Eysel UT, Eydin D, Schweigart G. Repetitive optical stimulation elicits fast receptive field changes in mature visual cortex. *Neuroreport*, 9(5):949–954, 1998.
- Falconbridge MS, Stamps RL, Badcock DR. A simple Hebbian/Anti-Hebbian network learns the sparse, independent components of natural images. *Neural Comput*, 18:415–429, 2006.
- Feidler JC, Saul AB, Murthy A, Humphrey AL. Hebbian learning and the development of direction selectivity: the role of geniculate response timings. *Network: Comput Neural Syst*, 8:195–214, 1997.
- Feldman DE. Timing-based LTP and LTD at vertical inputs to layer II/III pyramidal cells in rat barrel cortex. *Neuron*, 27:45–56, 2000.
- Felleman DJ, Van Essen DC. Distributed hierarchical processing in the primate cerebral cortex. *Cereb Cortex*, 1:1–47, 1991.
- Ferrera VP, Nealey TA, Maunsell JHR. Responses in macaque visual area V4 following inactivation of the parvocellular and magnocellular LGN pathways. *J Neurosci*, 14(4):2080–2088, 1994.
- Field DJ. Relations between the statistics of natural images and the response profiles of cortical cells. *J Opt Soc Am A*, 4:2379–2394, 1987.
- Field DJ, Hayes A, Hess RF. Contour integration by the human visual system: Evidence for a local "association field". *Vision Res*, 33(2):173–193, 1993.
- Fischer B. Overlap of receptive field centers and representation of the visual field in the cat's optic tract. *Vision Res*, 13:2113–2120, 1973.
- Földiák P. Forming sparse representations by local anti-Hebbian learning. *Biol Cybern*, 64:165–170, 1990.
- Földiák P. Learning invariance from transformation sequences. *Neural Comput*, 3(2):194–200, 1991.
- Földiák P. *Visual Constancies: Why Things Look As They Do*, chapter Learning constancies for object perception, pages 144–172. Cambridge University Press, 1997.
- Fox K, Daw N. A model for the action of NMDA conductances in the visual cortex. *Neural Comput*, 4:59–83, 1992.

- Fox K, Sato H, Daw NW. The location and function of NMDA receptors in cat and kitten visual cortex. *J Neurosci*, 9:2443–2454, 1989.
- Freeman E, Sagi D, Driver J. Lateral interactions between targets and flankers in low-level vision depend on attention to the flankers. *Nat Neurosci*, 4:1032–1036, 2001.
- Frome RC, Dan Y. Spike-timing-dependent synaptic modification induced by natural spike trains. *Nature*, 416:433–438, 2002.
- Frome RC, Poo MM, Dan Y. Spike-timing-dependent synaptic plasticity depends on dendritic location. *Nature*, 434(7030):221–225, 2005.
- Fu YX, Djupsund K, Gao H, Hayden B, Shen K, Dan Y. Temporal specificity in the cortical plasticity of visual space representation. *Science*, 296:1999–2003, 2002.
- Gabor D. Theory of communication. *J Inst Elec Eng*, 93:429–459, 1946.
- Gattass R, Pessoa LA, de Weerd P, Fiorani M. Filling-in in topographically organized distributed networks. *An Acad Bras Cienc*, 71:997–1015, 1999.
- Gattass R, Rosa MGP, Sousa APB, Pinon MCGP, Fiorani Jr M, Neuenschwander S. Cortical streams of visual information processing in primates. *Braz J Med Biol Res*, 23:375–393, 1990.
- Gattass R, Sousa APB, Ungerleider LG, Mishkin M. Cortical projections of area V2 in the macaque. *Cereb Cortex*, 7:110–129, 1997.
- Gattass R, Nascimento-Silva S, Soares JGM, Lima B, Jansen AK, Diogo ACM, Farias MF, Marcondes M, Botelho EP, Mariani OS, Azzi J, Fiorani M. Cortical visual areas in monkeys: location, topography, connections, columns, plasticity and cortical dynamics. *Phil Trans R Soc B*, 360(1456):709–731, 2005.
- Geisler WS, Perry JS, Super BJ, Gallogly DP. Edge co-occurrence in natural images predicts contour grouping performance. *Vision Res*, 41:711–724, 2001.
- Gilbert CD. Horizontal integration and cortical dynamics. *Neuron*, 9:1–20, 1992.
- Gilbert CD, Wiesel TN. Morphology and intracortical projections of functionally characterized neurones in the cat visual cortex. *Nature*, 280(5718):120–125, 1979.
- Gilbert CD, Wiesel TN. Columnar specificity of intrinsic horizontal and corticocortical connections in cat visual cortex. *J Neurosci*, 9:2432–2442, 1989.
- Gilbert CD, Wiesel TN. The influence of contextual stimuli on the orientation selectivity of cells in primary visual cortex of the cat. *Vision Res*, 30(11):1689–1701, 1990.
- Giorgi RG, Soong GP, Woods RL, Peli E. Facilitation of contrast detection in near-peripheral vision. *Vision Res*, 44:3193–3202, 2004.

- Goodale M, Meenan J, Bühlhoff H, Nicolle D, Murphy K, Racicot C. Separate neural pathways for the visual analysis of object shape in perception and prehension. *Current Biology*, 4(7):604–610, 1994.
- Goodale M, Milner A, Jakobson L, Carey D. A neurological dissociation between perceiving objects and grasping them. *Nature*, 349(6305):154–156, 1991.
- Goodale MA, Milner AD. Separate visual pathways for perception and action. *Trends Neurosci*, 15(1):20–25, 1992.
- Grinvald A, Lieke EE, Frostig RD, Hildesheim R. Cortical point-spread function and long-range lateral interactions revealed by real-time optical imaging of macaque monkey primary visual cortex. *J Neurosci*, 14:2545–2568, 1994.
- Grossberg S, Mingolla E, Ross WD. Visual brain and visual perception: how does the cortex do perceptual grouping? *Trends Neurosci*, 20(3):106–111, 1997.
- Grossberg S, Mingolla E, Pack C. A neural model of motion processing and visual navigation by cortical area MST. *Cereb Cortex*, 9:878–895, 1999.
- Grossberg S, Williamson JR. A neural model of how horizontal and interlaminar connections of visual cortex develop into adult circuits that carry out perceptual grouping. *Cereb Cortex*, 11:37–58, 2001.
- Grünert U, Greferath U, Boycott BB, Wässle H. Parasol (P alpha) ganglion-cells of the primate fovea: immunocytochemical staining with antibodies against GABA A-receptors. *Vision Res*, 33:1–14, 1993.
- Hancock PJB, Baddeley RJ, Smith LS. The principal components of natural images. *Network: Comput Neural Syst*, 3(1):61–70, 1992.
- Hansen T, Sepp W, Neumann H. Recurrent long-range interactions in early vision. In Wermter S, Austin J, Willshaw D, editors, *Emergent Neural Computational Architectures Based on Neuroscience : Towards Neuroscience-Inspired Computing*, volume 2036, pages 127–138. Springer Verlag: Berlin, Heidelberg, 2001.
- Hassenstein B, Reichardt W. Systemtheoretische Analyse der Zeitreihenfolgen- und Vorzeichenenauswertung bei der Bewegungsrezeption des Rüsselkäfers *Chlorophanus*. *Zeitschrift für Naturforschung*, 1956.
- Hebb DO. *The organization of behaviour*. Wiley, New York, 1949.
- Heeley DW, Buchanan-Smith HM, Cromwell JA, Wright JS. The oblique effect in orientation acuity. *Vision Res*, 37(2):235–242, 1997.
- Heinen SJ, Skavenski AA. Recovery of visual responses in foveal V1 neurons following bilateral foveal lesions in adult monkey. *Exp Brain Res*, 83(3):670–674, 1991.

- Hess RF, Dakin SC. Absence of contour linking in peripheral vision. *Nature*, 390:602–604, 1997.
- Hess RF, Dakin SC. Contour integration in the peripheral field. *Vision Res*, 39:947–959, 1999.
- Hicks TP, Lee BB, Vidyasagar TR. The responses of cells in macaque lateral geniculate nucleus to sinusoidal gratings. *J Physiol*, 337(1):183–200, 1983.
- Hirsch JA, Gilbert CD. Synaptic physiology of horizontal connections in the cat's visual cortex. *J Neurosci*, 11(6):1800–1809, 1991.
- Hoyer PO, Hyvärinen A. A multi-layer sparse coding network learns contour coding from natural images. *Vision Res*, 42:1593–1605, 2002.
- Hubel DH, Wiesel TN. Receptive fields of single neurons in the cat's visual cortex. *J Physiol*, 148:574–591, 1959.
- Hubel DH, Wiesel TN. Receptive fields, binocular interactions and functional architecture in the cat's visual cortex. *J Physiol (London)*, 160:106–154, 1962.
- Hubel DH, Wiesel TN. Binocular interaction in striate cortex of kittens reared with artificial squint. *J Neurophysiol*, 28(6):1041–1059, 1965.
- Hubel DH, Wiesel TN. Receptive fields and functional architecture of monkey striate cortex. *J Physiol (London)*, 195:215–243, 1968.
- Hubel DH, Wiesel TN. Uniformity of monkey striate cortex: a parallel relationship between field size scatter, and magnification factor. *J Comp Neurol*, 158:295–306, 1974.
- Hubel DH, Wiesel TN, LeVay S. Plasticity of ocular dominance columns in monkey striate cortex. *Philosophical Transactions of the Royal Society of London Series B*, 278:377–409, 1977.
- Hupé JM, James AC, Girard P, Lomber SG, Payne BR, Bullier J. Feedback connections act on the early part of the responses in monkey visual cortex. *J Neurophysiol*, 85:134–145, 2001.
- Hupé JM, James AC, Payne BR, Lomber SG, Girard P, Bullier J. Cortical feedback improves discrimination between figure and background by V1, V2 and V3 neurons. *Nature*, 394:784–787, 1998.
- Ito M, Gilbert CD. Attention modulates contextual influences in the primary visual cortex of alert monkeys. *Neuron*, 22:593–604, 1999.
- Jastorff J, Giese MA. Time-dependent Hebbian rules for the learning of templates for visual motion recognition. In Ilg U, Bülthoff HH, Mallot H, editors, *Dynamic Perception*, pages 151–156. Infix, Berlin, 2004.

- Jones JP, Palmer LA. An evaluation of the two-dimensional Gabor filter model of simple receptive fields in cat striate cortex. *J Neurophysiol*, 58(6):1233–1258, 1987.
- Kapadia MK, Ito M, Gilbert CD. Improvement in visual sensitivity by changes in local context: Parallel studies in human observers and in V1 of alert monkeys. *Neuron*, 15: 843–856, 1995.
- Kaplan E, Shapley E. X and Y cells in the lateral geniculate nucleus of macaque monkeys. *J Physiol*, 330(1):125–143, 1982.
- Kaplan E, Shapley RM. The primate retina contains two types of ganglion cells, with high and low contrast sensitivity. *P Natl Acad Sci USA*, 83:2755–2757, 1986.
- Kaplan E, Bernadete E. The dynamics of primate retinal ganglion cells. *Prog Brain Res*, 134:17–34, 2001.
- Kasamatsu T, Kitano M, Sutter EE, Norcia AM. Lack of lateral inhibitory interactions in visual cortex of monocularly deprived cats. *Vision Res*, 38(1):1–12, 1998.
- Katz LC, Callaway EM. Development of local circuits in mammalian visual cortex. *Annu Rev Neurosci*, 15, 1992.
- Keil MS, Cristóbal G. Separating the chaff from the wheat: possible origins of the oblique effect. *J Opt Soc Am A*, 2000.
- Kiorpes L, Bassin SA. Development of contour integration in macaque monkeys. *Vis Neurosci*, 20:567–575, 2003.
- Knierim JJ, van Essen DC. Neuronal responses to static texture patterns in area V1 of the alert macaque monkey. *J Neurophysiol*, 67:961–980, 1992.
- Koffka K. *Principles of Gestalt psychology*. London: Lund Humphries, 1935.
- Kohonen T. *Self-organization and associative memory*. Springer Verlag: Berlin, Heidelberg, 1989.
- Komatsu Y, Nakajima S, Toyama K, Fetz EE. Intracortical connectivity revealed by spike-triggered averaging in slice preparations of cat visual cortex. *Brain Res*, 442:359–362, 1988.
- Körding KP, König P. Neurons with two sites of synaptic integration learn invariant representations. *Neural Comput*, 13(12):2823–2849, 2001.
- Krebs WK, Essock EA, Buttrey SE, J. SM, McCarley JS. An oblique effect of chromatic gratings measured by color-mixture thresholds. *Perception*, 29:927–935, 2000.
- Krieger G, Rentschler I, Hauske G, Schill K, Zetzsche C. Object and scene analysis by saccadic eye-movements: an investigation with higher-order statistics. *Spat Vis*, 13(2–3): 201–214, 2000.

- Krüger N. Collinearity and parallelism are statistically significant second order relations of complex cell responses. *Neural Processing Letters*, 8:117–129, 1998.
- Kulikowski J, Vidyasagar T. Space and spatial frequency: analysis and representation in the macaque striate cortex. *Exp Brain Res*, 64:5–18, 1986.
- Lappe M, Bremmer F, van den Berg AV. Perception of self-motion from visual flow. *Trends Cogn Sci*, 3(9):329–336, 1999.
- Ledgeway T, Hess RF. Rules for combining the outputs of local motion detectors to define simple contours. *Vision Res*, 42:653–659, 2002.
- Ledgeway T, Hess RF, Geisler WS. Grouping local orientation and direction signals to extract spatial contours: Empirical tests of "association field" models of contour integration. *Vision Res*, 2005.
- Leventhal AG, Hirsch HVB. Receptive-field properties of different classes of neurons in visual cortex of normal and dark-reared cats. *J Neurophysiol*, 43(4):1111–1132, 1980.
- Levi DM, Klein SA, Aitsebaomo AP. Vernier acuity, crowding and cortical magnification. *Vision Res*, 25(7):963–977, 1985.
- Li B, Peterson MR, Freeman RD. Oblique effect: A neural basis in the visual cortex. *J Neurophysiol*, 90:204–217, 2003.
- Li Z. Pre-attentive segmentation in the primary visual cortex. *Spat Vis*, 13:25–50, 1999.
- Linsenmeier R, Frishman LJ, Jakiela HG, Enroth-Cugell C. Receptive field properties of X and Y cells in the cat retina derived from contrast sensitivity measurements. *Vision Res*, 22:1173–1183, 1982.
- Livingstone MS. Mechanisms of direction selectivity in macaque V1. *Neuron*, 20:509–526, 1998.
- Livingstone MS, Hubel DH. Anatomy and physiology of a color system in the primate visual cortex. *J Neurosci*, 4:309–356, 1984.
- Livingstone MS, Hubel DH. Segregation of form, color, movement, and depth: anatomy, physiology, and perception. *Science*, 240:740–749, 1988.
- Logothetis NK, Pauls J, Poggio T. Shape representation in the inferior temporal cortex of monkeys. *Current Biology*, 5:552–563, 1995.
- Lomo T. Potentiation of monosynaptic EPSPs in the perforant path-dentate granule cell synapse. *Exp Brain Res*, 12:46–63, 1971.
- Löwel S, Singer W. Selection of intrinsic horizontal connections in the visual cortex by correlated neuronal activity. *Science*, 255:209–212, 1992.

- Maffei L, Fiorentini A. The unresponsive regions of visual cortical receptive fields. *Vision Res*, 16(10):1131–1139, 1976.
- Magee JC, Johnston D. A synaptically controlled, associative signal for Hebbian plasticity in hippocampal neurons. *Science*, 275(5297):209–213, 1997.
- Makela P, Nasanen R, Rovamo J, Melmoth D. Identification of facial images in peripheral vision. *Vision Res*, 41(5):599–610, 2001.
- Malpeli JG, Lee D, Baker FH. Laminar and retinotopic organization of the macaque lateral geniculate nucleus: Magnocellular and parvocellular magnification functions. *J Comp Neurol*, 375(3):363–377, 1996.
- Mannan SK, Ruddock KH, Wooding DS. The relationship between the locations of spatial features and those of fixations made during visual examination of briefly presented images. *Spat Vis*, 10(3):167–188, 1996.
- Mannan SK, Ruddock KH, Wooding DS. Fixation patterns made during brief examination of two-dimensional images. *Perception*, 26(8):1059–1072, 1997.
- Mansfield RJ, Ronner SF. Orientation anisotropy in monkey visual cortex. *Brain Res*, 149(1):229–234, 1978.
- Marčelja S. Mathematical description of the response of simple cortical cells. *J Opt Soc Am A*, 70(11):1297–1300, 1980.
- Markram H, Lübke J, Frotscher M, Sakmann B. Regulation of synaptic efficacy by coincidence of postsynaptic APs and EPSPs. *Science*, 275:213–215, 1997.
- Marrocco RT, McClurkin JW, Young RA. Spatial summation and conduction latency classification of cells of the lateral geniculate nucleus of macaques. *J Neurosci*, 2:1275–1291, 1982.
- McIlhagga WH, Mullen KT. Contour integration with colour and luminance contrast. *Vision Res*, 36(9):1265–1279, 1996.
- Mehta MR, Quirk MC, Wilson MA. Experience-dependent asymmetric shape of hippocampal receptive fields. *Neuron*, 25:707–715, 2000.
- Merigan WH, Byrne C, Maunsell JH. Does primate motion perception depend on the magnocellular pathway? *J Neurosci*, 11:3422–3429, 1991a.
- Merigan WH, Katz LM, Maunsell JHR. The effects of parvocellular lateral geniculate lesions on the acuity and contrast sensitivity of macaque monkeys. *J Neurosci*, 11:994–1101, 1991b.
- Mignard M, Malpeli JG. Paths of information flow through visual cortex. *Science*, 251:1249–1251, 1991.

- Mineiro P, Zipser D. Analysis of direction selectivity arising from recurrent cortical interactions. *Neural Comput*, 10:353–371, 1998.
- Murakoshi T, Guo JZ, Ichinose T. Electrophysiological identification of horizontal synaptic connections in rat visual cortex in vitro. *Neuroscience Letters*, 163:211–214, 1993.
- Nakamura H, Gattass R, Desimone R, Ungerleider LG. The modular organization of projections from areas V1 and V2 to areas V4 and TEO in macaque. *J Comp Neurol*, 13: 3681–3691, 1993.
- Nelson JJ, Kupersmith MJ, Seiple WH, Weiss PA, Carr RE. Spatiotemporal conditions which elicit or abolish the oblique effect in man: direct measurement with swept evoked potential. *Vision Res*, 24:579–586, 1984.
- Neumann H, Sepp W. Recurrent V1-V2 interaction in early visual boundary processing. *Biol Cybern*, 81:425–444, 1999.
- Nowak LG, Bullier J. Axons, but not cell bodies, are activated by electrical stimulation in cortical gray matter: I. Evidence from chronaxie measurements. *Exp Brain Res*, 118: 477–488, 1998.
- O’Keefe J, Dostrovsky J. The hippocampus as a spatial map. preliminary evidence from unit activity in the freely-moving rat. *Brain Res*, 34:171–175, 1971.
- Olshausen BA, Field DJ. Wavelet-like receptive fields emerge from a network that learns sparse codes for natural images. *Nature*, 381:607–609, 1996.
- Orban GA, Kennedy H. The influence of eccentricity on receptive field types and orientation selectivity in areas 17 and 18 of the cat. *Brain Res*, 208(1):203–208, 1981.
- Orban GA, Kennedy H, Bullier J. Velocity sensitivity and direction selectivity of neurons in areas V1 and V2 of the monkey: influence of eccentricity. *J Neurophysiol*, 56(2):462–480, 1986.
- Ostkamp R. *Bildvorverarbeitung realer Szenen mit dynamischen Modellneuronen zur kontextabhängigen Merkmalsextraktion, Merkmalskopplung und Szenensegmentierung*. PhD thesis, Philipps-Universität Marburg, Fachbereich Physik, 1996.
- Perrett DL, Rolls ET, Caan W. Visual neurons responsive to faces in the monkey temporal cortex. *Exp Brain Res*, 47:329–342, 1982.
- Perry VH, Cowey A. The ganglion cell and cone distributions in the monkey’s retina: Implications for central magnification factors. *Vision Res*, 225:1795–1810, 1985.
- Perry VH, Oehler R, Cowey A. Retinal ganglion cells that project to the dorsal lateral geniculate nucleus in the macaque monkey. *Neuroscience*, 12(4):1101–1123, 1984.

- Pigarev IN, Nothdurft HC, Kastner S. Neurons with radial receptive fields in monkey area V4A: evidence of a subdivision of prelunate gyrus based on neuronal response properties. *Exp Brain Res*, 145:149–206, 2002.
- Polat U, Sagi D. Lateral interactions between spatial channels: suppression and facilitation revealed by lateral masking experiments. *Vision Res*, 33:993–999, 1993.
- Polat U, Sagi D. The architecture of perceptual spatial interactions. *Vision Res*, 34:73–78, 1994.
- Pollen DA, Ronner SF. Phase relationship between adjacent simple cells in the visual cortex. *Science*, 212:1409–1411, 1981.
- Popovic Z, Sjöstrand J. Resolution, separation of retinal ganglion cells, and cortical magnification in humans. *Vision Res*, 2001.
- Prodöhl C, Würtz RP, von der Malsburg C. Learning the Gestalt rule of collinearity from object motion. *Neural Comput*, 15:1865–1896, 2003.
- Purpura K, Kaplan E, Shapley RM. Background light and the contrast gain of primate P and M retinal ganglion cells. *P Natl Acad Sci USA*, 85:4534–4537, 1988.
- Purpura K, Tranchina D, Kaplan E, Shapley RM. Light adaptation in the primate retina: analysis of changes in gain and dynamics of monkey retinal ganglion cells. *Vis Neurosci*, 4:75–93, 1990.
- Quiroga RQ, Reddy L, Kreiman G, Koch C, Fried I. Invariant visual representation by single neurons in the human brain. *Nature*, 435:1102–1107, 2005.
- Reid RC, Shapley RM. Spatial structure of cone inputs to receptive fields in primate lateral geniculate nucleus. *Nature*, 356:716–718, 1992.
- Reinagel P, Zador AM. Natural scene statistics at the centre of gaze. *Network: Comput Neural Syst*, 10:1–10, 1999.
- Reitboeck HJ, Altmann J. A model for size- and rotation-invariant pattern processing in the visual system. *Biol Cybern*, 51:113–121, 1984.
- Rodieck RW. The primate retina. In *Comparative Primate Biology*, pages 203–278. New York: Alan R. Liss, 1988.
- Rolls ET. Functions of the primate temporal lobe cortical visual areas in invariant visual object and face recognition. *Neuron*, 27:205–218, 2000.
- Rolls ET, Milward T. A model of invariant object recognition in the visual system: Learning rules, activation functions, lateral inhibition, and information-based performance measures. *Neural Comput*, 12:2547–2572, 2000.

- Rovamo J, Virsu V. An estimation and application of the human cortical magnification factor. *Exp Brain Res*, 37(3):495–510, 1979.
- Rovamo J, Virsu V, Näsänen R. Cortical magnification factor predicts the photopic contrast sensitivity of peripheral vision. *Nature*, 271:54–56, 1978.
- Ruderman D, Bialek W. Statistics of natural images - scaling in the woods. *Phys Rev Lett* V, 73(6):814–817, 1994.
- Rushton WA. A theory of the effects of fibre size in medullated nerve. *J Physiol*, 115: 101–122, 1951.
- Ruthazer ES, Stryker MP. The role of activity in the development of long-range horizontal connections in area 17 of the ferret. *J Neurosci*, 16(22):7253–7269, 1996.
- Saam M, Eckhorn R. Lateral spike conduction velocity in the visual cortex affects spatial range of synchronization and receptive field size without visual experience: A learning model with spiking neurons. *Biol Cybern*, 83:1–9, 2000.
- Salin PA, Bullier J. Corticocortical connections in the visual system: Structure and function. *Physiol Rev*, 75(1):107–154, 1995.
- Saudargiene A, Porr B, Wörgötter F. How the shape of pre- and postsynaptic signals can influence STDP: A biophysical model. *Neural Comput*, 16:595–625, 2004.
- Schlack A, Hoffmann KP, Bremmer F. Interaction of linear vestibular and visual stimulation in the macaque ventral intraparietal area (VIP). *Eur J Neurosci*, 16(10):1877, 2002.
- Schmidt KE, Goebel R, Löwel S, Singer W. The perceptual grouping criterion of colinearity is reflected by anisotropies of connections in the primary visual cortex. *Eur J Neurosci*, 9 (5):1083–1089, 1997.
- Schwartz EL. Afferent geometry in the primate visual cortex and the generation of neuronal trigger features. *Biol Cybern*, 28:1–24, 1977.
- Schwartz EL. Computational anatomy and functional architecture of striate cortex: A spatial mapping approach to perceptual coding. *Vision Res*, 20(8):645–669, 1980.
- Schwartz EL. Cortical anatomy, size invariance, and spatial frequency analysis. *Perception*, 10:455–468, 1981.
- Sclar G, Maunsell JHR, Lennie P. Coding of image contrast in central visual pathways of the macaque monkey. *Vision Res*, 30:1–10, 1990.
- Shani R, Sagi D. Eccentricity effects on lateral interactions. *Vision Res*, 45:2009–2024, 2005.
- Shapley R, Kaplan E, Soodak R. Spatial summation and contrast sensitivity of X and Y cells in the lateral geniculate nucleus of the macaque. *Nature*, 292:543–545, 1981.

- Shon AP, Rao RPN, Sejnowski TJ. Motion detection and prediction through spike-timing dependent plasticity. *Network: Comput Neural Syst*, 15:179–198, 2004.
- Sigman M, Cecchi GA, Gilbert CD, Magnasco MO. On a common circle: Natural scenes and gestalt rules. *P Natl Acad Sci USA*, 98(4):1935–1940, 2001.
- Sillito AM, Grieve KL, E. JH, J. C, J. D. Visual cortical mechanisms detecting focal orientation discontinuities. *Nature*, 378(6556):492–496, 1995.
- Silveira LCL, Perry VH. The topography of magnocellular projecting ganglion cells (M ganglion cells) in the primate retina. *Neuroscience*, 40:217–237, 1991.
- Sincich LC, Horton JC. Independent projection streams from macaque striate cortex to the second visual area and middle temporal area. *J Neurosci*, 23(13):5684–5692, 2003.
- Sincich LC, Blasdel GG. Oriented axon projections in primary visual cortex of the monkey. *J Neurosci*, 21(12):4416–4426, 2001.
- Sirosh J, Miikkulainen R. Topographic receptive fields and patterned lateral interaction in a self-organizing model of the primary visual cortex. *Neural Comput*, 9(3):577–594, 1997.
- Sjöström PJ, Turrigiano GG, Nelson SB. Rate, timing, and cooperativity jointly determine cortical synaptic plasticity. *Neuron*, 32:1149–1164, 2001.
- Slotnick SD, Klein SA, Carney T, Sutter E. Electrophysiological estimate of human cortical magnification. *Clinical Neurophysiology*, 112:1349–1356, 2001.
- Slovin H, Arieli A, Hildesheim R, Grinvald A. Long-term voltage-sensitive dye imaging reveals cortical dynamics in behaving monkeys. *J Neurophysiol*, 88:3421–3438, 2002.
- Snyder AW, Miller WH. Photoreceptor diameter and spacing for highest resolving power. *J Opt Soc Am*, 67(5):696–698, 1977.
- Spelke ES, Breinlinger K, Jacobson K, Phillips A. Gestalt relations and object perception: a developmental study. *Perception*, 22(12):1483–1501, 1993.
- Spitzer H, Hochstein S. Complex-cell receptive field models. *Prog Neurobiol*, 31:285–309, 1988.
- Stettler DD, Das A, Bennett J, Gilbert CD. Lateral connectivity and contextual interactions in macaque primary visual cortex. *Neuron*, 36:739–750, 2002.
- Stringer SM, Rolls ED. Invariant object recognition in the visual system with novel views of 3d objects. *Neural Comput*, 14:2585–2596, 2002.
- Stuart GJ, Sakmann B. Active propagation of somatic action potentials into neocortical pyramidal cell dendrites. *Nature*, 367:69–72, 1994.

- Sur M, Leamey CA. Development and plasticity of cortical areas and networks. *Nat Rev Neurosci*, 2(4):251–262, 2001.
- Tanaka K. Neuronal mechanisms of object recognition. *Science*, 262:685–688, 1993.
- Trachtenberg JT, Stryker MP. Rapid anatomical plasticity of horizontal connections in the developing visual cortex. *J Neurosci*, 21(10):3476–3482, 2001.
- Ts'o DY, Gilbert CD, Wiesel TN. Relationships between horizontal interactions and functional architecture in cat striate cortex as revealed by cross-correlation analysis. *J Neurosci*, 6:1160–1170, 1986.
- Ungerleider L, Mishkin M. Two cortical visual systems. In Ingle D, Goodale M, Mansfield R, editors, *Analysis of Visual Behavior*, pages 549–586. Cambridge, Mass.: MIT Press, 1982.
- Ungerleider LG, Desimone R. Cortical connections of visual area MT in the macaque. *J Comp Neurol*, 248:190–222, 1986.
- van de Grind WA, van Doorn AJ, Koenderink JJ. Detection of coherent movement in peripherally viewed random-dot patterns. *J Opt Soc Am A*, 73(12):1674–1683, 1983.
- Van der Schaaf A, Hateren JH. Modelling the power spectra of natural images. *Vision Res*, 36:2759–2770, 1996.
- Van Essen DC, Anderson CH, Felleman DJ. Information processing in the primate visual system: An integrated systems perspective. *Science*, 255:419–423, 1992.
- Van Essen DC, Gallant JL. Neural mechanisms of form and motion processing in the primate visual system. *Neuron*, 13:1–10, 1994.
- Van Essen DC, Newsome WT, Maunsell HR. The visual field representation in striate cortex of the macaque monkey: Asymmetries, anisotropies and individual variability. *Vision Res*, 24:429–448, 1984.
- Van Essen DC, Anderson CH. Information processing strategies and pathways in the primate visual system. In Zornetzer SF, Davis LL, Lau C, McKenna T, editors, *An Introduction to Neural and Electronic Networks*, pages 45–76. Academic Press, 2. edition, 1995.
- van Hateren JH, Ruderman DL. Independent component analysis of natural image sequences yields spatio-temporal filters similar to simple cells in primary visual cortex. *Proc. R. Soc. Lond. B.*, 265:2315–2320, 1998.
- van Hateren JH, Van der Schaaf A. Independent component filters of natural images compared with simple cells in primary visual cortex. *Proc. R. Soc. London B*, 265:359–366, 1998.

- Virsu V, Rovamo J. Visual resolution, contrast sensitivity, and the cortical magnification factor. *Exp Brain Res*, 37(3):475–494, 1978.
- Virsu V, Rovamo J, Laurinen P, Nasanen R. Temporal contrast sensitivity and cortical magnification. *Vision Res*, 22(9):1211–1217, 1982.
- Virsu V, Hari R. Cortical magnification, scale invariance and visual ecology. *Vision Res*, 36(18):2971–2977, 1996.
- von der Heydt R, Peterhans E, Baumgartner G. Illusory contours and cortical neuron responses. *Science*, 224(4654):1260–1262, 1984.
- Wallis G. Using spatio-temporal correlations to learn invariant object recognition. *Neural Netw*, 9(9):1513–1519, 1996.
- Wallis G, Rolls ET. Invariant face and object recognition in the visual system. *Prog Neurobiol*, 51(2):167–194, 1997.
- Wässle H, Grünert U, Röhrenbeck J, Boycott BB. Retinal ganglion cell density and cortical magnification factor in the primate. *Vision Res*, 30(11):1897–1911, 1990.
- Wässle H, Levick WR, Cleland BG. The distribution of the alpha type of ganglion cells in the cat's retina. *J Comp Neurol*, 159:419–438, 1975.
- Watanabe M, Rodieck RW. Parasol and midget ganglion cells of the primate retina. *J Comp Neurol*, 289(3):434–454, 1989.
- Waxman SG, Bennett MV. Relative conduction velocities of small myelinated and non-myelinated fibres in the central nervous system. *Nature*, 238:217–219, 1972.
- Wenisch OG, Noll J, van Hemmen JL. Spontaneously emerging direction selectivity maps in visual cortex. *Biol Cybern*, 93(4):239–247, 2005.
- Wertheimer M. Untersuchungen zur Lehre von der Gestalt II. *Psychologische Forschung*, 4: 301–350, 1923.
- Westheimer G. Scaling of visual acuity measurement. *Archives of Ophthalmology*, 97:327–330, 1979.
- Wiesel TN, Hubel DH. Single cell responses in striate cortex of kittens deprived of vision in one eye. *J Neurophysiol*, 26:1003–1017, 1963.
- Williams CB, Hess RF. Relationship between facilitation at threshold and suprathreshold contour integration. *J Opt Soc Am A*, 15:2046–2051, 1998.
- Wimbauer S, Wenisch OG, Miller KD, van Hemmen JL. Development of spatiotemporal receptive fields of simple cells: I. Model formulation. *Biol Cybern*, 77:453–461, 1997.

- Wiskott L, Sejnowski T. Slow feature analysis: Unsupervised learning of invariances. *Neural Comput*, 14(4):715–770, 2002.
- Woods RL, Nugent AK, Peli E. Lateral interactions: Size does matter. *Vision Res*, 42: 733–745, 2002.
- Xing J, Heeger DJ. Center-surround interactions in foveal and peripheral vision. *Vision Res*, 40:3065–3072, 2000.
- Xu X, Bonds AB, Casagrande VA. Modeling receptive-field structure of koniocellular, magnocellular, and parvocellular LGN cells in the owl monkey (*Aotus trivigatus*). *Vis Neurosci*, 19:703–711, 2002.
- Yabuta NH, Sawatari A, Callaway EM. Two functional channels from primary visual cortex to dorsal visual cortical areas. *Science*, 292(5515):297–300, 2001.
- Yao H, Dan Y. Stimulus timing-dependent plasticity in cortical processing of orientation. *Neuron*, 32:315–323, 2001.
- Yen SC, Finkel LH. Extraction of perceptually salient contours by striate cortical networks. *Vision Res*, 38(5):719–741, 1998.
- Zeki SM. Representation of central visual fields in prestriate cortex of monkey. *Brain Res*, 14:271–291, 1969.
- Zeki SM. A direct projection from area V1 to area V3A of rhesus monkey visual cortex. *Proc. R. Soc. B.*, 107:499–506, 1980.
- Zenger-Landolt B, Koch C. Flanker effects in peripheral contrast discrimination- psychophysics and modeling. *Vision Res*, 41:3663–3675, 1996.
- Zetsche C, Röhrbein F. Nonlinear and extra-classical receptive field properties and the statistics of natural scenes. *Network: Comput Neural Syst*, 12(3):331–350, 2001.
- Zhang LI, Tao, H. W. Holt CE, Harris WA, Poo M. A critical window for cooperation and competition among developing retinotectal synapses. *Nature*, 395:37–44, 1998.
- Zigmond MJ. *Fundamental Neuroscience*. Academic Press, San Diego, 1999.

Acknowledgements

Scientific work is seldom an individual endeavor. This is also true for the current thesis. Many people have influenced this thesis and me due to their knowledge and their generosity in sharing it with me. Therefore, it would be impossible to list everyone who contributed.

First and foremost, I would like to thank my advisor, Prof. Dr. Reinhard Eckhorn, for his enduring commitment and continuous interest in the subject, and his encouragement throughout this research. I wish to thank Prof. Dr. Heiko Neumann for his willingness to serve as a referee for this this thesis.

I would like to thank (in no particular order) Dr. Andreas Gabriel, Timm Zwickel, Frank Michler, Dr. Thomas Wachtler, Tobias Teichert, Markus Wittenberg, Kerstin Königs, Susanne Klauke, Steffen Klingenhöfer, and Prof. Dr. Reinhard Eckhorn for inspiring discussions and helpful comments on the manuscript.

I am very grateful to all other members of our research group for their cooperation and friendship, which provided a nice work environment and made daily work very motivating. I especially thank the former and current contributors to the *Neural Assembly Simulation Environment* (N.A.S.E.) for the cooperative development of elementary simulation and analysis tools.

I would like to thank Rachel Hoover for her dedication to the correction of mistakes concerning the correct use of the English language.

This work would not have been possible without financial support from the Friedrich-Ebert-Foundation.

My sincerest thanks goes to my mother, who has been very caring and supportive throughout my life, and without whom all this would not have been possible.

Scientific CV

Name: Basim Samir Al-Shaikhli
Date of Birth: January, 19th, 1975
Place of Birth: Kassel, Germany
Nationality: German
Present Address: Emil-Mannkopff Str. 6
35037 Marburg
☎ +49 6421 988192
✉ basimo@gmail.com

Education:

04/2004 - 06/2006 **Graduate Scholarship**
Friedrich-Ebert-Foundation, Bonn

09/2001 - 10/2003 **Research Associate**
Neurophysics Group, Dept. Physics,
Philipps University Marburg

06/2001 **Physics Diploma**
Subjects of examination: Theoretical Physics, Experimental
Physics, Solid State Physics, Computer Science
Diploma thesis: "Figur/Hintergrund-Trennung durch
Signalentkopplung" (Figure/ground segregation by decoupling
of neural signals)

04/1996 - 06/2001 **Physics Studies**
including Vordiplom (intermediate examination)
Philipps University Marburg

06/1994 **Abitur**
Gustav-Stresemann-Gymnasium, Bad Wildungen